# Three-dimensional turbulent flow generation considering correlation of fluctuating components and SCADA data

# 変動風速の相関とSCADAデータを考慮した3次元乱流場の生成

Hélène Huang

| Signature | Date | Seal |
|---|---|---|
| Advisor: | | |
| Co-advisor: | | |

Department of Civil Engineering
The University of Tokyo

A thesis submitted for the degree of
Master of Engineering

September 2012

**Abstract**

Generation of a turbulent wind field based on prescribed turbulence characteristics is required for physical model-based condition monitoring of wind turbines. Kaimal's and Mann's models are specified in the IEC 61400-1 standard and have been widely used for the design of wind turbines. However, these models cannot directly be used for wind generation for monitoring purposes. Kaimal's model lacks a theoretical background and is incomplete in terms of cross-correlations between different components of wind. Mann's model is derived from von Karman's theoretical model, but it cannot be easily linked to measured time series of wind. The aim of this study is to propose a set of turbulence models and investigate the applicability of the proposed model to dynamic simulation of wind turbines for monitoring.

First, von Karman's model is modified to satisfy measured wind data characteristics and the IEC requirements, and a model for Reynolds stress components is proposed. Von Karman's model has expressions in both frequency and time domain. The consistency of the proposed model with IEC requirements is validated in the frequency domain. Implementation in the wind generation method is carried out in the time domain, based on an adaptation of Iwatani's autoregressive method for wind generation. The generation algorithm can be linked to any number of measured wind speed data at any number of points. The turbulent wind fields generated in this study satisfy the IEC requirements and the proposed turbulence model, and are consistent with measured time series of wind speed.

Then, three wind fields are generated based on the proposed method, and the response of a wind turbine to each wind field is calculated. The first wind field satisfies the turbulence description but is not linked with any measured wind speed. The second and third wind fields are respectively linked to one and three components of measured wind speed. When one component of measured wind speed is included, the estimated maximum base moment shows a closer value to measurements and shows smaller variations over several random seeds realizations. Including three components of measured wind speed further increases the stability both in the fore-aft tower base bending moment and side-by-side tower base bending moment.

# Acknowledgements

First of all, I would like to express my utmost gratitude to my advisor, Professor Takeshi Ishihara, for allowing me to conduct this research and for his guidance and support. I would especially like to thank him for letting me participate to the EWEA conference, in which I discovered a lot about other research topics and industry issues in the field of wind energy.

I would also like to acknowledge the constant support of Dr. Atsushi Yamaguchi, whose advice was always valuable. His patience and good humour helped me find the strength to carry out this research. Also, to Professor Fujino, I would like to express my deepest appreciation for his lectures and the ones he organized with international professors.

I am grateful to Professor Fuse, my co-advisor, for his enlightening insights about time series analysis. And of course, I am extremely thankful to the Japanese Ministry of Education, Culture, Sports, Science and Technology for supporting me financially during these two years. I would also like to thank the Foreign Student Office and the Japanese Language Class in Civil Engineering and in the School of Engineering, who made our lives easier as foreign students and were like another family in the department.

I would like to give my special thanks to other members of the Bridge and Structure laboratory as well as members of the Concrete laboratory, who made studying hours at the lab much more enjoyable. In particular, special cheers to Sun, Amin, Umar, LanAnh, Youssef, Max, and my desk neighbour Takahashi-san.

A very, very special thanks to my tutor and friend, Yuka Kikuchi, who not only helped me a lot when I first landed at the University of Tokyo, but also kept on being funny, cheery, supportive and generous ever since we met.

Thanks to all my friends in Japan. Life would not have been so enjoyable without you.

# Contents

# List of Figures

# List of Tables

# Chapter 1

# Introduction

In the recent years, concerns about the depletion of fossil fuel sources and environmental awareness has pushed the development of renewable sources of energy. Among these, wind energy has known a fast development in the last 10 years [17]. In particular, the possibility of using the open sea as a possible location for wind farms attracts attention as the offshore wind resource potential is much larger than that of onshore wind, if only for lack of land availability.

## 1.1 The cost of condition monitoring

In spite of the growing interest in wind energy, its cost is still high. Unexpected failures are the main reason for the downtime of wind farms, and the traditional way of carrying out maintenance by scheduled on-site visits is no longer efficient enough, as the industry is shifting towards building wind farms in remote, difficult to access locations. As such, the European Wind Energy Association (EWEA) estimated that, in 2009, the operation and maintenance accounted for 20 to 35% of the total life cost of wind farms [17]. These costs are then reflected on the electricity price.

Operation and maintenance (O& M) costs need to be reduced to make wind energy more attractive. Innovative maintenance strategies can be adopted, such as condition-based maintenance. In such a strategy, by monitoring the condition of the wind turbines, minor damage can be detected early and immediate repair can be conducted when necessary; thus, major failures can be avoided and downtime can be reduced.

Several condition-based monitoring methods have been developed recently.

The most obvious one is the measurement-based method, in which measurements are made on the structure and insights about loads and structural response can be obtained directly. Although this seems to be the most natural choice, its main drawback is related to its strength: in order to obtain detailed real-time measurements, numerous sensors have to be deployed on every structure. This method can be acceptable for large, single structure systems such as bridges, but the sheer number and high costs of sensors are prohibitive if they are to be installed on a whole wind farm, without even thinking about the sensors' lifetime and the need to replace them. Another method, the statistics-based condition monitoring, consists of fitting a model based on short-term measurements and extrapolating it. It solves the cost issue by reducing drastically the need for sensors, but lacks flexibility to implement large variations in the conditions, making it less effective in case of sudden system changes.

A new method, called physical model-based condition monitoring (PCM), has been developed by Yoon in 2011 [29]. This method is based on measurements from a SCADA (System control and data acquisition) system, which are always installed for wind turbines since they are used for controlling the turbine operation; therefore the PCM has the advantage of not needing additional sensors, yet providing real-time data during the entire operation time. The measurements are used to update the aeroelastic model of the wind turbine, and finite-element simulations are conducted to estimate the structure's behaviour.

## 1.2 Wind field simulation for physical model-based condition monitoring

### 1.2.1 Concept of physical-model based condition monitoring

The main idea behind PCM is to understand the state of the structure by reproducing the structural response of the turbine using a limited number of measurements, with at least one anemometer (for wind speed measurement) and one strain gauge or one accelerometer (for the response). In order to have a good estimation of the response, and therefore an accurate understanding of the state of the structure, two points are essential: having an accurate model, and applying adequate external forces. The monitoring can be done in almost real-time, on a given period of time that we will denote $T$. The process is described on the flowchart in Fig. 1.1 and can be summarized as follows:

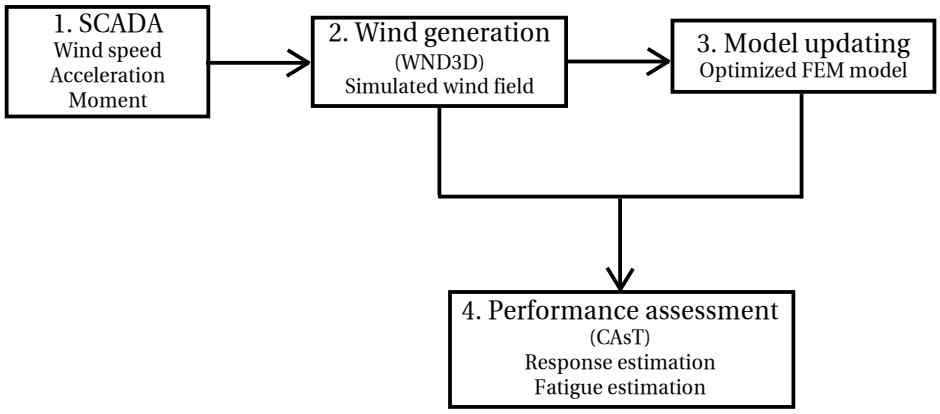


Figure 1.1: Flowchart of physical model-based condition monitoring method.

1. SCADA measurements are recorded. On the one hand, characteristics of the measured wind speed over $T$, such as mean wind speed $U$ and standard deviation $\sigma$, as well as the time series, are obtained. On the other hand, time history of the structural response is available (acceleration or moment time series).
2. The known wind turbulence characteristics are extrapolated over the area where the wind affects the wind turbine, then used to generate a three-dimensional turbulent wind field around that area, using the WND3D software, developed at the University of Tokyo [18][29] ("Wind generation").
3. The turbulent wind field is applied to a finite element model of the turbine, using the software CAsT (Computer-Aided Aerodynamic and Aeroelastic Technology, developed at the University of Tokyo [10]) to simulate the structural response. A modal analysis is conducted on the simulated response and the measured response to optimize the finite element model ("Model updating").
4. Finally, the optimized model is used with CAsT to estimate the response and assess the performance of the wind turbine ("Performance assessment").

In his research, Yoon [29] has developed a parameter optimization technique to improve the fitness between the response of finite element model and the actual structure, which makes up step 3 of the PCM process. This step ensures that the finite element model represents the real structure accurately. Moreover, during the lifetime of the structure, the adjustment of the model makes it possible

to understand changes in the structure and, eventually, damage.

Another important step of the process to obtain an accurate estimation of the wind turbine response is to apply an accurate wind field in the dynamic simulation. In PCM, a three-dimensional autoregressive method (Iwatani [11], Phuc [18]) is used to simulate the turbulent wind field. Wind field simulation is discussed in 1.2.2 below.

Estimating the loads (moment, force) and displacement (or acceleration) of the structure allows to adjust the operation of the wind turbine. For example, if fatigue loads are less than expected, the operation lifetime could be extended, or the other way around, if we detect that fatigue loads are higher than expected, the operation lifetime must be reduced. Additionally, estimating the real-time loads allows to detect when design loads are exceeded, and control can then be applied to the wind turbine (by adjusting the blade pitch for instance) to reduce the loads.

The PCM strategy can therefore reduce the O&M costs by avoiding extreme damage thanks to early detection, reducing the chance of damage by controlling the turbine to reduce loads, and can be used to determine if the lifetime of a wind farm can be prolonged.

### 1.2.2 Turbulent flow simulation

The PCM strategy requires an accurate estimation of the external forces in order to estimate the wind turbine loads accurately. Our focus will be on the aerodynamic forces, which are induced by the turbulent wind flow. In absence of detailed measurements of the wind speed, wind loads have to be estimated from a limited set of data about the wind flow; in the case of SCADA data, we usually only have access to the wind speed time series at one point, and only one component of the wind speed is available, that is, the longitudinal wind speed. Therefore, we need to simulate the wind field acting on the whole wind turbine from this small amount of information.

Several methods for generating turbulence fields have been proposed for wind turbine applications. The main obstacle arises from the nonlinear relationship between the wind flow and the aerodynamic forces, as shown in equation (1.1).

$$\begin{cases} \text{Drag force:} & F_D = \frac{1}{2}\rho A C_D(\alpha)|u-\dot{x}|^2 \\ \text{Lift force:} & F_L = \frac{1}{2}\rho A C_L(\alpha)|u-\dot{x}|^2, \end{cases} \tag{1.1}$$

where $A$ is the cross-section of the affected structure, $\rho$ is the fluid density, $C_D$ and $C_L$ are the drag and lift coefficients, $\alpha$ is the angle of attack, $u$ is the velocity of the flow and $\dot{x}$ is the velocity of the moving structure.

Because of that nonlinearity between turbulence and aerodynamic forces, a numerical step-by-step simulation is necessary, thus the need to calculate the time series of the flow velocity. In the case of wind turbines, the rotation of the blades also makes it necessary to understand the spatial variations of turbulence across the swept area.

One method, developed by Shinozuka in 1971 [20] and popularized by Sandia laboratories and Veers in 1988 [24], uses the spectral properties of the wind speed and generates time series by means of a Fourier transform. Another approach was introduced by Iwatani in 1982 [11], where the power spectral densities (PSD) of the wind turbulence are first translated to time-domain correlation functions by Fourier transform, then correlations applied to a time-domain, autoregressive method to generate wind speed time series at any desired point. Both approaches are quite similar in the sense that they start from standard turbulence power spectral densities models to use in their simulation method, and a Fourier transform is required at some point to obtain time series of wind speeds. Very little information from measurement is necessary to run these simulations: only the mean wind speed and the standard deviation of turbulence have to be provided, and a turbulence model can be chosen.

An interesting development for improved generation of wind flows, based on measured wind speed time series, has been proposed by Iwatani a few years later, in 1996 [12]. An improved version of his autoregressive approach allows to include not only usual statistical data such as mean and standard deviation of the wind speed, but the measured wind speed time series itself, in the simulation. Because the simulation uses the spatial relationships provided by the spectral turbulence models, the phase characteristics of the measured data can influence neighbouring points in space, resulting in an intuitively better simulation of the actual wind field. Iwatani's original study only simulates the longitudinal component of wind speed and only considers vertically-spaced points, but the method was extended to three components and three dimensions by Phuc

[18] (2005). This latter method has been chosen for wind generation in the PCM method, and included in the WND3D software dedicated to turbulent wind flow generation.

Since any of these wind field simulation methods have to be parametrized using turbulence models, which describe the spatial relationships behind the variations of turbulence, the next section will discuss the availability of turbulence models and the requirements of international and Japanese standards.

### 1.2.3 Turbulence models in design guidelines and standards

A basic step of understanding the dynamic response of a structure is to study the frequency distribution of the external force. For such a purpose, a natural approach is to use a frequency-domain description: therefore, in wind engineering, we mostly use power spectral density models, as well as coherence or co-spectrum models (section 2.1.2 and appendix B defines the particular terms used for turbulence description). The frequency-domain approach is adopted by most standards and guidelines today.

Also, as for most aspects of civil engineering, design wind loads are described in international and local design codes. In Japan, the wind engineering reference currently in use is the Recommendations for Loads on Buildings from the AIJ [1]. The AIJ recommendations give general advice on modelling wind loads for structural design. With a more specific approach, the IEC "prepares and publishes standards for all electrical, electronic and related technologies"[1], including wind turbines. The IEC standards offer guidelines [9] for designing onshore and offshore wind turbines, considering basic structural needs and environmental loads, such as the wind, of course, but also wave and earthquake loads when applicable.

The work of these two institutions will be used in this study. However one can notice that although the IEC standards should be applied for wind turbines, it often lacks generality. In particular, the wind speed and turbulence models are proposed for the wind around the hub height, and the standards only suggest a couple of turbulence models in its annex, with very little detail about the lateral and vertical components of the wind as opposed to the longitudinal (and main) component. On the other hand, the AIJ recommendations are not specific to wind turbines nor international in nature and shall be regarded as indicative

[1] Quoted from `http://www.iec.ch/about/`, last visited: August 3, 2012

when opposed to the IEC requirements.

Moreover, the wind simulation method adopted in PCM is strongly based on a time-domain approach. However, in IEC, the two suggested models are only available in the frequency domain. On the one hand, Kaimal's model is purely empirical and lacks a theoretical background; it also lacks descriptions for the lateral and vertical components' coherence relationships. On the other hand, Mann's model is derived from von Karman's theoretical work and provides a complex yet exhaustive three-dimensional spectral description; but this complexity means that it is currently not possible to use it with a link to measurement data, like we do in PCM. A time-domain description of the turbulence would allow a faster and more accurate method by getting rid of the Fourier transform necessity, and would also facilitate the link with measured time series of wind speed.

A time-domain description has however been introduced by von Karman in the course of the development of his turbulence model [26]. Although wind engineering guidelines often use his spectral model [25], his work is based on an understanding of correlations, which are the time-domain equivalent of spectral densities. Hinze [8] proposes a thorough review of this theory, with a clear analytical equivalence between the correlation and the spectral form of von Karman's turbulence models. Von Karman's model is currently the best foundation for a complete time-domain description of turbulence, but it is derived from the theory of isotropic turbulence, which is an ideal state assumption. Thus, compliance with IEC requirements, which are mainly empirical, is not guaranteed.

## 1.3 Objectives

Shortcomings in the description of turbulence by the models proposed in IEC prompts us to review the available models, theoretical and empirical, and to propose a more exhaustively defined model which satisfies general consensus on the boundary layer turbulence while complying with IEC requirements. For PCM applications, a correlation-based description is desirable; although von Karman's model is not empirically validated, it will serve as a strong foundation for the development of a time and frequency domain turbulence model.

The purpose of this research is therefore to propose a modified version of von Karman's model that would describe turbulence in both frequency and time domain, with an analytical relationship between these two approaches. This

model should also:

- ⋆ comply with the IEC requirements and correct some inconsistencies related to the difference between the ideal isotropic turbulence and the actual turbulence structure;
- ⋆ propose a description of Reynolds stress, which is unavailable or incomplete in the commonly used models;
- ⋆ and finally, this proposed model should be validated by actual wind speed measurements.

Chapter 2 starts with a review of turbulence modelling and useful statistical descriptors. With a focus on the IEC requirements and empirical observations, the empirical Kaimal model and the theoretical von Karman model are studied and a new turbulence model is proposed and validated with measurements.

Chapter 3 details the autoregressive model used for turbulent wind generation. The stochastic nature of the wind is introduced and mathematical assumptions are described. Iwatani's improved method is explained and a discussion about the generality and limits of the autoregressive model is sketched out.

In Chapter 4, the applicability of the wind generation method and the choice of a turbulence model are investigated though evaluation of the improvements in response estimation. We will study the impact of generated wind linked to one component of measured wind speed on the wind turbine response estimation, as opposed to the response estimated using a wind field generated without any link. Then, the impact of linking with more than one component of measured wind speed will be compared to the result of linking with just one component.

Finally, Chapter 5 gives the conclusions of this study.

Appendices give an insight in future applications for which additional study is required, and provide a review of the mathematical concepts used in this thesis, in particular in relation with spectral analysis.

# Chapter 2

# Wind turbulence

Wind turbulence refers to the fluctuations of the wind speed on a small time scale, typically 10 minutes. While the wind speed has seasonal and diurnal variations on larger time scales, turbulence represents the deviations from the 10-min mean wind speed. Therefore, turbulent fluctuations have a zero-mean over a 10-min average. Turbulence is generated from friction and thermal effects. In this chapter, we would like to define all the parameters needed for generating a turbulent wind field using the WND3D software. WND3D was first developed by Phuc [18] based on Iwatani's idea [11][12]. The algorithm itself is described in Chapter 3.

Several textbooks propose a thorough review of the physical background [14][23] and statistical descriptors [2]. These will be summarized in Section 2.1 and 2.2. To describe the frequency distribution of the fluctuations, spectral turbulence models are commonly used and the IEC international standards give requirements in the frequency domain. We review these requirements as well as existing turbulence models in Section 2.3. A new turbulence model, based on von Karman's theoretical model and available in both time and frequency domain, is introduced in Section 2.4. Finally, in Section 2.5, the proposed turbulence model is validated using sonic anemometer measurements.

## 2.1 Description of turbulence

The behaviour of the atmospheric flow is complex and nonlinear. The dynamics of the atmosphere are usually described using equations of motion based on the principles of conservation of mass, momentum, etc. For wind energy applica-

tions, the relevant part of the atmosphere to consider is the planetary boundary layer, made of the first one to five kilometers above the ground.

Th following paragraphs will quickly explain the origins of turbulence from the Navier-Stokes equation, and introduce the descriptions of turbulence in the time and frequency domain, which will be used in the rest of this thesis.

### 2.1.1 Physics of the atmospheric boundary layer

#### 2.1.1.1 Navier-Stokes equation

In the atmosphere, a fluid element is exposed to external and internal forces: on the one hand, the pressure gradient force, the Coriolis force and the gravity; on the other hand, internal forces such as molecular friction. From the conservation of momentum, we can equate the rate of change of momentum with the total forces exerted on the fluid particle, leading to the Navier-Stokes equation, written in vector form in (2.1).

$$\rho\left(\partial_t \overrightarrow{u} + (\overrightarrow{u}\cdot\nabla)\overrightarrow{u}\right) = -\nabla p + 2\rho(\overrightarrow{u}\times\overrightarrow{\Omega}) + \eta\nabla^2\overrightarrow{u} - f_g, \tag{2.1}$$

where the unknown variables are $\overrightarrow{u} = (u_1, u_2, u_3)$, the three-dimensional velocity vector, and $p$, the atmospheric pressure. $\partial_t$ indicates the partial derivative with regards to time, $\overrightarrow{\Omega}$ is the rotational speed of the earth, $\rho$ is the air density, $\eta$ is the dynamic viscosity.

One might notice that there are four unknowns (three for the velocity plus one for the pressure), but only three equations in (2.1). An additional equation is the continuity equation, derived from the conservation of mass and the assumption that the air density is constant:

$$\nabla\cdot\overrightarrow{u} = 0. \tag{2.2}$$

#### 2.1.1.2 Reynolds averaging

However, the strong nonlinearity of the Navier-Stokes equation does not allow for general analytic solutions to be found. Moreover, real flows are mostly turbulent which means that the variables must take into account a fluctuating part. Each variable is thus decomposed in a mean component and a fluctuating component, such as

$$u_i(t) = U_i + u_i'(t), \tag{2.3}$$

and similarly for the pressure. This procedure adds even more unknowns to the initial problem. One technique to simplify this system is to consider only the mean flow, by using Reynolds averaging.

The averaging process is, theoretically, an ensemble averaging, because the variables that we work with are random variables: we must therefore average on all the realisations of the variable. However, most of the time we can only take the time or space average, as an approximation to the ensemble average. That is,

$$U_i = \overline{u_i(t)} \approx \frac{1}{T}\int_t^{t+T} u_i(t')\mathrm{d}t'. \tag{2.4}$$

Substituting the decomposed variables into (2.1), and applying ensemble averaging over the equation, we obtain the Reynolds-averaged Navier-Stokes equation (2.5), in which a new term appears. This new term describes an additional force applied to the flow, due to turbulence only; it is usually referred to as the Reynolds stress.

$$\rho\left(\partial_t \overrightarrow{U} + (\overrightarrow{U}\cdot\nabla)\overrightarrow{U}\right) = -\nabla p + 2\rho(\overrightarrow{U}\times\overrightarrow{\Omega}) + \eta\nabla^2\overrightarrow{U} - f_g - \underbrace{\nabla\tau_t}_{\text{turbulent momentum flux}} \tag{2.5}$$

The terms in the Reynolds stress tensor, $\tau_t$, are defined as

$$\tau_{t,ij} = \rho\overline{u_i' u_j'}, \tag{2.6}$$

which are the correlations between the fluctuating wind components.

Therefore, the Reynolds stress represents the influence of the fluctuations on the mean flow. The correlations are a time-domain description of the driving relationships of turbulence. Another description can be defined in the frequency domain.

### 2.1.2 Time and frequency domain description of turbulence

As implied by the Navier-Stokes equation, the relationships between turbulence components can be described using the correlations between them. Correlations are a time-domain description; however, in wind engineering, we most commonly encounter frequency-domain descriptions using power spectral densities or cross-spectral densities. The following paragraphs aim at clarifying the basic time-and-frequency-domain vocabulary that will be used in this thesis.

#### 2.1.2.1 What is the power spectral density?

In equation (2.6), the fluctuating components of the wind are described using correlations. In statistical terms, the correlation series between two random processes $x(t)$ and $y(t)$ (see definition of a random process in section 3.1.1) is given by

$$\mathrm{Corr}(x,y)(\tau) = \mathbb{E}[(x(t)-\mu_x)(y^*(t-\tau)-\mu_y)], \tag{2.7}$$

where $\mathbb{E}$ denotes the expectation, similar to Reynolds' ensemble averaging described in the previous subsection, and the star denotes complex transposition (or complex conjugation in the case of a scalar variable); $\mu_x$ and $\mu_y$ are the respective means of $x(t)$ and $y(t)$. For simplicity we will always assume that the random processes have a zero mean.

In spectral analysis, the correlation theorem is derived from the convolution theorem (see appendix A, equation (A.9) and (A.11)), thus we have the following Fourier transform pair:

$$\mathrm{Corr}(x,y)(\tau) \Longleftrightarrow X(f)Y^*(f) \tag{2.8}$$

where $X(f)$ and $Y(f)$ are the Fourier transforms of $x$ and $y$, $f$ being the frequency. The correlation theorem becomes the Wiener-Khinchin theorem when $x = y$ i.e.

$$\mathrm{Corr}(x,x)(\tau) \Longleftrightarrow |X(f)|^2 \tag{2.9}$$

In this case, we also say that the correlation is an *autocorrelation* sequence.

In wind engineering, turbulence is most often described using the power spectral density. For a deterministic signal, we can define an energy spectral density as the squared magnitude of the Fourier transform (see Appendix A). We can see in equation (2.9) that in this sense, the energy spectral density is the Fourier transform of the autocorrelation sequence.

However, for random signals, one realization does not have finite energy and thus we cannot use the energy spectral density directly. A random signal will have a finite average power, which is called the power spectral density (PSD). The PSD can be estimated using the periodogram method, which basically is a discrete form of the correlation theorem, defined as

$$\mathrm{Periodogram}(x,f) = \frac{1}{N}\left|X_n(f)\right|^2, \tag{2.10}$$

Table 2.1: Equivalence between correlation and spectral form.

| Correlation form | Spectral form |
|---|---|
| Autocorrelation $\mathrm{Corr}(x,x)(t)$ | PSD or Autospectrum $S(f)$ |
| Cross-correlation $\mathrm{Corr}(x,y)(t)$ | Cross-spectrum $S_{xy}(f)$ |

where $X_n(f)$ is the discrete Fourier transform of $\{x(t), t = 1 \dots n\}$.

More details are given in Appendix A, in particular for relationships between cross-correlation and cross-spectrum, and estimation methods. What is important to remember here is that the correlation and the spectral density are closely linked, as they contain the same information, and thus they can be used in an equivalent way.

#### 2.1.2.2 Definitions of correlations and the corresponding spectral form

Table 2.1 presents the equivalence between the correlations and the corresponding spectral form used to describe turbulence. The expressions "spectrum" and "spectral density" will be used indifferently.

For turbulent wind fields, we are typically interested in the fluctuations in the three directions and at several points separated in space. In this case, we denote $(u, v, w)$ the longitudinal, lateral and vertical fluctuating components; we will use an index to denote the point, e.g. $u_1$ will denote the longitudinal fluctuation for point 1, which Cartesian coordinates would be $(x_1, y_1, z_1)$. We can then introduce the specific terms and notations that will be used in the other parts of the thesis:

1. Same point, same component:
   - ⋆ "Autocorrelation for $u$ component at point $i$": $\mathrm{Corr}(u_i, u_i)(t)$ or $\tilde{R}_u(t)$
   - ⋆ "Autospectrum for $u$ component at point $i$": $S_{u_i}(f)$
2. Two points, same component:
   - ⋆ "Cross-correlation, $u$ component, between $i$ and $j$": $\mathrm{Corr}(u_i, u_j)(t)$ or $\tilde{R}_u(r, t)$
   - ⋆ "Cross-spectrum, $u$ component, between $i$ and $j$": $S_{u_i u_j}(f)$

- ⋆ "Coherence, $u$ component, between $i$ and $j$": $\mathrm{Coh}_u(r,f)$, where

$$r = \sqrt{(x_i - x_j)^2 + (y_i - y_j)^2 + (z_i - z_j)^2}$$
$$\mathrm{Coh}_u(r,f) = \left| \frac{S_{u_i u_j}(f)}{\sqrt{S_{u_i} S_{u_j}}} \right|^2$$

3. Same point, two components ("Reynolds stress")
   - ⋆ "$u\,v$ cross-correlation at point $i$": $\mathrm{Corr}(u_i, v_i)(t)$
   - ⋆ "$u\,v$ cross-spectrum at point $i$": $S_{u_i v_i}(f)$
   - ⋆ "$u\,v$ co-spectrum at point $i$": $\mathrm{Co}_{u_i v_i}(f)$, where

$$\mathrm{Co}_{u_i v_i}(f) = Re(S_{u_i v_i}(f))$$

4. Two points, two components ("two-point Reynolds stress")
   - ⋆ "$u\,v$ cross-correlation between $i$ and $j$": $\mathrm{Corr}(u_i, v_i)(t)$
   - ⋆ "$u\,v$ cross-spectrum between $i$ and $j$": $S_{u_i v_j}(f)$
   - ⋆ "Two-point $u\,v$ co-spectrum between $i$ and $j$": $\mathrm{Co}_{u_i v_j}(r,f)$, where

$$r = \sqrt{(x_i - x_j)^2 + (y_i - y_j)^2 + (z_i - z_j)^2}$$
$$\mathrm{Co}_{u_i v_j}(r,f) = Re\left(S_{u_i v_j}(f)\right)$$

In general, for frequency-domain description of turbulence, the coherence and co-spectrum are used rather than the cross-spectrum. This is another reason why a new turbulence model is desired: using coherence and co-spectrum rather than the cross-spectrum means that the imaginary part, i.e. the phase, is disregarded.

## 2.2 Statistical properties of turbulent wind

Turbulent fluctuations of the wind can be considered as random processes. As a first approximation, the turbulence is supposed to be Gaussian, i.e. the fluctuations are normally distributed with mean $U$ and standard deviation to that mean value, $\sigma$. This approximation is not applicable if one wants to study the extreme cases, but it is roughly acceptable for most usual cases.

This section will define the basic statistical descriptors of the turbulent wind, namely the mean wind speed and the turbulence intensity or the standard devi-

ation, and review the various theoretical and empirical formulas used to model them.

### 2.2.1 Mean wind speed

In the study of wind turbulence, the typical time scale is 10 minutes, and therefore the mean wind speed commonly refers to the 10-min average wind speed. We would like to define the mean wind speed profile, i.e. the variation of the mean wind speed as a function of the height.

#### 2.2.1.1 Theoretical logarithmic profile

In the surface boundary layer, the wind speed profile can be derived from equation (2.5) [14], which, in neutral or near-neutral atmospheric conditions, leads to the logarithmic profile equation:

$$U(z) = \frac{u_*}{\kappa} \ln\left(\frac{z}{z_0}\right), \tag{2.11}$$

where $u_*$ is the friction velocity, which is constant with height; and $\kappa$ is the von Karman constant, which is approximately 0.4 [2]. The roughness length, $z_0$, is related to the surface roughness and varies according to the type of terrain (typical values: $10^{-4}$ m for the open sea, up to the order of 1 m in cities).

For non-neutral conditions, a corrective term must be added to equation (2.11), but for our purposes, this correction will not be considered.

#### 2.2.1.2 Power law approximation

A power law approximation is adopted in the AIJ and IEC standards, with slight variations between the two definitions. Both standards are described in the following paragraphs.

**AIJ profile** The AIJ standards define a wind profile:

$$U(z) = \begin{cases} 1.7U_{100}\left(\dfrac{z}{z_G}\right)^{\alpha} & \text{for } z \geq z_b \\ 1.7U_{100}\left(\dfrac{z_b}{z_G}\right)^{\alpha} & \text{for } z \leq z_b \end{cases} \tag{2.12}$$

Table 2.2: Description of terrain category in AIJ standards.

| | Category | Condition at construction site and upwind region |
|---|---|---|
| Smooth | I | Open, no significant obstruction, sea, lake |
| ↑ | II | Open, few obstructions, grassland, agricultural field |
| | III | Suburban, wooded terrain, few tall buildings (4 to 9-story) |
| ↓ | IV | City, tall buildings (4 to 9-story) |
| Rough | V | City, heavy concentration of tall buildings (> 10-story) |

Table 2.3: Parameters for each terrain category in AIJ standards.

| Category | I | II | III | IV | V |
|---|---|---|---|---|---|
| $z_b$ (m) | 5 | 5 | 10 | 20 | 30 |
| $z_G$ (m) | 250 | 350 | 450 | 550 | 650 |
| $\alpha$ | 0.1 | 0.15 | 0.2 | 0.27 | 0.35 |

The parameters $\alpha$, $z_b$ and $z_G$ are determined by the terrain category, as detailed in Tables 2.2 and 2.3. $U_{100}$ "corresponds to the 100-year-recurrence 10-minute mean wind speed over a flat, open terrain at an elevation of 10m."

However, the AIJ suggests, in the comments, that when the boundary layer is fully developed, i.e. when the surface roughness is uniform in the area, a simpler form, shown in equation (2.13)

$$U(z) = \begin{cases} U_0 \left(\dfrac{z}{z_0}\right)^{\alpha} & \text{when } z \geq z_b \\ U_0 \left(\dfrac{z_b}{z_0}\right)^{\alpha} & \text{when } z \leq z_b \end{cases} \tag{2.13}$$

In that case, $U_0$ is the mean wind speed at reference height $z_0$.

**IEC power law** The IEC standard also uses a power law profile, using the hub height wind speed as a reference and fixing the exponent at 0.2.

$$U(z) = U_{\text{hub}} \left(\frac{z}{z_{\text{hub}}}\right)^{0.2} \tag{2.14}$$

The third edition ([9], 2003) does not give any explicit lower or upper limit to this wind profile. This is because the IEC standard only discusses the rotor swept area. The exponent used in IEC corresponds to terrain category III in AIJ; as such, it is an average value and, compared to the AIJ, underestimates the value of the mean wind speed in areas with a low roughness. Fig. 2.1 shows the power

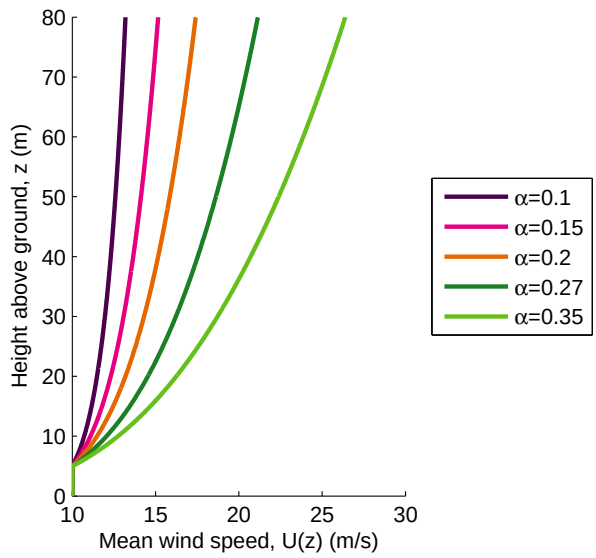


Figure 2.1: Power law profile for the mean wind speed.

law profiles for all exponents in Table 2.3, with a reference wind speed of 10 m/s at a reference height of 5 m above ground.

### 2.2.2 Turbulence intensity

Turbulence intensity is a way to describe the level of turbulence; it is defined as the standard deviation of the fluctuation, $\sigma$, divided by the mean wind speed $U$ (usually this is the 10-min mean wind speed).

$$I = \frac{\sigma}{U} \tag{2.15}$$

The following paragraphs will discuss the various models adopted in the AIJ and IEC standards, with some mention of other guidelines such as the Danish DNV/Risø [5].

#### 2.2.2.1 Standard deviation

The standard deviation, $\sigma$, exhibits some variability between different 10-min periods: it is, in itself, a random variable. The DNV/Risø guidelines indicate that the distribution of $\sigma$ conditioned on $U$ can be modelled by a lognormal law. However, in this study, we will consider the average value, i.e. the expectation, of $\sigma$ conditioned on $U$.

**DNV/Risø guidelines** The guidelines indicate the mean value of $\sigma$ derived from the boundary layer theory:

$$\mathbb{E}[\sigma] = UA_z\kappa\frac{1}{\ln(z/z_0)}, \tag{2.16}$$

with $A_z$ a constant, dependent on the roughness length, $\kappa \approx 0.4$ being von Karman's constant.

For simplicity, in the following parts, we will assume $\sigma = \mathbb{E}[\sigma]$. It will therefore be considered constant for a given mean wind speed on a 10-minute period.

**IEC requirement for the standard deviation** In the second edition of the IEC 61400-1 standard, the characteristic standard deviation is defined as the mean value of $\sigma$ plus its standard deviation.

$$\sigma_c = \mathbb{E}[\sigma] + \mathrm{Var}(\sigma) = I_{15}\frac{U_{15} + aU}{a+1}, \tag{2.17}$$

where $U_{15} = 15$m/s is a reference wind speed, $I_{15}$ is the characteristic value of the turbulence intensity at 15m/s and $a$ is a slope parameter. Suggested parameters for higher turbulence characteristics are $I_{15} = 0.18$ and $a = 2$; for lower turbulence, $I_{15} = 0.16$ and $a = 3$.

The third edition of the IEC61400-1 simplifies this expression and defines the "representative value" of the turbulence standard deviation for the longitudinal component, $\sigma_u$, by the 90% quantile for a given hub wind speed.

$$\sigma_u = I_{\mathrm{ref}}(0.75U_{\mathrm{ref}} + 5.6), \tag{2.18}$$

where $I_{\mathrm{ref}}$ and $U_{\mathrm{ref}}$ are chosen according to the wind turbine class, as defined in Table 2.4.

Table 2.4: Basic parameters for wind turbine classes in IEC 61400-1.

| Wind turbine class | I | II | III | S |
|---|---|---|---|---|
| $U_{\mathrm{ref}}$ (m/s) | 50 | 42.5 | 37.5 | Specified by the designer |
| Higher turbulence $I_{\mathrm{ref}}$ | 0.16 | 0.16 | 0.16 | |
| Medium turbulence $I_{\mathrm{ref}}$ | 0.14 | 0.14 | 0.14 | |
| Lower turbulence $I_{\mathrm{ref}}$ | 0.12 | 0.12 | 0.12 | |

#### 2.2.2.2 Turbulence intensity profile

In the AIJ standards, instead of defining the standard deviation of turbulence, a turbulence intensity profile is given for the longitudinal component $u$.

$$I_u(z) = \begin{cases} 0.1\left(\dfrac{z}{z_G}\right)^{-\alpha-0.05} & \text{for } z \geq z_b \\ 0.1\left(\dfrac{z_b}{z_G}\right)^{-\alpha-0.05} & \text{for } z \leq z_b \end{cases} \tag{2.19}$$

In equation (2.19), $z_G$, $z_b$ and $\alpha$ are given by Table 2.3.

One might notice that, as opposed to the DNV or IEC recommendations, the AIJ suggests that the standard deviation of turbulence is not constant over the height of the structure, since from the AIJ profiles in equations (2.12) and (2.19) and the definition of turbulence intensity (2.15), one obtains

$$\sigma(z) = 0.17U_{100}\left(\frac{z}{z_G}\right)^{-0.05} \quad \text{for } z \geq z_b. \tag{2.20}$$

## 2.3 Stochastic turbulence models

Spectral turbulence models describe the frequency distribution of the turbulence. They are commonly used in wind engineering, since they are convenient to understand the static response to wind excitation. From the numerous existing turbulence models, we will focus on two: first, the Kaimal model, which is empirical and suggested by the IEC 61400-1 in its Annex B; and second, the von Karman model, which theoretical foundations and analytical time and frequency domain descriptions are of greatest interest for our study.

### 2.3.1 IEC requirements

In its third edition, the IEC [9] gives three requirements.

1. The standard deviation of the turbulence is assumed to be invariant with height. Additionally, minimum values for the standard deviation of the lateral and vertical components of turbulence are given by

$$\begin{cases} \sigma_v \geq 0.7\sigma_u \\ \sigma_w \geq 0.5\sigma_u \end{cases} \tag{2.21}$$

2. A longitudinal turbulence scale parameter is defined at hub height as

$$\Lambda_1 = \mathrm{Min}(42, 0.7 z_{\mathrm{hub}}), \tag{2.22}$$

and the power spectral densities of the three components must "asymptotically approach the following forms as the frequency in the inertial subrange increases"

$$S_u(f) = 0.05\sigma_u^2 \left(\frac{\Lambda_1}{U_{\mathrm{hub}}}\right)^{-2/3} f^{-5/3} \tag{2.23}$$

$$S_v(f) = S_w(f) = \frac{4}{3} S_u(f) \tag{2.24}$$

3. A "recognized model for the coherence shall be used".

One can notice that the first, and in particular the third, requirements leave some flexibility over the choice of the parameters or the models. Moreover, the IEC only deals with the turbulence at hub height, while we would like to use the requirements for the turbulence over the entire turbine. We will therefore consider slightly modified versions of these requirements, rewriting the length scale parameter of equation (2.22) as

$$\Lambda_1 = \mathrm{Min}(42, 0.7z), \tag{2.25}$$

with $z$ any given height, and the high-frequency forms of the power spectral densities of the third requirement will be used for all heights as well, by replacing $U_{\mathrm{hub}}$ by $U(z)$.

### 2.3.2 Kaimal model

In Annex B of the IEC 61400-1 standard [9], some turbulence models are proposed with the corresponding choice of standard deviations and coherence model. In the following section, the Kaimal model will be discussed, with the choices proposed by the IEC Annex B but also with extended choices that are necessary to complete the model.

#### 2.3.2.1 Kaimal autospectrum and model parameters

Kaimal proposed a model based on experimental results. The original model, originally described by Kaimal ([13], 1972), is defined as

$$\frac{fS_u(f)}{u_*^2} = \frac{105\frac{f\tilde{z}}{U}}{(1+33\frac{f\tilde{z}}{U})^{5/3}}, \tag{2.26}$$

where $f$ is the frequency, $S_u(f)$ is the power spectral density, also called power spectrum or autospectrum, for the longitudinal component $u$, $U$ is the mean wind speed and $\tilde{z}$ is a normalized height.

The IEC defines, in its Annex B, another form of the Kaimal spectrum:

$$\frac{fS_i(f)}{\sigma_i^2} = \frac{4\frac{fL_i}{U}}{(1+6\frac{fL_i}{U})^{5/3}}, \tag{2.27}$$

where $L_i$ is the turbulence length scale for the $i$-th component ($i = u, v, w$). Annex B also gives the standard deviation for each component as

$$\begin{cases} \sigma_v = 0.8\sigma_u \\ \sigma_w = 0.5\sigma_u, \end{cases} \tag{2.28}$$

which satisfies the first requirement in equation (2.21).

When equating the IEC form (2.26) with the original form (2.26), we obtain

$$\frac{\sigma}{u_*} = 2.185 \tag{2.29}$$

$$\frac{L_u}{\tilde{z}} = 5.5 \tag{2.30}$$

Following the second requirement of the IEC, by writing the high-frequency form of the spectrum and applying the conditions (2.23) and (2.24), one obtains

$$\frac{4\frac{fL_i}{U}}{(1+6\frac{fL_i}{U})^{5/3}} \equiv \frac{4\frac{fL_i}{U}}{(6\frac{fL_i}{U})^{5/3}} = 0.2019\left(\frac{fL_i}{U}\right)^{-2/3}, \tag{2.31}$$

where $i = u, v, w$ indicates the component. Thus, we can obtain the ratio between the longitudinal component and the two other components, leading to

the ratio between the length scales (2.32).

$$\begin{aligned}\frac{S_v}{S_u} &= \left(\frac{\sigma_v}{\sigma_u}\right)^2 \left(\frac{L_v}{L_u}\right)^{-2/3} \\ \frac{L_v}{L_u} &= \left(\frac{\sigma_v}{\sigma_u}\right)^3 \left(\frac{S_v}{S_u}\right)^{-3/2}\end{aligned} \tag{2.32}$$

We have a similar relation for $L_w/L_u$. Finally, from (2.24),

$$\begin{cases} L_u = 8.1\Lambda_1 \\ L_v = 0.33 L_u \\ L_w = 0.08 L_u, \end{cases} \tag{2.33}$$

which are the indicated length scales in IEC Annex B.

#### 2.3.2.2 Coherence and Reynolds stress

IEC requirement number three calls for a "recognized turbulence model", and Annex B suggests a model for longitudinal coherence, seemingly empirical, to use with the Kaimal model, as follows.

$$\mathrm{Coh}(r,f) = \exp\left(-12\sqrt{\left(\frac{fr}{U}\right)^2 + \left(\frac{0.12r}{L_u}\right)^2}\right) \tag{2.34}$$

However, the IEC does not provide any detail about coherence for the two other components. One option is to use the Davenport coherence model, given in equation (2.35); this choice was made for the GH Bladed software [7] as well as Iwatani's wind generation method [11].

$$\sqrt{\mathrm{Coh}(r,f)} = \exp\left(-12\frac{fr}{U}\right) \tag{2.35}$$

Davenport's model has been developed out of an empirical study of horizontal winds [3], and thus might be unsuitable for vertical winds.

It has to be noted that no clear model is given for the Reynolds stress in the IEC. Kaimal, in his original publication [13], has introduced an empirical co-spectrum model to describe the relationship between the longitudinal compo-

nent $u$ and the vertical component $w$ at a given point:

$$-\frac{f\mathrm{Co}_{uw}(f)}{u_*^2} = \frac{14\frac{fz}{U}}{\left(1+9.6\frac{fz}{U}\right)^{7/3}}, \tag{2.36}$$

which can be rewritten using the relationships we derived previously in (2.29) and (2.30) as

$$-\frac{f\mathrm{Co}_{uw}(f)}{\sigma_u\sigma_w} = \frac{1.066\frac{fL_u}{U}}{\left(1+1.745\frac{fL_u}{U}\right)^{7/3}}. \tag{2.37}$$

In any case, this does not give any information about the two-point Reynolds stress. The Kaimal model, in its current IEC form, is therefore incomplete. Although the empirical aspect guarantees good agreement with measured turbulence properties, many cross-spectral terms are undefined and most importantly for our study, there is no easy way to define a time domain model that would be analytically equivalent to the frequency domain description.

### 2.3.3 Original von Karman model

Von Karman proposed a theoretical model defined both in the frequency and the time domain. As explained in section 2.1.2, the correlation can be linked to the spectrum through a Fourier transform; this relation has been studied analytically by von Karman [25] and detailed in Hinze's book [8].

#### 2.3.3.1 Autocorrelation and autospectrum model

Von Karman's working hypothesis is isotropic turbulence, i.e.

$$\sigma_u = \sigma_v = \sigma_w \tag{2.38}$$

and, as a consequence [8], defines the turbulence length scale ratios:

$$L_v^x = L_w^x = 0.5L_u^x \tag{2.39}$$

where $L_u^x$ can be defined using the AIJ formula [1]

$$L_u^x(z) = \mathrm{Max}\left(100\text{ m}, 100\sqrt{\frac{z}{30}}\right). \tag{2.40}$$

The original von Karman longitudinal spectrum is described in equation

(2.41), where the parameters are the standard deviation $\sigma_u$ and the length scale $L_u^x$.

$$\frac{fS_u(f)}{\sigma_u^2} = \frac{4\frac{fL_u^x}{U}}{\left(1+70.8\left(\frac{fL_u^x}{U}\right)^2\right)^{5/6}} \tag{2.41}$$

This spectrum has, according to Hinze [8] and Takeuchi and Maeda [22], the analytical equivalent in the time domain given by the autocorrelation function:

$$\tilde{R}_u(\tau) = \mathsf{f}(U\tau). \tag{2.42}$$

$\mathsf{f}$ is the longitudinal separation function; it describes the correlation between the turbulent component time series at two points separated in the same direction as the component, as explained on Fig. 2.2. Using Taylor's frozen turbulence hypothesis, illustrated in Fig. 2.3, we have the space-time equivalence $\Delta x = U\tau$. The autocorrelation takes advantage of that assumption, by considering

$$u(t-\tau, x, y, z) = u(t, x+U\tau, y, z),$$

hence equation (2.42). $\mathsf{f}$ is described in equation (2.43), with $L = L_u$:

$$\mathsf{f}(r) = \alpha_1 |a_1 r|^{1/3} K_{1/3}(|a_1 r|), \tag{2.43}$$

where:

$$\alpha_1 = \frac{2^{2/3}}{\Gamma(1/3)} \approx 0.5926 \tag{2.44}$$

$$a_1 = \frac{\pi^{1/2}\Gamma(5/6)}{L\Gamma(1/3)} \approx \frac{0.7468}{L}. \tag{2.45}$$

$K_q$ is the $q$-th order modified Bessel function of the second kind, and $\Gamma$ is the Euler gamma function.

For the lateral and vertical components, $v$ and $w$, von Karman's spectrum is given by

$$\frac{fS_i(f)}{\sigma_i^2} = \frac{2\left(\frac{fL_u^x}{U}\right)\left(1+188.8\left(\frac{fL_u^x}{U}\right)^2\right)}{\left(1+70.8\left(\frac{fL_u^x}{U}\right)^2\right)^{11/6}} \tag{2.46}$$

where the reader's attention is called to the use of $L_u^x$, the longitudinal length scale. The corresponding correlation function is given by the lateral separation

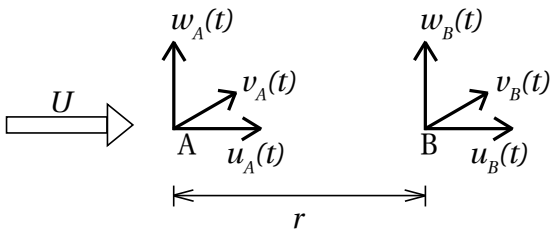


Figure 2.2: Von Karman's separation functions depends on the components. For the longitudinal component $u$, the spatial separation $r$ is in the same direction as the turbulent component considered, thus the longitudinal separation function applies. For $v$ and $w$, the separation is orthogonal to the turbulence direction, therefore the lateral separation function must be used.

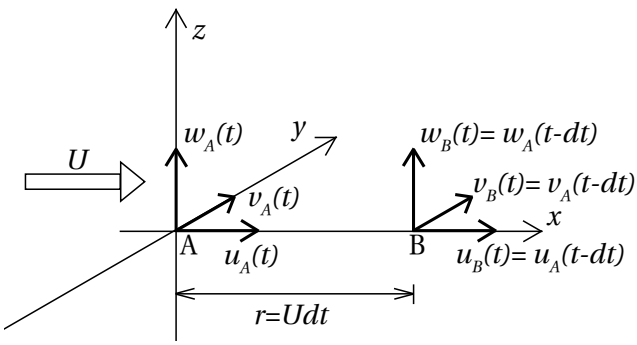


Figure 2.3: Taylor's hypothesis of frozen turbulence. It assumes that turbulence moves with the mean flow speed $U$, unchanged. Therefore the turbulence at point B is the same as the one at point A some time before.

function g:

$$\tilde{R}_i(\tau) = \mathrm{g}(U\tau), \quad i = v, w \tag{2.47}$$

$$g(r) = \alpha_1 |a_1 r|^{1/3} \left( K_{1/3}(|a_1 r|) - \frac{|a_1 r|}{2} K_{2/3}(|a_1 r|) \right), \tag{2.48}$$

with $L = L_v$ or $L_w$ respectively (in $a_1$). g is supposed to describe the correlation between components at spatially separated points when the separation is orthogonal to the direction of the considered component.

#### 2.3.3.2 Cross-correlation and coherence model

Like autocorrelation and autospectrum, there is a cross-correlation and coherence function for the $u$ component on the one hand, and the $v$ and $w$ compo-

nents on the other hand. For the longitudinal component, the cross-correlation at two points separated by a distance $r$ is given by

$$\tilde{R}_u(r,\tau) = \big(\mathrm{f}(r_1) - \mathrm{g}(r_1)\big)\,\frac{(U\tau)^2}{r_1^2} + \mathrm{g}(r_1), \tag{2.49}$$

where $r_1 = \sqrt{(U\tau)^2 + r^2}$. The corresponding cross-spectrum is described in equation (2.50) for two points, indexed by 1 and 2.

$$\begin{aligned}\tilde{S}_u(r,f) &= \frac{S_u(r,f)}{\sqrt{S_{u_1}(f)S_{u_2}(f)}} \\ &= \frac{2}{\Gamma(5/6)}\left(\left(\frac{\theta}{2}\right)^{5/6} K_{5/6}(\theta) - \left(\frac{\theta}{2}\right)^{11/6} K_{1/6}(\theta)\right),\end{aligned} \tag{2.50}$$

where

$$\theta = \sqrt{(a_1 r)^2 + \left(\frac{2\pi f r}{U}\right)^2}. \tag{2.51}$$

For the other components, the cross-correlation has a slightly different form (2.52).

$$\tilde{R}_i(r,\tau) = \big(\mathrm{f}(r_1) - \mathrm{g}(r_1)\big)\,\frac{\Delta x_i^2}{r_1^2} + \mathrm{g}(r_1) \quad i = v, w, \tag{2.52}$$

where $\Delta x_v = \Delta y$ and $\Delta x_w = \Delta z$, for notation convenience. The cross-spectrum has the same form as (2.50) but $\theta$ in (2.51) must be modified to

$$\theta = \sqrt{(a_1 \Delta x_i)^2 + \left(\frac{2\pi f \Delta x_i}{U}\right)^2}, \quad i = v, w. \tag{2.53}$$

In all of the above equations, the appropriate length scale must be used for $a_1$.

**Remark:** The cross-spectrum has only real values, which means that the phase of the spectrum is supposed to be zero.

Hinze [8] has given a general cross-correlation expression, supposedly valid for different components of turbulence, but Fujimura (Takeuchi) and Maeda [6][22] have shown that this expression only gives very small values and are negligible compared to the actual measured Reynolds stress correlation values.

Finally, we can see that von Karman's model provides a good starting point for developing a time and frequency-domain description of turbulence, thanks to the analytical relationships between the spectral and correlation forms of the model. However, it has two clear shortcomings:

- ⋆ The starting assumption of isotropic turbulence is an ideal situation and thus, not verified in observed data; Maeda has shown discrepancies in an empirical study [15].
- ⋆ The model has generally not been adapted to IEC requirements.

Neither Kaimal nor Von Karman's models satisfy all of the desired features completely. This leaves space for improvement; from this review of both models, we will propose a new turbulence model that would be inspired by empirical observations and the analytical knowledge derived from von Karman's study, while satisfying the IEC requirements.

## 2.4 Proposed turbulence model

The main objective of this research is to propose a model in time and frequency domain, using a correlation approach as well as the more common spectral approach, while complying with the international standards that are defined using the spectral approach. Von Karman's model offers a good foundation to do that. Additional research has been conducted by Maeda, who first observed the fit between von Karman's model and measurement data, then used von Karman's model in a correlation-based method similar to the one we will use. Maeda has shown discrepancies between the measurements and the model, but did not propose a correction in his later studies. Moreover, no consideration of the international standards have been taken in the previous correlation-based studies.

The review proposed in the previous section has exposed some shortcomings of the existing turbulence models, but has also shown some good ideas and observations. We will use this knowledge to propose a new turbulence model that will be:

- ⋆ available in both correlation and spectral form;
- ⋆ consistent with empirical data and validated by measurements;
- ⋆ and complying with IEC requirements.

In this section, a modification of the original von Karman power spectrum model is proposed based on the empirical observations from Kaimal's model and Maeda's results. The model's parameters are then fitted to comply with the IEC requirements. Finally, the original von Karman cross-spectral model is modified to bring consistency with the modified power spectrum model.

The very first assumption in this proposed model is that turbulence is not isotropic; as such, in order to verify the first IEC requirement (2.23), while being a bit conservative, the ratio of standard deviations is chosen to be like the IEC Annex B Kaimal model [9]:

$$\begin{cases} \sigma_v = 0.8\sigma_u \\ \sigma_w = 0.5\sigma_u. \end{cases} \tag{2.54}$$

### 2.4.1 Autocorrelation and autospectrum

Several empirical observations, either from Kaimal's model or an experimental study by Maeda [15], show that the shape of the autospectrum is quite similar for all three components of wind turbulence. Indeed, instead of having isotropic turbulence with the same standard deviation in all directions, it seems that the standard deviations are different, but the behaviour is the same.

Therefore, taking a cue from Kaimal's model while keeping the advantage of von Karman's correlation model, we propose to use the same shape for the autocorrelation and autospectrum of all three components, based on von Karman's longitudinal autocorrelation and spectrum.

$$\frac{fS_i(f)}{\sigma_i^2} = \frac{4\frac{fL_i}{U}}{\left(1+70.8\left(\frac{fL_i}{U}\right)^2\right)^{5/6}} \tag{2.55}$$

$$\tilde{R}_i(\tau) = \mathsf{f}(U\tau) \quad i = u, v, w \tag{2.56}$$

The parameters left to be determined in this model are:

- ⋆ the standard deviations $\sigma_i$: available from measurements, or calculated using the IEC equation (2.18), and expanded to all heights using the turbulence intensity profile defined later;
- ⋆ the mean wind speed $U$: available from measurements or average meteorological data, and expanded to all heights using the wind speed profile defined later;
- ⋆ the turbulence length scales $L_i$.

For the turbulence length scales, as we have seen in the IEC Kaimal model in section 2.3.2.1, it should be derived from the IEC requirements on the high-frequency shape of the spectral densities. Applying the same calculation to (2.55),

we obtain the expression of the turbulence length scale as a function of the scale parameter $\Lambda_1$ (2.25) and thus of height.

$$\begin{cases} L_u = 3.49\Lambda_1 \\ L_v = 0.33 L_u \\ L_w = 0.08 L_u . \end{cases} \tag{2.57}$$

Alternatively, when measurements are available, the spectral form (2.55) can be fitted to the PSD estimated from measured time series to obtain the empirical length scale. The profile offered by $\Lambda_1(z)$ can then be adjusted, and used to obtain length scales at other heights.

### 2.4.2 Cross-correlation and coherence

As we have modified von Karman's autocorrelation model by assuming that all components had the same "behaviour", the cross-correlation must be changed accordingly so that the whole turbulence model stays consistent. Therefore, the cross-correlation function for one component at two spatially separated points will be the same for all components and given by

$$\tilde{R}_i(r,\tau) = \left(\mathrm{f}(r_1) - \mathrm{g}(r_1)\right) \frac{(U\tau)^2}{r_1^2} + \mathrm{g}(r_1) \tag{2.58}$$

$$\tilde{S}_i(r,f) = \frac{2}{\Gamma(5/6)} \left( \left(\frac{\theta}{2}\right)^{5/6} K_{5/6}(\theta) - \left(\frac{\theta}{2}\right)^{11/6} K_{1/6}(\theta) \right), \tag{2.59}$$

where $\theta$ is the same as (2.51) and the turbulence length scale in $a_1$ (2.45) depends on the component, and is averaged between the two points, e.g. between points 1 and 2,

$$L_i = \frac{1}{2}(L_i(z_1) + L_i(z_2)) \quad i = u, v, w. \tag{2.60}$$

### 2.4.3 Reynolds stress

Fujimura (Takeuchi) and Maeda [6][22] have suggested an empirical modification of the original von Karman model for Reynolds stress. Their proposition only applies to vertical separation, since their observations were obtained from a vertical measurement mast. We suggest a generalisation of their empirical model for all spatial separations. As a first approach, we assume that the $uv$ and $vw$ cross-correlations are negligible and only define the $uw$ cross-

correlation.

$$\frac{f\mathrm{Co}_u w(f)}{\sigma_u \sigma_w} = \frac{\overline{uw}}{\sigma_u \sigma_w} \frac{4fL_{uw}/U}{(1+70.8(fL_{uw}/U)^2)^{5/3}} \tag{2.61}$$

$$\tilde{R}_i(\tau) = \frac{\overline{uw}}{\sigma_u \sigma_w} \mathrm{f}(U\tau) \tag{2.62}$$

$$L_{uw} = \frac{1}{2}(L_u + L_w). \tag{2.63}$$

It appears that these expressions are simply derived from the autocorrelation and PSD models with adjusted parameters and a correcting factor $\frac{\overline{uw}}{\sigma_u \sigma_w}$. This correcting factor can be approximated using the geostrophic wind speed:

$$\overline{uw} \approx u^{*2}$$

$$\sigma_u \sigma_w = 0.5\sigma_u^2$$

$$\frac{\overline{uw}}{\sigma_u \sigma_w} \approx \frac{u^{*2}}{0.5\sigma_u^2}.$$

According to (2.29) we can then conclude

$$\frac{\overline{uw}}{\sigma_u \sigma_w} \approx 2\left(\frac{1}{2.185}\right)^2. \tag{2.64}$$

Similarly, for two-point $uw$ cross-correlation, we will adapt the one component cross-correlation and cross-spectrum expressions with a correcting factor:

$$\tilde{R}_i(r,\tau) = \frac{\overline{uw}}{\sigma_u \sigma_w}\left((\mathrm{f}(r_1) - \mathrm{g}(r_1))\frac{(U\tau)^2}{r_1^2} + \mathrm{g}(r_1)\right) \tag{2.65}$$

$$\tilde{S}_i(r,f) = \frac{\overline{uw}}{\sigma_u \sigma_w}\frac{2}{\Gamma(5/6)}\left(\left(\frac{\theta}{2}\right)^{5/6} K_{5/6}(\theta) - \left(\frac{\theta}{2}\right)^{11/6} K_{1/6}(\theta)\right), \tag{2.66}$$

where $\theta$ is defined as in (2.51) with the length scale $L_{uw}$ (2.63).

Finally, this concludes the description of turbulence. All correlations have been determined, although it must be noted that we have chosen to neglect the $uv$ and $vw$ cross-correlations as a first approach.

### 2.4.4 Other parameters

Parameters such as wind speed and standard deviation can be estimated from the measurements, but these measurements are usually only available at some points. To obtain the relevant values for all heights, we shall use a wind speed

and turbulence intensity profile. The following profiles are implemented in the WND3D software and reference values can be modified as appropriate.

#### 2.4.4.1 Wind speed profile

Although our target is to implement IEC specifications, in this case we will refer to the AIJ standards, which have a similar power law profile but propose a choice of exponent depending on the terrain category (see (2.13)). In addition, since we are trying to reproduce the three-dimensional turbulent field based on measurements, these measurements can be used as a reference for the profile equation.

$$U(z) = \begin{cases} U_0 \left(\dfrac{z}{z_0}\right)^{\alpha} & \text{when } z \geq z_b \\ U_0 \left(\dfrac{z_b}{z_0}\right)^{\alpha} & \text{when } z \leq z_b \end{cases} \tag{2.67}$$

The user can define the following parameters:

- ⋆ $U_0$ and $z_0$ are the reference values, typically chosen as the mean wind speed at hub height, and the hub height, respectively. When available, the user can define these values from a measurement point.
- ⋆ $\alpha$ and $z_b$ can be chosen from Table 2.3, or determined at the user's will (for example, following the IEC requirements we would have $\alpha = 0.02$). When measurements at several points are available, the exponent can be fitted to the observed profile.

#### 2.4.4.2 Turbulence intensity profile

In order to adjust the turbulence intensity at one's will in WND3D, the AIJ profile (2.19) is adopted with adjustable parameters, in a similar way to the wind profile.

$$I_u(z) = \begin{cases} I_0 \left(\dfrac{z}{z_0}\right)^{-\beta} & \text{for } z \geq z_b \\ I_0 \left(\dfrac{z_b}{z_0}\right)^{-\beta} & \text{for } z \leq z_b \end{cases} \tag{2.68}$$

In this model, the following parameters can be determined by the user:

- ⋆ $I_0, z_0$ are reference values, obtained using the IEC expression (2.18), from the AIJ (2.19) or from a measurement point when available;

- ⋆ the exponent term $\beta$ can be chosen equal to $\alpha+0.05$ to follow AIJ requirements, or adjusted to be equal to $\alpha$ so that the standard deviation of turbulence is constant over the height of the structure (IEC requirement);
- ⋆ $z_b$, the bottom limit for the profile, can also be modified.

## 2.5 Validation of the proposed model

### 2.5.1 Measurement data

For the validation, we will use measurement data from a wind turbine on the island of Hachijojima, Japan. The site is at the foot of a mountain, with an elevation of about 100 meters. The 500 kW wind turbine was installed by TEPCO and operation started in 2000.

A sonic anemometer is positioned at 6.23 meters, which can measure the wind speed for all three components, giving $\{u(t), v(t), w(t)\}$ time series. Observations from the sonic anemometer are available from December 2004 to October 2006. The measurements from the sonic anemometer will be used to validate the proposed turbulence model of section 2.4. For simplicity in the presentation of results, the figures shown in this validation are obtained from the data of March 23, 2005 only.

For the validation, we will use the frequency domain in order to make comparisons with the existing Kaimal and von Karman models as well. The measured time series will be used to estimate the spectral densities; the PSD are estimated using the MEM method, and the cross-spectral densities are obtained using Welch's modified periodogram estimation method (defined in Appendix A).

The correlation can also be used to validate the model. In this case, we calculate the correlation using the biased expression, e.g.

$$\mathrm{Corr}(u(t))(\tau) = \frac{1}{N}\sum_{t=1}^{N-\tau} u(t)u(t-\tau) \tag{2.69}$$

for the autocorrelation of a sequence of $N$ samples. The biased expression is used because it smooths the correlation function for large offsets $\tau$, ensuring that, for the autoregressive applications in Chapter 3 and 4, the function decreases rapidly enough.

Other parameters must be estimated. The mean wind speed $U$ and standard

deviation $\sigma_u, \sigma_v, \sigma_w$ are easily obtained from the measurements using

$$U = \frac{1}{N}\sum_{t=1}^{N} u(t)$$
$$\sigma_u^2 = \frac{1}{N-1}\sum_{t=1}^{N}(u(t)-U)^2.$$

It should be noted that we use the unbiased estimator for the standard deviation.

Finally, the turbulence length scale can also be estimated from the measurements. According to the equations for the autospectrum in any of the models and for any component, the value at $f = 0$ Hz shall follow the expression

$$S(0) = \sigma^2 \frac{4L}{U}. \tag{2.70}$$

Therefore, from the estimated values of the power spectrum, the mean wind speed and the standard deviation, we can also estimate the turbulence length scale from the observations.

### 2.5.2 Assumption of non-isotropic turbulence

First of all, the measurement data shows that the real turbulence structure is non-isotropic. Table 2.5 reviews the measured data for the week of March 20 to March 27, 2005. The given values are the 1-day average. The data from this week confirm that the ratios adopted in the IEC and in the proposed model are reasonable, since the average ratios for the week are very close to (2.54).

### 2.5.3 Validation of the proposed autospectrum model

To validate the autospectrum model, we observe several 10-min samples of measured wind speed and compare them to the available turbulence models. In Fig. 2.4, we have represented the estimated power spectral density of the measured wind speed, obtained by averaging the PSD of every 10-min sample on the day of March 23, 2005; the average autocorrelations are also shown. They are shown with the original von Karman model and the proposed model for comparison. For the turbulence models, parameters are estimated as explained in section 2.5.1. In this figure, the length scale is estimated from measurements.

The models are all rather similar and accurate for the longitudinal component. However, we can see that for the lateral and vertical components, where

Table 2.5: Measured mean wind speed and standard deviations, 1-day average values for the week of March 20 to 27, 2005.

| | $U$ (m/s) | $\sigma_u$ (m/s) | $\sigma_v$ (m/s) | $\sigma_w$ (m/s) |
|---|---|---|---|---|
| 20-Mar-05 | 3.041 | 1.407 | 1.091 | 0.636 |
| 21-Mar-05 | 2.759 | 1.552 | 1.300 | 0.731 |
| 22-Mar-05 | 3.096 | 1.631 | 1.287 | 0.820 |
| 23-Mar-05 | 5.381 | 2.695 | 1.951 | 1.210 |
| 24-Mar-05 | 4.003 | 1.948 | 1.516 | 0.881 |
| 25-Mar-05 | 5.448 | 2.742 | 2.348 | 1.232 |
| 26-Mar-05 | 4.374 | 2.127 | 1.737 | 0.948 |
| 27-Mar-05 | 2.572 | 1.273 | 1.031 | 0.592 |

| | $\sigma_v/\sigma_u$ | $\sigma_w/\sigma_u$ |
|---|---|---|
| 20-Mar-05 | 0.775 | 0.452 |
| 21-Mar-05 | 0.837 | 0.471 |
| 22-Mar-05 | 0.789 | 0.503 |
| 23-Mar-05 | 0.724 | 0.449 |
| 24-Mar-05 | 0.778 | 0.452 |
| 25-Mar-05 | 0.856 | 0.449 |
| 26-Mar-05 | 0.816 | 0.446 |
| 27-Mar-05 | 0.810 | 0.465 |
| Average | 0.798 | 0.461 |

von Karman's original model differs from the proposed model, there is a small difference for the lateral component and a clear difference for the vertical component.

In both frequency and time domain, the proposed model gives satisfying results when compared to observations. An additional study, about the accuracy of the length scale model, would be required in the future shall these models be used for wind generation. In particular, the turbulence length scale can only be estimated from available measurement points, meaning that a validation of the proposed length scale model is required to verify its applicability for other points where measurement is not available.

### 2.5.4 Validation of the proposed Reynolds stress model

For the Reynolds stress, we have also calculated cross-components co-spectral densities for every 10-min sample and averaged them over one day, for the data of March 23, 2005. Fig. 2.5 shows the comparison between the measured wind

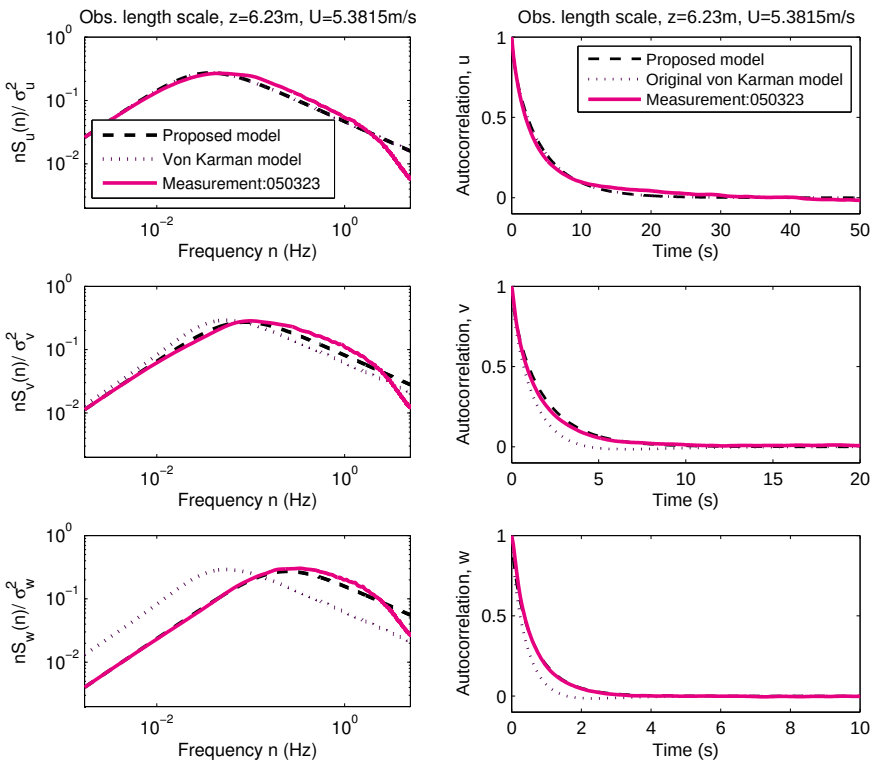


(a) Normalized power spectral densities (b) Autocorrelations

Figure 2.4: Normalized power spectral densities and autocorrelations of three components of measured wind speed, averaged, on March 23, 2005. The proposed model shows better fit with the measurements than the original von Karman model.

data, Kaimal's co-spectrum model and our proposed co-spectrum model.

First, let us discuss the choice to neglect the $uv$ and $vw$ cross-component correlation as a first approach. According to the observations, the assumption is clearly true for $vw$, while it is not verified for $uv$ as it appears that a slight relationship exist between the longitudinal and lateral components (Fig. 2.5, top.)

In any case, the proposed Reynolds stress model fits very well with the empirical data for the $uw$ relationship. Further improvements of the proposed model should include a model for $uv$ correlation.

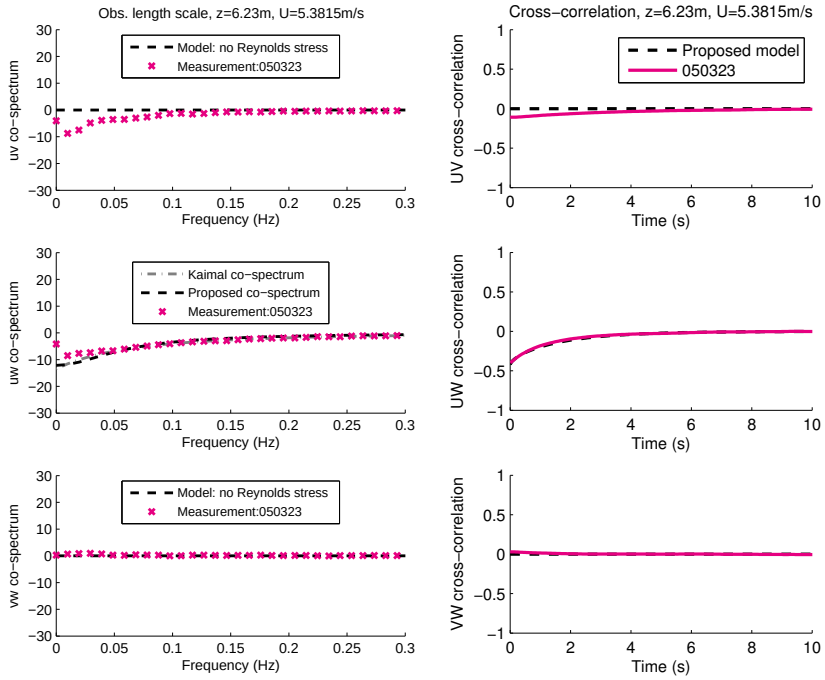


(a) Co-spectra between components

(b) Cross-correlations between components

Figure 2.5: Average co-spectrum and cross-correlation for different components of measured wind speed on March 23, 2005. Validation of the proposed co-spectrum model, assuming no Reynolds stress for $uv$ and $vw$, with additional comparison to Kaimal's empirical co-spectrum.

# Chapter 3

# Autoregressive model for turbulence generation

Wind generation methods can be separated in two classes: on the one hand, frequency domain methods, and on the other hands time domain methods. A widely used frequency domain method has been first introduced by Veers [24]. Veers' method is developed around the use of a spectral matrix to describe turbulence. This is consistent with the common approach in wind engineering which mostly uses a frequency-domain approach. Therefore, this method has the advantage of using the turbulence models from the standards, which are given in spectral form, directly.

However, aside from issues related to the turbulence models, this approach requires the application of a Fourier transform to obtain the time series of the generated flow. Additionally, as we would like to reproduce the time series of measured data, phase has a great importance, thus working in the time domain is more natural and convenient.

The approach proposed here is a time domain method to generate a turbulent flow by taking into consideration the turbulence properties through the correlation and with a possibility to include measured data into the simulation. The use of an autoregressive model for wind modelling has been introduced by Iwatani in 1982 [11], which was then reused by Maeda and Fujimura [6][16][22]. Iwatani also improved this method by enabling the inclusion of measurement data to obtain wind fluctuations similar to observed ones [12]. In this chapter, Section 3.1 introduces the general background to define autoregressive models. Section 3.2 describes the application of an autoregressive model to describe

wind turbulence and makes a review of Iwatani's method for linking measured data to the turbulence generation. Finally, Section 3.3 discusses the choice of model order and the limitations of the method.

This method is implemented in a software called WND3D, developed in the University of Tokyo by Phuc [18] based on Iwatani's method. The present research has modified the software to include the turbulence models in correlation form as described in Chapter 2, and to output the characteristics of the wind field (spectral densities, correlations, statistical properties) directly, using the estimations methods described in Appendix A.

## 3.1 Autoregressive model

Autoregressive models (thereafter, AR models) belong to the larger group of linear prediction models. AR models are a particular case of linear regression: a variable is explained by its own past values rather than the value of other independent variables.

The present section does not pretend to provide a rigorous mathematical description of AR modelling, but aims to build a solid enough background for the good application of these models.

### 3.1.1 Autoregressive stochastic processes

A stochastic process is a collection of random variables, generally represented as an indexed family. Typically, in this thesis, we will deal with time series. Time series are simply a time-indexed sequence of random variables, which are the discrete time observations.

Let us consider a stochastic process $\{x(t), t \in \mathbb{T}\}$, where $\mathbb{T}$ is an index set that represents time, such as $\mathbb{Z}$ or $\mathbb{N}$. We suppose that the process takes values in $\mathbb{K} = \mathbb{R}$ or $\mathbb{C}$. For convenience, we will suppose that the process is normalized, i.e. the expectation is zero and the standard deviation is 1. While random variables can be explained by other independent variables via a linear regression model, it seems natural to explain, and *predict*, a time-dependent variable represented by a stochastic process by using its values at past time indices.

The basic form of the univariate AR model of order $p$, also denoted AR(p), is

$$x(t) = \sum_{i=1}^{p} a(i)x(t-i) + \varepsilon(t), \tag{3.1}$$

where the $a(i)$ are the autoregressive parameters and $\varepsilon(t)$ is a stationary random process with zero mean, called the *innovation process*. The innovation process satisfies the following properties.

$$\mathbb{E}[\varepsilon(t)\varepsilon^*(t')] = \begin{cases} 0 & \text{for } t \neq t' \\ \sigma_\varepsilon^2 & \text{for } t = t' \end{cases} \tag{3.2}$$

$$\mathbb{E}[\varepsilon(t)x^*(t')] = \begin{cases} 0 & \text{for } t \neq t' \\ \sigma_\varepsilon^2 & \text{for } t = t' \end{cases} \tag{3.3}$$

where $\mathbb{E}[\cdot]$ denotes the expectation.

### 3.1.2 Yule-Walker equations

A traditional way of fitting this model is to use the Yule-Walker equations [27][30]. These equations are simply derived. Let's multiply equation (3.1) with $x^*(t-m)$ for any $m \in T$, and take the expectation:

$$\begin{aligned} \forall t, m \in \mathbb{T} \quad x(t)x(t-m) &= \sum_{i=1}^{p} a(i)x(t-i)x^*(t-m) + \varepsilon(t)x^*(t-m) \\ \mathbb{E}[x(t)x^*(t-m)] &= \mathbb{E}\left[\sum_{i=1}^{p} a(i)x(t-i)x^*(t-m)\right] + \mathbb{E}[\varepsilon(t)x^*(t-m)], \end{aligned} \tag{3.4}$$

where the star exponent denotes complex conjugation (or later, for vectors and matrices, the conjugate transpose).

The left-hand term is what we will call *covariance sequence* or *covariance function*. In addition, if it is normalized by the variance of the process $\{x(t)\}$, we can also call it *correlation* sequence or function. In our case $\sigma[x] = 1$, and for convenience we will always work with the correlation sequence. We can suppose that

$$\mathbb{E}[x(t)x^*(t-m)] = r(m), \tag{3.5}$$

which means that the correlation sequence only depends on the lag between the two variables. This assumption, along with the assumption that $\mathbb{E}[x(t)] = 0$, means that the process $\{x(t)\}$ is weak-sense stationary. This also leads to other

properties such as

$$\forall m \in \mathbb{T} \quad r(m) = r^*(-m) \tag{3.6}$$

$$r(0) \geq |r(m)|. \tag{3.7}$$

The property (3.7) derives from the properties of positive semidefinite matrices, and the fact that the covariance matrix $R_m$ is positive semidefinite is proven in appendix A (equation (A.21)).

Going back to the derivation in (3.4), we can rewrite it using the correlation sequence $r(m)$.

$$r(m) = \sum_{i=1}^{p} a(i) \underbrace{\mathbb{E}\left[x(t-i)x^*(t-m)\right]}_{r(m-i)} + \underbrace{\mathbb{E}[\varepsilon(t)x^*(t-m)]}_{0 \text{ for } m \neq 0}, \tag{3.8}$$

in which the second term is simplified using the property (3.3). For $m = 0$, we obtain another equation

$$r(0) = \sum_{i=1}^{p} a(i) r(-i) + \underbrace{\mathbb{E}[\varepsilon(t)x^*(t)]}_{\sigma_\varepsilon^2}, \tag{3.9}$$

which can be simplified from property (3.3) again (note also that from (3.6), $r(-i) = r^*(i)$).

Finally, we can regroup equations (3.8) and (3.9) which give us the following set of Yule-Walker equations to find the parameters $a(i)$ of this AR(p) model.

$$\begin{bmatrix} r(1) \\ r(2) \\ \vdots \\ r(p) \end{bmatrix} = \begin{bmatrix} r(0) & r^*(1) & \cdots & r^*(p-1) \\ r(1) & r(0) & & \vdots \\ \vdots & & \ddots & r^*(1) \\ r(p-1) & r(p-2) & \cdots & r(0) \end{bmatrix} \begin{bmatrix} a(1) \\ a(2) \\ \vdots \\ a(p) \end{bmatrix} \tag{3.10}$$

$$\sigma_\varepsilon^2 = r(0) - \sum_{i=1}^{p} a(i) r^*(i) \tag{3.11}$$

While the first matrix equation gives the parameters directly, some additional work is required to obtain the innovations. One way of evaluating the innovation process is to use a gaussian white noise process $\{o(t)\}$, which has the following

properties:

$$\mathbb{E}[o(t)] = 0$$
$$\mathbb{E}[o(t)o^*(t')] = \begin{cases} 0 & \text{if } t \neq t' \\ 1 & \text{if } t = t', \end{cases}$$

and calculating the innovation using

$$\varepsilon(t) = \sigma_\varepsilon o(t). \tag{3.12}$$

This guarantees that the innovation process has the desired properties (equation (3.2)), indeed:

$$\begin{aligned} \mathbb{E}[\varepsilon(t)] &= \mathbb{E}[\sigma_\varepsilon o(t)] = \sigma_\varepsilon \mathbb{E}[o(t)] \\ &= 0 \\ \mathbb{E}[\varepsilon(t)\varepsilon^*(t')] &= \mathbb{E}[\sigma_\varepsilon o(t)(\sigma_\varepsilon o(t'))^*] \\ &= \sigma_\varepsilon^2 \mathbb{E}[o(t)o^*(t)] \\ &= \begin{cases} 0 & \text{if } t \neq t' \\ \sigma_\varepsilon^2 & \text{if } t = t'. \end{cases} \end{aligned}$$

## 3.2 Application to turbulent flow generation

In order to generate a turbulent wind field, we need to simulate turbulence at any point in space. For wind turbines, that will be generally points across the rotor's swept area, or, given a finite element model, nodes of the model. In any case, the wind field simulation must include multiple points.

This section will therefore expand the AR process of the previous section in order to apply it to multiple points: this will be called a multivariate autoregressive model. Then, parametrisation of the model will be done using the proposed turbulence model of Chapter 3. Finally, Iwatani's idea of linking with measurement data to improve the wind field's accuracy is explained.

In the following parts, we will consider

- ⋆ that we want to simulate turbulent wind time series at $N$ spatially separated points;

- ⋆ that the three components of the wind, which are denoted $u, v, w$, are defined along the Cartesian coordinate system $(x, y, z)$ where the longitudinal $x$-axis has been chosen to be parallel to the direction of the wind, so that the mean wind speed is equal to the mean of the longitudinal wind speed ($U = \mathbb{E}[u]$), and that the mean lateral and vertical wind speed is zero ($\mathbb{E}[v] = \mathbb{E}[w] = 0$).

### 3.2.1 Multivariate autoregressive model for wind generation

The multivariate autoregressive (MAR) or vector autoregressive (VAR) model is simply an extension of the AR model described in section 3.1. Instead of a single scalar process $\{x(t)\}$, we consider a vector of processes

$$\begin{aligned}\mathbf{u}(t) &= [u_1(t), u_2(t), ..., u_N(t), v_1(t), ..., v_N(t), w_1(t), ..., w_N(t)]^T \\ &= [u_{11}(t), u_{12}(t), ..., u_{1N}(t), u_{21}(t), ..., u_{2N}(t), u_{31}(t), ..., u_{3N}(t)]^T,\end{aligned}$$

where $N$ is the number of spatial positions where the wind is described, and $^T$ denotes the transpose. Two notations can be adopted; the first one uses $u, v, w$ to distinguish the components, the other uses two indices, where the first indicates component with $(u, v, w) = (u_1, u_2, u_3)$, and the second indicates the point in space.

Note that wind turbulence is typically a real process, but we will keep the star notation (complex conjugate transpose) for the sake of generality.

The MAR($p$) process (multivariate autoregressive process of order $p$) is written as

$$\mathbf{u}(t) = \sum_{i=1}^{p} A(i)\mathbf{u}(t-i) + \epsilon(t), \tag{3.13}$$

where the innovation is also a $3N \times 1$ vector defined by

$$\epsilon(t) = [\varepsilon_{11}(t), \varepsilon_{12}(t), \varepsilon_{13}(t), \ldots, \varepsilon_{21}(t), \ldots \varepsilon_{3N}(t)]^T$$

$$\mathbb{E}[\epsilon(t)\epsilon(t')] = \begin{cases} \mathbf{S}_\varepsilon & \text{if } t = t' \\ 0 & \text{if } t \neq t'. \end{cases}$$

$\mathbf{S}_\varepsilon$ is a $3N \times 3N$ correlation matrix; the expectation of the innovation is, like in the univariate case, zero.

Parameters and correlations are also matrices of size $3N \times 3N$:

$$\begin{aligned}\forall m = 1,\dots,p \quad R(m) &= \mathbb{E}[\mathbf{u}(t)\mathbf{u}^*(t-m)] \\ &= \left(\overline{u_{ij}u_{kl}}(m)\right)_{i,k=1,2,3 \text{ and } j,l=1,\dots,N},\end{aligned}$$

where we have denoted the scalar correlation

$$\overline{u_{ij}u_{kl}}(m) = \mathbf{E}[u_{ij}(t)u^*_{kl}(t-m)]. \tag{3.14}$$

The basic structure of the correlation matrix is given in equation (3.15) (using $u, v, w$ rather than $u_1, u_2, u_3$ for clarity). Also note that the correlation matrix is symmetric due to assumption (3.6).

$$\begin{bmatrix}
\overline{u_1u_1} & \cdots & \overline{u_1u_N} & \overline{u_1v_1} & \cdots & \overline{u_1v_N} & \overline{u_1w_1} & \cdots & \overline{u_1w_N} \\
\vdots & \ddots & \vdots & \vdots & \ddots & \vdots & \vdots & \ddots & \vdots \\
\overline{u_Nu_1} & \cdots & \overline{u_Nu_N} & \overline{u_Nv_1} & \cdots & \overline{u_Nv_N} & \overline{u_Nw_1} & \cdots & \overline{u_Nw_N} \\
\overline{v_1u_1} & \cdots & \overline{v_1u_N} & \overline{v_1v_1} & \cdots & \overline{v_1v_N} & \overline{v_1w_1} & \cdots & \overline{v_1w_N} \\
\vdots & \ddots & \vdots & \vdots & \ddots & \vdots & \vdots & \ddots & \vdots \\
\overline{v_Nu_1} & \cdots & \overline{v_Nu_N} & \overline{v_Nv_1} & \cdots & \overline{v_Nv_N} & \overline{v_Nw_1} & \cdots & \overline{v_Nw_N} \\
\overline{w_1u_1} & \cdots & \overline{w_1u_N} & \overline{w_1v_1} & \cdots & \overline{w_1v_N} & \overline{w_1w_1} & \cdots & \overline{w_1w_N} \\
\vdots & \ddots & \vdots & \vdots & \ddots & \vdots & \vdots & \ddots & \vdots \\
\overline{w_Nu_1} & \cdots & \overline{w_Nu_N} & \overline{w_Nv_1} & \cdots & \overline{w_Nv_N} & \overline{w_Nw_1} & \cdots & \overline{w_Nw_N}
\end{bmatrix} \tag{3.15}$$

The MAR parameters are obtained using the Yule-Walker equations as well. The multivariate form of the Yule Walker equations is written as (3.16) and (3.17).

$$\begin{bmatrix} R(1) \\ R(2) \\ \vdots \\ R(p) \end{bmatrix} = \begin{bmatrix} R(0) & R^*(1) & \cdots & R^*(p-1) \\ R(1) & r(0) & & \vdots \\ \vdots & & \ddots & R^*(1) \\ R(p-1) & R(p-2) & \cdots & R(0) \end{bmatrix} \begin{bmatrix} A(1) \\ A(2) \\ \vdots \\ A(p) \end{bmatrix} \tag{3.16}$$

$$\mathbf{S}_\varepsilon = R(0) - \sum_{i=1}^{p} A(i)R^*(i) \tag{3.17}$$

As for the univariate AR model, the parameters $A(i)$ can be obtained by inverting equation (3.16), but an additional operation is required to obtain the innovation processes. We will use the same approach as in section 3.1. First, we should

rewrite the innovation vector's correlation matrix, which is, by definition, positive semi-definite. It is therefore possible to apply a Cholesky decomposition to obtain

$$\mathbf{S}_\varepsilon = LL^*, \tag{3.18}$$

where $L$ is a lower triangular matrix. Then, let's define the innovation as

$$\epsilon(t) = L\mathbf{o}(t), \tag{3.19}$$

with $\mathbf{o}(t)$ a gaussian white noise vector process:

$$\mathbb{E}[\mathbf{o}(t)] = 0$$
$$\mathbb{E}[\mathbf{o}(t)\mathbf{o}^*(t')] = \begin{cases} 0 & \text{if } t \neq t' \\ \mathbb{I} & \text{if } t = t'. \end{cases}$$

$\mathbb{I}$ is the identity matrix. Thus, $\mathbb{E}[\epsilon(t)] = 0$ and

$$\begin{aligned} \mathbb{E}[\epsilon(t)\epsilon^*(t')] &= \mathbb{E}[L\mathbf{o}(t)\mathbf{o}^*(t')L^*] \\ &= L\mathbb{E}[\mathbf{o}(t)\mathbf{o}^*(t')]L^* \\ &= \begin{cases} 0 & \text{if } t \neq t' \\ LL^* = \mathbf{S}_\varepsilon & \text{if } t = t' \end{cases} \end{aligned}$$

which clearly satisfies the properties of the innovation vector process.

Now, in order to solve the parameters equation, (3.16), the sequence of correlation matrices $\{R(i), i = 1 \dots p\}$ must be estimated in some way. Generally, as mentioned in the case of the univariate AR model, the correlation sequence is estimated from measured data and we can say that the model is then fitted to these measurements. However in the case of wind field modelling, in particular in our study where we want a complete field over the height of a structure, we obviously cannot expect to possess information at all considered points. Another method must be used to obtain these matrices.

### 3.2.2 Obtaining the correlations matrices

The MAR model for predicting, or generating, a fully-fledged three dimensional turbulent wind field, must be parametrized. As we have seen in the previous

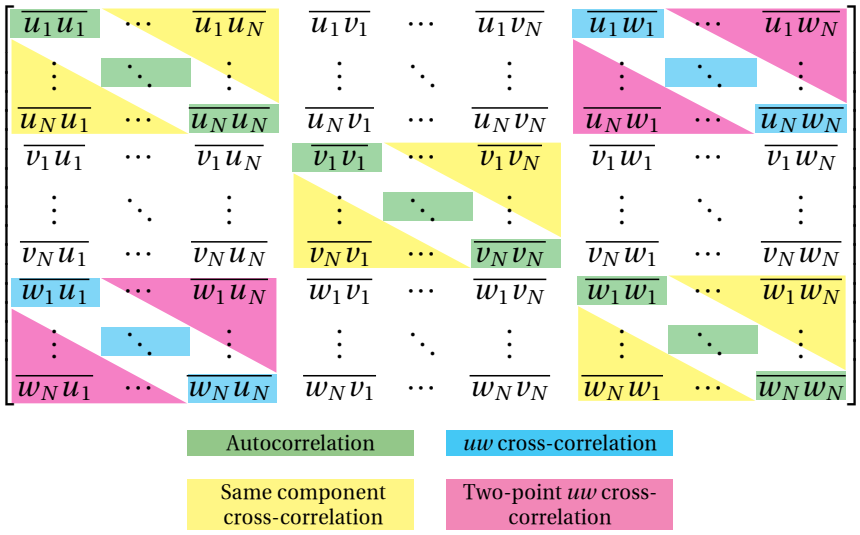


Figure 3.1: Contents of the correlation matrix, with the vocabulary of turbulence description defined in Chapter 2. Note that the $uv$ and $vw$ cross-correlations are neglected in the proposed turbulence model.

sections, parameters can be calculated with the Yule-Walker equations, but to solve these equations we need to know the sequence of correlation matrices $\{R(i), i = 1 \dots p\}$.

It appears that the turbulence relationships described in Chapter 2 correspond exactly to the contents of the $R(i)$ matrices. Turbulence models aim at giving an idea of the average behaviour and relationships between the components of turbulence at spatially separated points, and this is exactly what is needed for the correlations matrices in the MAR model. The $R(i)$ matrices contain autocorrelations (diagonal terms), same component cross-correlation in the diagonal blocks, and cross-component correlations; Fig. 3.1 shows the partition of the correlation matrix, with the particular vocabulary related to wind modelling that we have defined in Chapter 2.

For this kind of model, it is clear that a correlation-based description of turbulence is the most convenient. For legacy frequency-domain models, a discrete Fourier transform must be applied to obtain, numerically, the necessary correlations. In this study, the proposed turbulence model can be used directly in correlation form.

### 3.2.3 Linking with measured wind speed time series

Evaluating the correlations using the turbulence models requires some additional parameters. The three parameters to be provided in the turbulence models are the mean wind speed, the standard deviation and the length scale. These are usually estimated using the measurements of the SCADA system, but at other points where no measurement is available, the estimated parameters from SCADA are extrapolated using standards models, such as, for example, the wind speed profile.

However, these are only "average" statistical values and a lot information concerning the phase is lost in the averaging process. The simulated wind lacks time-domain similarity with the real wind. For this reason, an improved method to link time series of measurement data to the MAR generation method has been introduced by Iwatani [11].

In addition to the three parameters mentioned above, the MAR method can include more information from the measured time series using the observed correlation, but also using the measured time series to correct the prediction error and provide a corrected evaluation of the innovation process. This procedure can be seen as adding a constraint to the generated wind field: the wind field generation algorithm is constrained by the known measured time series at given points.

#### 3.2.3.1 Adjusting the innovation process

The main feature of Iwatani's method for including information from measured wind speed data is to modify the innovation process according to the known data. Let's assume that, out of the $K = 3N$ terms in the MAR model, $k$ are known. The innovation vector has been defined as (3.19), which can be rewritten in full matrix form as

$$\begin{bmatrix} \varepsilon_1(t) \\ \vdots \\ \varepsilon_k(t) \\ \varepsilon_{k+1}(t) \\ \vdots \\ \varepsilon_K(t) \end{bmatrix} = \begin{bmatrix} L_{11} & 0 & \cdots & \cdots & \cdots & 0 \\ \vdots & \ddots & \ddots & & & \vdots \\ L_{k1} & \cdots & L_{kk} & \ddots & & \vdots \\ L_{k+1,1} & \cdots & L_{k+1,k} & L_{k+1,k+1} & \ddots & \vdots \\ \vdots & & \vdots & \vdots & \ddots & 0 \\ L_{K1} & \cdots & L_{Kk} & L_{K,k+1} & \cdots & L_{KK} \end{bmatrix} \begin{bmatrix} o_1(t) \\ \vdots \\ o_k(t) \\ o_{k+1}(t) \\ \vdots \\ o_K(t) \end{bmatrix} \tag{3.20}$$

Note that we have reindexed the variables from 1 to $K = 3N$.

On the one hand, we have the predicted wind speed, minus the innovations, $\hat{u}_1(t)$ to $\hat{u}_k(t)$ defined as

$$\hat{u}_i(t) = \sum_{m=1}^{p} \sum_{j=1}^{K} A(m)_{ij} u_j(t-m) \quad i = 1, \ldots, k, \tag{3.21}$$

and on the other hand, the measured wind speed for the same components, $u_1^m(t)$ to $u_k^m(t)$. The prediction error can be calculated as

$$e_i(t) = u_i^m(t) - \hat{u}_i(t) \quad i = 1, \ldots, k. \tag{3.22}$$

We can use this prediction error to adjust the MAR model, by assuming that the prediction error is equal to the innovation. Thus, $\varepsilon_1(t)$ to $\varepsilon_k(t)$ are equal to $e_1(t)$ to $e_k(t)$. The first $k$ lines of equation (3.20) can therefore be used to calculate the values of $o_1(t)$ to $o_k(t)$, guaranteeing that the final values of $u_1(t)$ to $u_k(t)$, innovation included, are equal to the measured ones. The $K - k + 1$ other lines are used to derive the other terms of the innovation vector from $o_{k+1}(t)$ to $o_K(t)$ generated as a Gaussian white noise.

Note that the lower triangular matrix $L$ has been obtained from the parameters matrices $A(i)$ calculated in the Yule-Walker equations, and both L and the $A(i)$ depend on the correlation matrices $R(i)$.

#### 3.2.3.2 Including the measured correlation

In section 3.2.2, the turbulence models have been used to evaluate the correlations. But as we have available wind speed time series data, why not also use the measured correlations to parametrize the model?

The possibility to use the measured correlations is offered in the WND3D software developed with this study and the PCM method. In such a situation, the correlations obtained from the measurements are included in the correlation matrices $R(i)$ instead of using the standard turbulence models.

The main shortcoming comes from the uncertainty in the estimation of the correlation function. As suggested in *Spectral Analysis of Signals* [21], the use of the biased correlation estimator is preferred as it helps guarantee that the correlation function decreases rapidly enough to ensure a good definition of the power spectral density. However, due to possible inconsistency between the standard turbulence models, which describe an average behaviour, and the ac-

tual measured turbulence which is just one realization, the correlation matrices are not guaranteed to be well-conditioned or even positive semidefinite. A quick overview of the limitations of the MAR model is conducted in the next section.

## 3.3 Model order and shortcomings of autoregressive processes

Autoregressive models have been extensively studied over the years and Yule-Walker's equations are a conventional way of evaluating the parameters for the regression. However, some authors mention the shortcomings of this approach in particular cases. Limits of this approach are reviewed in section 3.3.1. Additionally, choosing the "optimal" order for the autoregressive process is also a major issue. Various criteria for choosing a model order are discussed in section 3.3.2.

The discussion will mostly deal with the univariate AR model, but all conclusions can be extended to the multivariate case.

### 3.3.1 Stability of the autoregressive process

Concerns about the stability of an AR model must be tackled. For instance, de Hoon et al. [4] show that under some circumstances, the Yule-Walker approach give poor results, such a when the correlation matrices are ill-conditioned (i.e. the largest and smallest eigenvalue are of a very different orders of magnitude), or if there are issues with the stationarity condition. Indeed, the main assumption that was used to solve the Yule-Walker equations is related to the stationarity of the process, such as in (3.4).

An autoregressive process has a characteristic polynomial, which roots must lie inside the unit circle for the process to be stationary.

**Lag operator** The lag operator, denoted $z$, can be used to express the AR process in the form of a polynomial. Given a time series $\{x(t), t \in \mathbb{T}\}$, then

$$\forall t \in \mathbb{T}, \quad zx(t) = x(t-1). \tag{3.23}$$

Thus, the univariate AR process (3.1) can be rewritten as

$$\varepsilon(t) = \left(1 - \sum_{m=1}^{p} a(i) z^i\right) x(t), \tag{3.24}$$

which gives the form of the characteristic polynomial by replacing the lag operator by the unknown $X$

$$\Psi(X) = 1 - \sum_{m=1}^{p} a(i) X^i. \tag{3.25}$$

**Stability condition** For the AR process to be stable, all the roots of the characteristic polynomial must lie inside the unit circle. As the roots get closer to the unit circle, the process will tend to become pseudo-periodic, and it is harmonic if the roots are exactly on the unit circle [4]

Since the characteristic polynomial's coefficients are the parameters $a(i)$, it seems clear that the correlations used to calculate the parameters have a large influence over the polynomial's roots. In the case of the Yule-Walker method to estimate the parameters, de Hoon et al. show that when the correlation matrix is ill-conditioned, the solution of equation (3.10) will be very sensitive to perturbations in the correlation coefficients.

In particular, for the purpose of generating an accurate wind field, cross-component correlations (Reynolds stress) represent an added "stress" on the model and tend to produce poorly conditioned correlation matrices. The consequences are quite obvious when we try to generate a wind field using such parameters, as shown in Appendix B, where we tried to simulate a turbulent wind field with Reynolds stress using a MAR autoregressive method. The generated wind shows the pseudo-periodic characteristics mentioned by de Hoon et al. for AR processes with a poorly verified stability condition.

This study has not solved the issue of poorly conditioned matrices for wind field generation. Improvements of the wind generation method should consider other methods to estimate the AR parameters, such as Burg's method suggested by de Hoon et al. In the current situation, the AR model as described in this chapter cannot be solved accurately and reliably for turbulence that includes Reynolds stress correlations.

### 3.3.2 Choice of the autoregressive model order

The choice of the autoregressive order can be done using Akaike's information criterion (AIC) or the final prediction error (FIP). The AIC consists in minimizing the log-likelihood of the innovation variance, while the FIP aims at minimizing the average error of the prediction. Several other criteria exist, such as the criterion autoregressive transfer (CAT), or the Bayesian information criterion (BIC).

The principle of order selection is quite simple: each criterion is given in the form of a function $IC(p)$ to be minimized. Usually, criteria take into account the error or the variance of the error and penalize too large orders. The approach is to fit the AR model for orders $p = 1, \ldots, p_{max}$ and evaluate the $IC(p)$ function for each order.

AR models for wind generation have been studied and used by Takeuchi and Maeda [22], as well as Phuc [18] and Yoon [29]. In this study, the order will be chosen according to these previous results.

# Chapter 4

# Application to wind turbine response estimation

Chapter 2 introduced a new turbulence model and Chapter 3 described an autoregressive wind generation method. The final target of the wind generation method is to provide an accurate external force to estimate the response of the wind turbine using finite element simulation. To validate this estimation method, measurements from a wind turbine in Miyakojima, Japan, are used. We will first evaluate the improvements brought by the improved wind generation method that links the simulated wind with time series of one component measured wind speed. The estimated response will be compared to the measured response to assess its accuracy. Additionally, a numerical validation is conducted to assess the effect of linking with three components of measured wind speed rather than one. An additional result showing the advantage of the proposed turbulence model over the original von Karman model is described in Appendix C.

Characteristics of the generated wind fields used in each section are summarized in Table 4.1.

## 4.1 Wind turbine and measurement data

For this chapter, the studied wind turbine is a 400 kW turbine on Miyakojima island, Japan. Field measurement were conducted from January 16, 2004 to March 16, 2004 by Ishihara et al. [10]. Measurements contain longitudinal wind speed data from a cup anemometer, as well as moment and acceleration time series obtained from strain gauges and accelerometers respectively. Positions of the

Table 4.1: Description of the generated turbulent wind fields studied in each section.

| | Wind generation method | Link with measured data | Turbulence model | Standards |
|---|---|---|---|---|
| Section 4.2 | Artificial | No | Proposed | IEC |
| | Linked | 1 component | Proposed | IEC |
| Section 4.3 | Linked | 1 component | Proposed | IEC |
| | Linked | 3 component | Proposed | IEC |

sensors are described in Fig. 4.1, as well as a few relevant nodes that will be often mentioned in the study.

The chosen time span for this study is the 10-min data measured on January 21, 2004 between 03:40 and 03:50. The sampling frequency is 20 Hz (i.e. $\Delta t = 0.05$ s). The principal wind direction is 56 degrees from the longitudinal axis of the wind turbine. The mean wind speed is 19.87 m/s and turbulence intensity is 10.8% at hub height (36 m). Terrain category for the wind speed profile is chosen as category I according to Table 2.2, with the corresponding parameters determined according to Table 2.3.

For the PCM method, the finite element model of the wind turbine has already been updated by Yoon [29]; this updated model will be used thereafter. Thus, for the purpose of validating the wind generation method, the target will be to reproduce the time series of the moment at the tower base for the selected 10-min time span using the WND3D wind generation software described in the previous chapters, and CAsT [10] for simulating the response.

## 4.2 Improvements in response estimation with the linked wind generation method

### 4.2.1 Wind field generation with the proposed model

We will use the term *artificial* for the generated wind without link, and *linked* for the generated wind with link to the time series. For each case, 10 realizations of the wind are generated by changing the random number generator's seed. To study turbulence properties, we should use ensemble averaging to estimate, for example, the power spectral density. Therefore, for spectral densities and correlations, the figures that are shown are the average over the 10 realizations, while

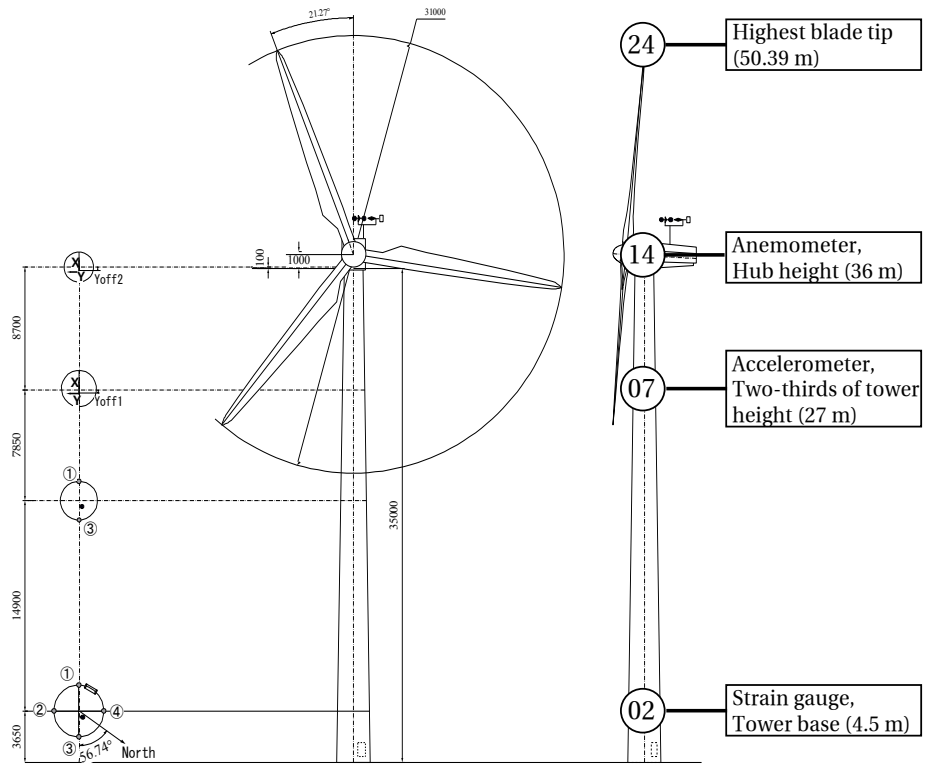


Figure 4.1: 400 kW wind turbine in Miyakojima. Position of the sensors and nodes relevant to this study.

particular realizations might be shown for time series.

We will compare two cases: the first one without link to measured data, and the other with link to the time measured series of longitudinal wind speed. Then, results for each case will be compared in terms of turbulence properties and estimation of the wind turbine response.

The order of the autoregressive model is chosen, according to previous studies by Phuc [18] and Yoon [29], as 200. The time step for the simulated wind is, like the measurements, $\Delta t = 0.05$ s.

#### 4.2.1.1 Wind generation parameters

For the wind generation, the parameters have been chosen as follows.

**Wind speed and turbulence intensity profile** WND3D includes the power law profile for the wind speed and turbulence intensity described in section 2.4.4.1

and 2.4.4.2 with

- ⋆ $U_0 = 19.87$ m/s and $z_0 = 36$ m (from measurements),
- ⋆ $\alpha = 0.1$,
- ⋆ $I_0 = 0.108$ and $z_0 = 36$ m (from measurements),
- ⋆ $\beta = 0.1$ to have a constant standard deviation as required by the IEC.
- ⋆ For both profiles, $z_b = 5$ m is set up as the lower boundary.

Standard deviations are chosen as in (2.28) (turbulence is not isotropic).

**Turbulence length scale** The turbulence length scale is calculated using the expression (2.57). To keep the same logic as the wind and turbulence intensity profiles, a lower boundary is set up at 5 m, under which the length scale is constant and equal to the length scale at 5 m.

**Correlations** The correlations are evaluated using the proposed turbulence model of section 2.4. Even for the linked case, we will not use the measured data to estimate the correlation.

Additionally, as a first approach, we neglect the Reynolds stress i.e. there is no correlation between different components of the wind.

#### 4.2.1.2 Quality of the generated wind field

Let us compare the properties of turbulence generated with and without linking to measured wind speed time series.

**Time series** We can compare the time series of the generated wind for both cases in Fig. 4.2; the figure shows time series of the longitudinal wind speed at different heights. In the artificial case, the generated wind has very little in common with the measured data, other than mean wind speed and standard deviations. In the linked case, however, the generated wind looks much more similar to the measured wind at 36 meters. Indeed, at the measurement height it appears that the generated wind is perfectly equal to the measured wind, due to the way we link the data as explained in section 3.2.3. Additionally, the turbulence at other heights is influenced by the linked data as we can observe that the low frequency variation is reproduced. This influence can be attributed to the same-component correlation, or equivalently the coherence relationship, which binds the turbulence at two different points to have similarities.

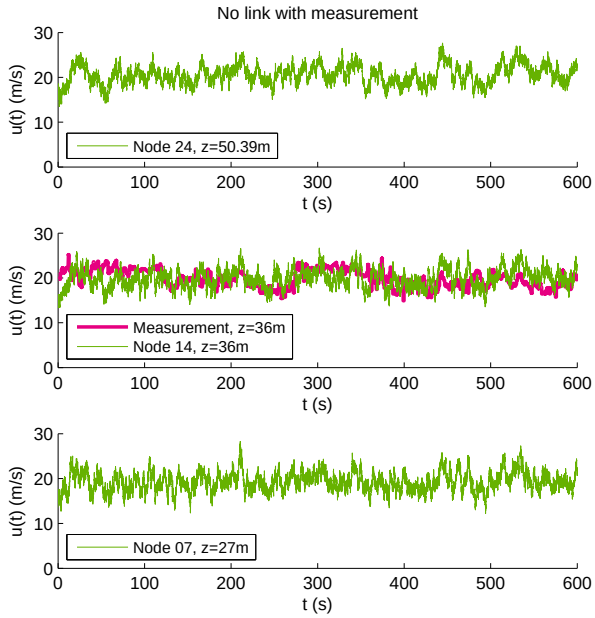


(a) Artificial case

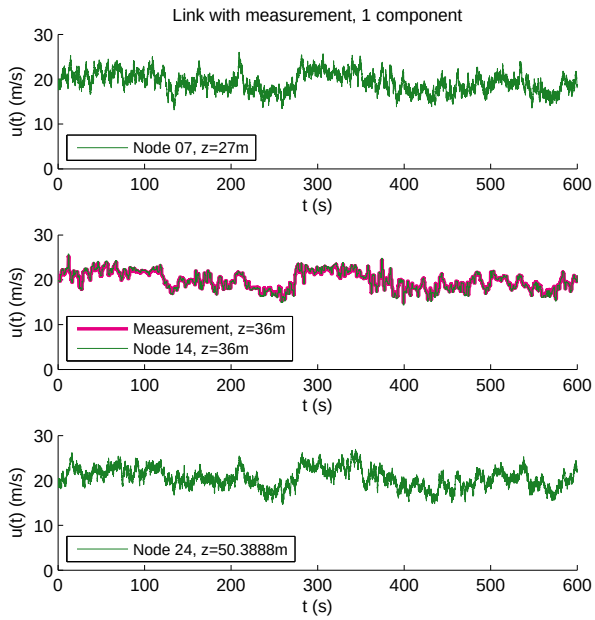


(b) Linked case

Figure 4.2: Time series of the wind speed generated using WND3D, for one realization, artificial and linked case.

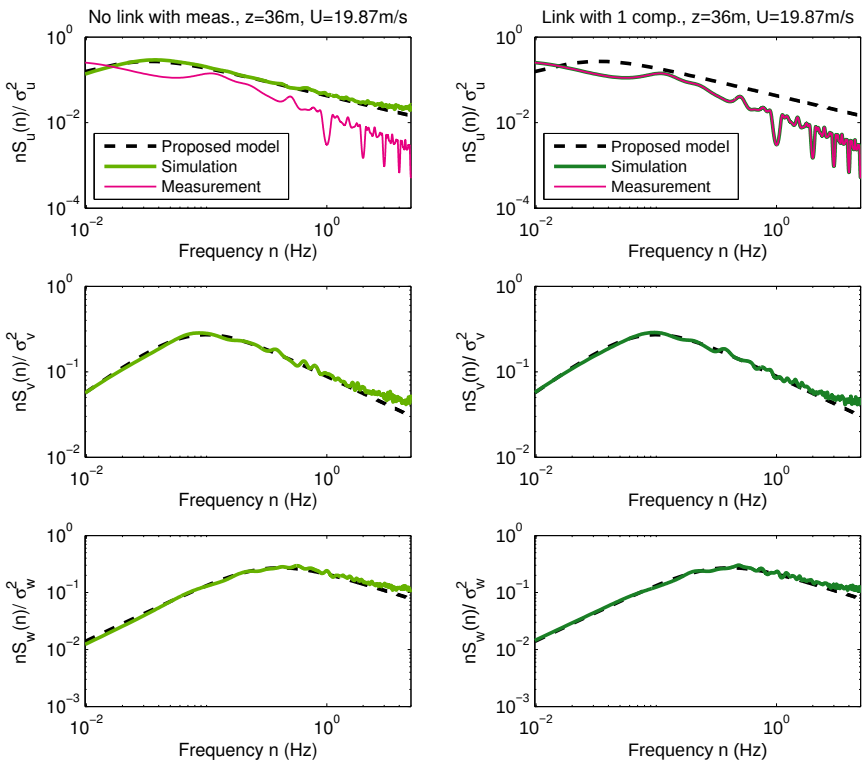


(a) Artificial case

(b) Linked case

Figure 4.3: Power spectral density of the generated wind speed at measurement height (36 m), average over 10 realizations, artificial and linked case.

**Power spectral density** The power spectral density of the generated wind is calculated using the MEM estimation. Fig. 4.3(a) shows the PSD of the three turbulence components in the artificial case. The autoregressive method used to generate the turbulent field appears to fit satisfyingly with the target spectra. When linking with measured time series, because we only link with the longitudinal component at one point, the lateral and vertical spectra are not impacted as shown on Fig. 4.3(b). For the upcoming verifications, we will limit ourselves to studying the behaviour of the longitudinal component only.

We can notice that for the selected 10-min sample, the power spectral density of the measured wind is much different from the average behaviour described in the turbulence model. Not only is the amplitude different, but the asymptotic slope also differs from the IEC requirement. We already guess that

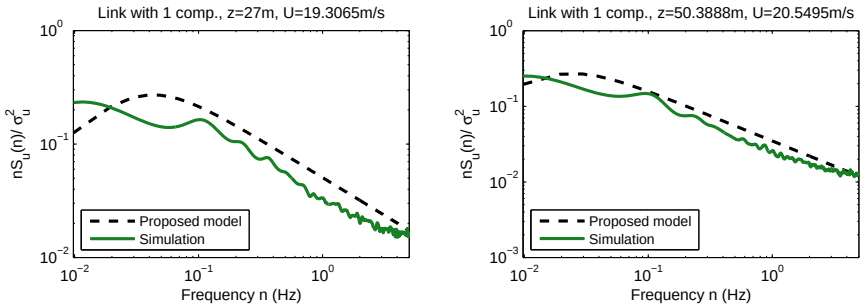


(a) At two-thirds of tower height, 27 m (b) At the highest blade tip's height, 50.4 m

Figure 4.4: Power spectral density of the generated wind at two-thirds of tower height and highest blade tip, average over 10 realizations, linked case.

linking with measured time series could significantly improve the accuracy of the generated wind by reproducing particular trends and behaviours.

In the linked case, the similarity that we have found in the time series is also observed in the frequency domain. Fig. 4.4 shows the PSD at heights below and above the measurement point in the linked case. The frequency distributions show similarities with the measurement and differ from the turbulence model.

**Coherence** The autoregressive method reproduces the target coherence satisfyingly. The target coherence is usually reached in both artificial and linked case; however, coherence with the measurement point is impacted as shown on Fig. 4.5. One possible explanation is that, in the linked case, we did not use the correlation estimate from the measurements, due to possible instability issues mentioned in section 3.2.3.2. The "correction" to fit with measurement data is done on the innovations, thus it is possible that during the generation process, the wind speed at other points is calculated to respect the coherence with the non-corrected wind speed at measurement point.

It would be interesting to see if including the correlation estimate, while ensuring stability of the process, from measured data improves this result.

**Reynolds stress** The wind has been generated with no Reynolds stress. This assumption is respected by the generated wind as shown on Fig. 4.6.

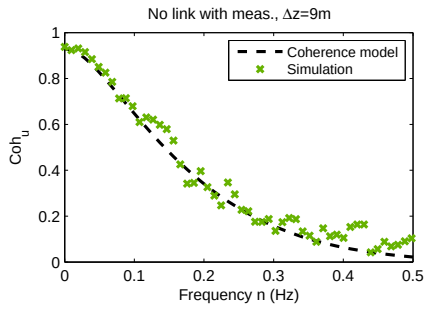


(a) Artificial case, between measurement point (node 14) and two-thirds of tower height (node 7)

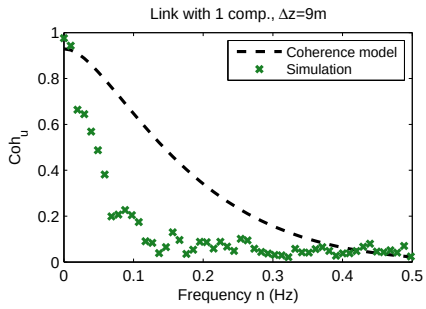


(b) Linked case, between measurement point (node 14) and two-thirds of tower height (node 7)

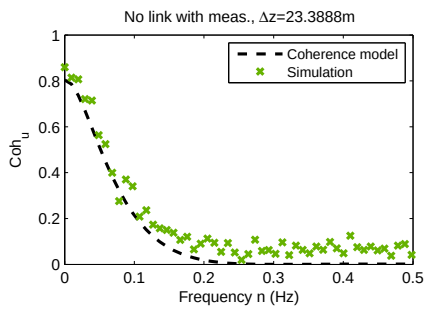


(c) Artificial case, between blade tip (node 24) and two-thirds of tower height (node 7)

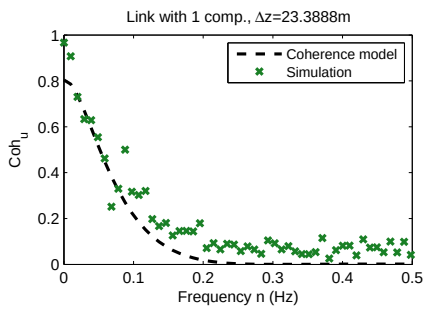


(d) Linked case, between blade tip (node 24) and two-thirds of tower height (node 7)

Figure 4.5: Coherence for longitudinal component, artificial and linked case, using the proposed turbulence model. In the linked case, the coherence involving the measurement point is impacted.

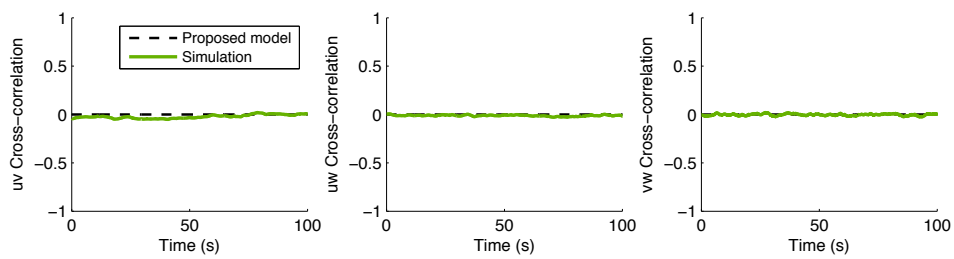


Figure 4.6: Reynolds stress correlations at 27 m. We have assumed no Reynolds stress.

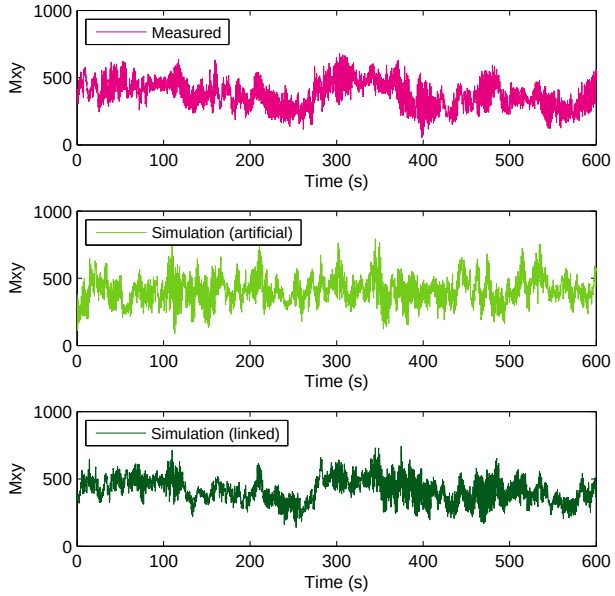


Figure 4.7: Time series of the moment at tower base for one realization. Comparison between measurement, artificial and linked case.

### 4.2.2 Reponse estimation

Using the generated turbulent wind fields, a dynamic finite element simulation is conducted with the CAsT software. The simulated response is compared to the measured response. In this section, the results obtained with the artificial and linked wind fields described in the previous section are compared, to demonstrate that the wind generation method linked to measurement data leads to a significant improvement in response estimation.

#### 4.2.2.1 Moment time series

The time series of the tower base moment are shown in Fig. 4.7. The observations that we have made on the wind field, in Fig. 4.2, also apply for the response: it is clear that in the linked case, the low-frequency trend of the measured moment is reproduced while in the artificial case the time series seem to have very little in common. This is a logical consequence of the quality of the simulated wind field, where the linked generation reproduces the measurements more accurately.

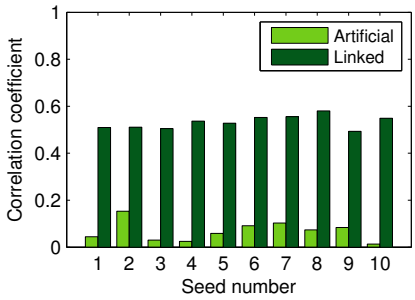


Figure 4.8: Correlation coefficients between measurement and simulations done with artificial and linked wind fields.

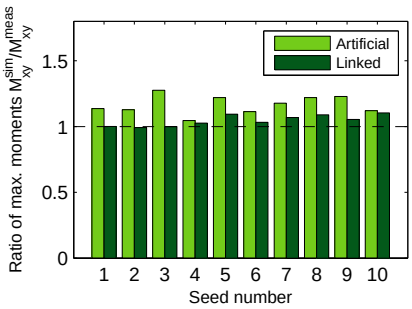


Figure 4.9: Maximum moment ratio between measurement and simulations done with artificial and linked wind fields.

Table 4.2: Correlation coefficients between simulated and measured tower base moment time series, comparison of artificial and linked case.

| Seed no. | 1 | 2 | 3 | 4 | 5 | 6 | 7 | 8 | 9 | 10 |
|---|---|---|---|---|---|---|---|---|---|---|
| Artificial | 0.045 | 0.153 | 0.030 | 0.025 | 0.059 | 0.092 | 0.103 | 0.074 | 0.084 | 0.014 |
| Linked | 0.510 | 0.511 | 0.505 | 0.537 | 0.528 | 0.552 | 0.556 | 0.580 | 0.493 | 0.549 |

#### 4.2.2.2 Correlation between simulation and measurement

As a measure of the similarity between simulated and measured moment time series in the linked case, as opposed to the artificial case, we can calculate the correlation coefficient between simulated and measured moment time series.

The (unbiased) correlation coefficient between two real sequences $\{x(t), t = 1 \dots N\}$ and $\{y(t), t = 1 \dots N\}$ is calculated as

$$\text{Corrcoef}(x,y) = \frac{1}{N-1} \frac{\sum_{t=1}^{N} (x(t)-\mu_x)(y(t)-\mu_y)}{\sqrt{\sigma_x \sigma_y}}, \tag{4.1}$$

where $\mu_x$, $\mu_y$ are the respective means of $x$ and $y$, and $\sigma_x$, $\sigma_y$ are the unbiased standard deviations of the sequences.

Fig. 4.8 and Table 4.2 show these correlation coefficients between the simulated and the measured time series of tower base moment. The coefficients are greatly increased when the external force is calculated from the wind generated with link to measured wind speed.

Table 4.3: Maximum moment ratios, comparison of artificial and linked case.

| Seed no. | 1 | 2 | 3 | 4 | 5 | 6 | 7 | 8 | 9 | 10 |
|---|---|---|---|---|---|---|---|---|---|---|
| Artificial | 1.137 | 1.128 | 1.276 | 1.046 | 1.220 | 1.113 | 1.178 | 1.220 | 1.229 | 1.121 |
| Linked | 1.000 | 0.992 | 0.999 | 1.026 | 1.094 | 1.033 | 1.069 | 1.089 | 1.054 | 1.104 |

| Seed no. | Average | Std. dev. |
|---|---|---|
| Artificial | 1.167 | 0.070 |
| Linked | 1.046 | 0.042 |

#### 4.2.2.3 Estimation of the maximum tower base moment

We have already shown that the linked method improves the correlation between the simulated and measured response. An even more interesting result is that we can also observe an improvement in the estimation of the maximum moment. In Fig. 4.9, we have calculated the ratio between the maximum moment estimated by simulation and the maximum measured moment, i.e.

$$\text{Maximum moment ratio} = \frac{M^{\text{simulated}}_{\text{tower base}}}{M^{\text{measured}}_{\text{tower base}}} \tag{4.2}$$

Results are also shown in Table 4.3.

To evaluate the accuracy of the estimation, we will consider the prediction error $e_i = M_i^{\text{simulated}} - M_i^{\text{measured}}$, with $i$ the realization index, and the bias and the standard deviation of error $\sigma_e$ defined as:

$$\text{bias} = \mathbb{E}[e_i] = \mathbb{E}[M_i^{\text{simulated}} - M_i^{\text{measured}}] \tag{4.3}$$

$$\sigma_e^2 = \mathbb{E}\left[(e_i - \text{bias})^2\right] \tag{4.4}$$

In the artificial wind case, the maximum moment overestimates the actual maximum load by an average of 16.7% over the 10 realizations. Moreover, the standard deviation of error represents 7% of the actual moment value. The estimation of the tower base moment using the artificial wind generation method does not give very stable results and tends to overestimate the load.

On the other hand, the linked wind generation method gives more stable results. The bias for 10 realizations is only 4.6% and the standard deviation of error represents 4.2% of the actual maximum moment. In some cases the results are even surprisingly perfect, such as for the first realization.

## 4.3 Linking with more than one component of measured wind speed

In this section, we will study the effect of linking the generated wind field with more than one component of measured wind speed. Section 4.2 indicated a clear improvement in response estimation when the generated wind field was linked to the times series of the longitudinal wind speed measured at one point.

Unfortunately, for the studied 400 kW wind turbine, sonic anemometer data is not available. Therefore, we will use the sonic anemometer measurements used in the turbulence model validation in section 2.5 as measured turbulence data. Since no corresponding response measurements are available, we will only conduct a numerical validation by observing the differences between the wind and the response in the two cases.

### 4.3.1 Wind field generation with link to three components of measured data

The turbulence is extracted from the measurements at Hachijojima, on March 23, 2005, between 14:20 and 14:30. The sonic anemometer was placed at 6.23 m above ground; in order to obtain a clearer comparison, the measured turbulence will be applied at the hub height instead of the actual measurement height. The standard deviation is not changed, but the mean wind speed is increased to match the measured mean wind speed at hub height, corresponding to the same 10-min sample.

#### 4.3.1.1 Simulation parameters

For the simulation, the proposed model of turbulence is chosen to parametrize the AR process.

**Wind speed and turbulence intensity profile** In WND3D, the profiles 2.4.4.1 and 2.4.4.2 are parametrized with

- ⋆ $U_0 = 17.31$ m/s and $z_0 = 36$ m,
- ⋆ $\alpha = 0.15$ (terrain category II),
- ⋆ $I_0 = 0.198$ and $z_0 = 36$ m (from measurements),
- ⋆ $\beta = 0.15$ (constant standard deviation, following the IEC),
- ⋆ For both profiles, $z_b = 5$ m is set up as the lower boundary.

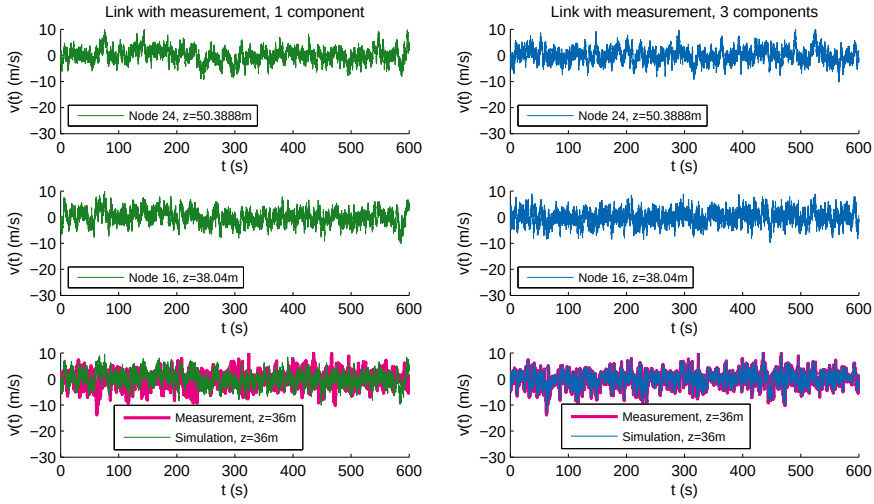


(a) Link with 1 component

(b) Link with 3 components

Figure 4.10: Time series of the generated lateral wind at several heights, link with 1 and 3 components.

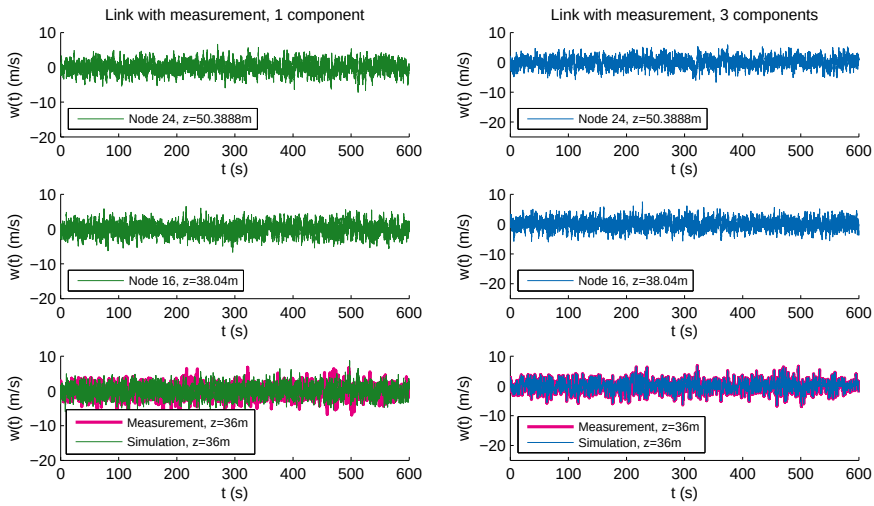


(a) Link with 1 component

(b) Link with 3 components

Figure 4.11: Time series of the generated vertical wind at several heights, link with 1 and 3 components.

Turbulence is non-isotropic and selected as indicated in the proposed model.

**Turbulence length scale** The turbulence length scales are evaluated using the formula corresponding to the proposed model, equation (2.57).

**Correlations** The correlations are evaluated using the proposed turbulence model. We will not use the measured data to estimate the correlation due to the issues mentioned in 3.2.3. We also neglect the Reynolds stress; however, due to the addition of three components of measured wind speed, where Reynolds stress is present, some cross-component correlations might appear; we will study this effect in the next part.

#### 4.3.1.2 Quality of the generated wind field

**Time series** The longitudinal component is linked in both cases so the generated longitudinal wind speed is quite similar for both fields. However, the lateral and vertical components are naturally impacted when three components of measured data are linked to the wind generation process. Fig. 4.10 and 4.11 show the lateral and vertical wind speeds at several heights in the case of linking with 1 and 3 components of measured data.

**Power spectral density and autocorrelation** Fig. 4.12 shows the power spectral densities and autocorrelations for the three components of wind speed at the measurement point. As expected the link with all three components of measurement data will influence the lateral and vertical wind components, which were not modified when there was only one component linked. Such a modification of the wind field, although occurring on seemingly less significant components of the wind since the longitudinal component is the largest in magnitude, is expected to have an impact on the estimated response of the wind turbine.

Linking with three components of measured data also influences the three components at other points, as shown on Fig. 4.13. The impact on the v and w is however quite small, since the proposed turbulence model is actually already quite close to measured data.

**Coherence** The coherence show the same properties as in Fig. 4.5, so no additional figures will be shown. It is to be remarked that the deviation from the

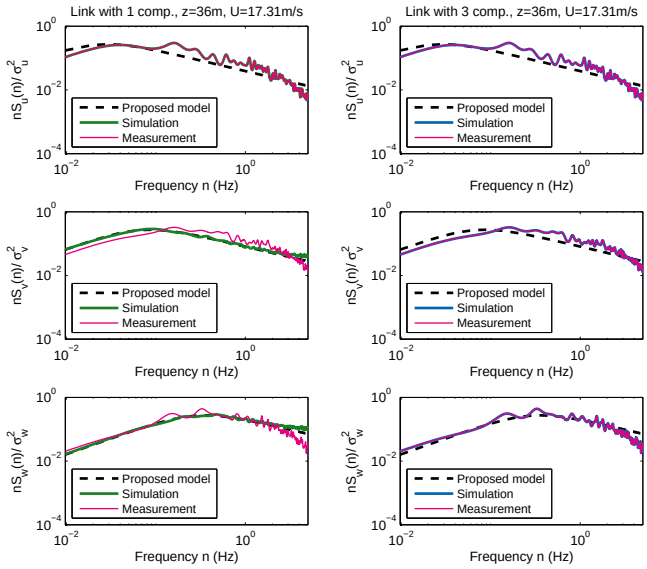


(a) Link with 1 component (b) Link with 3 components

Figure 4.12: Power spectral densities of winds generated with link to 1 and 3 components of measured data, proposed model, at hub height (measurement point).

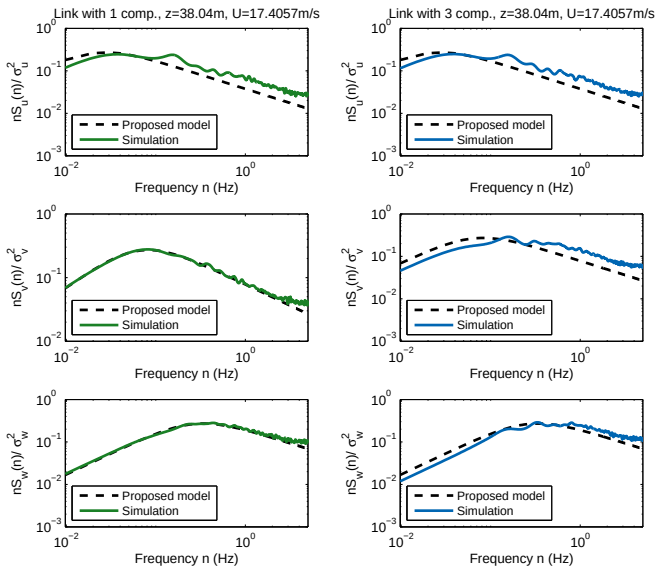


(a) Link with 1 component (b) Link with 3 components

Figure 4.13: Power spectral densities of winds generated with link to 1 and 3 components of measured data, proposed model, 2 m above hub height.

longitudinal coherence model for generated coherence involving the measurement point, Fig. 4.5(b), is also observed on the lateral and vertical coherence.

**Reynolds stress** Since the sequence of correlation matrices in the AR model have been parametrized to neglect Reynolds stress, the AR process itself will not include any cross-component correlations. However, when linking with three components of measured wind speed, the Reynolds stress correlations do exist between these three components at the measurement point.

It was thought that the cross-component correlation at measurement point could, in a way, spread to other points through the simple spatial relationships that exist for same-component cross-correlation (or coherence). Actually, comparing Fig. 4.14 to Fig. 4.15, this spreading effect seems insufficient to account for the Reynolds stress that we defined in the turbulence model based on actual observations.

### 4.3.2 Response estimation

The wind fields with link to 1 and 3 components are both applied on the wind turbine structure to estimate its response by finite element simulation. Since no measured response is available to use as a reference, the two simulated responses will simply be compared. Fore-aft moment (around the $y$-axis) and side-by-side moment (around the $x$-axis) are studied separately.

#### 4.3.2.1 Moment time series

One realization of the times series of the tower base moment, for the two simulation cases, is shown in Fig. 4.16. Although they are quite similar, some differences between the two estimated responses are visible, in particular for the side-by-side moment $M_x$.

#### 4.3.2.2 Estimation of the maximum moment

To quantify the differences, the maximum estimated moment for each simulation is compared, Fig. D.12. Numerical values are also given in Table 4.4 and Table 4.5. On average (over the 10 realizations), it appears that the maximum moment estimated with only one linked component is between 2.7% (fore-aft) and 4.9% (side-by-side) higher than with three components. The results of the estimation are also more stable with three components, as shown by the standard

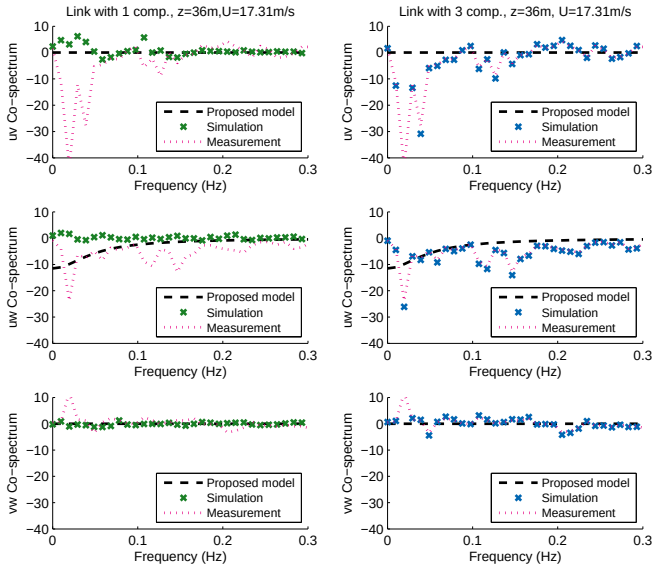


(a) Link with 1 component (b) Link with 3 components

Figure 4.14: Co-spectrum (Reynolds stress), link with 1 and 3 components, hub height (measurement point).

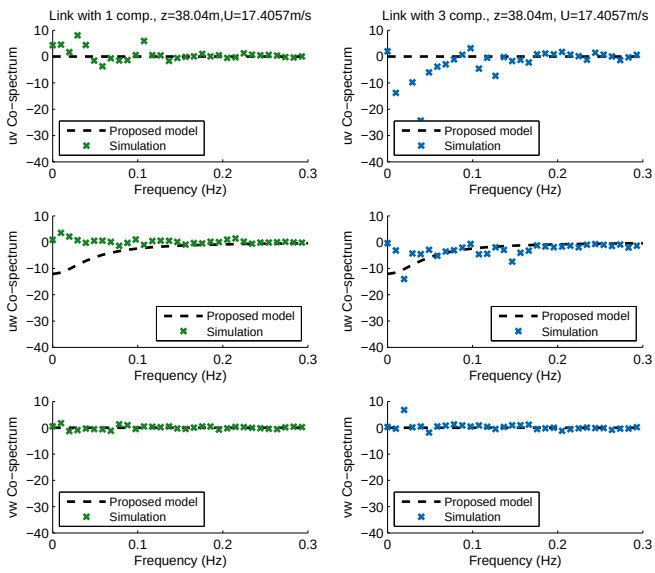


(a) Link with 1 component (b) Link with 3 components

Figure 4.15: Co-spectrum (Reynolds stress), link with 1 and 3 components, 2 m above hub height.

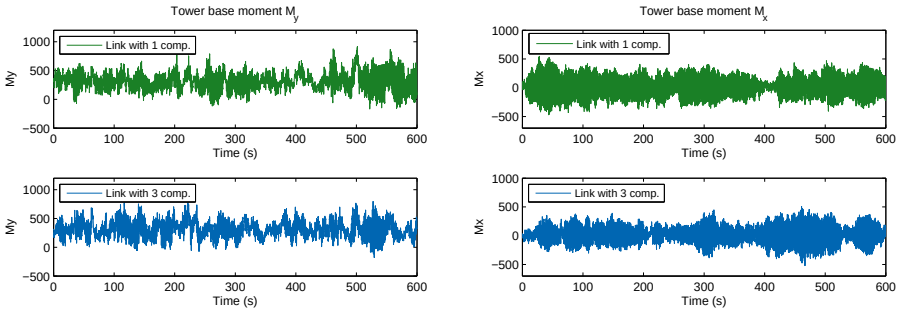


(a) Fore-aft (b) Side-by-side

Figure 4.16: Times series of the tower base moment, simulation using wind fields with link to 1 and 3 components of measured data. The moments are shown in kNm.

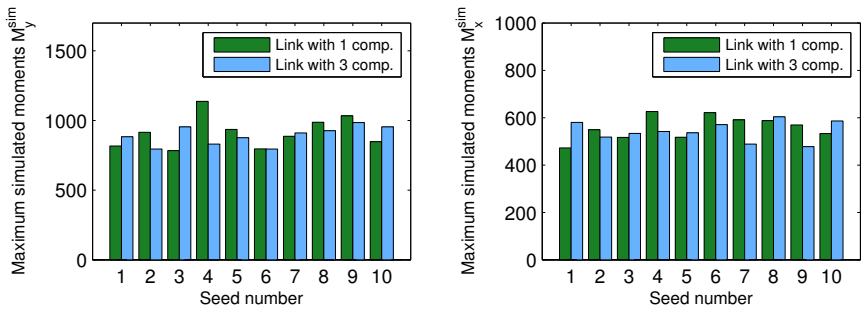


(a) Fore-aft (b) Side-by-side

Figure 4.17: Maximum tower base moment, simulation with link to 1 and 3 components of measured wind speed. The moments are shown in kNm.

deviation of the estimated moments for 10 realizations: for the fore-aft moment, it is reduced by more than half.

Although it would be advised to conduct additional simulations for cases when measured response is available, the intuition would dictate that the estimation is more accurate when more measurement data is included. This numerical validation is an encouraging step to show that including several components of measured data, maybe at several measurement points if possible, can improve the estimation of the wind turbine response.

Table 4.4: Values of the maximum simulated fore-aft moment when linked to 1 and 3 components of measured wind speed, 10 realizations. The moments are shown in kNm.

| | Seed no. | 1 | 2 | 3 | 4 | 5 | 6 |
|---|---|---|---|---|---|---|---|
| $M_y$ | 1 comp. | 816.80 | 915.60 | 783.40 | 1137.80 | 935.60 | 796.20 |
| | 3 comp. | 883.30 | 794.80 | 954.00 | 830.50 | 876.50 | 794.60 |

| | Seed no. | 7 | 8 | 9 | 10 | Average | Std. dev. |
|---|---|---|---|---|---|---|---|
| $M_y$ | 1 comp. | 886.80 | 987.40 | 1032.60 | 847.60 | 897.57 | 133.65 |
| | 3 comp. | 910.40 | 927.30 | 985.00 | 954.20 | 855.62 | 61.54 |

Table 4.5: Values of the maximum simulated side-by-side moment when linked to 1 and 3 components of measured wind speed, 10 realizations. The moments are shown in kNm.

| | Seed no. | 1 | 2 | 3 | 4 | 5 | 6 |
|---|---|---|---|---|---|---|---|
| $M_x$ | 1 comp. | 472.39 | 548.90 | 516.86 | 626.17 | 517.29 | 621.10 |
| | 3 comp. | 580.12 | 518.11 | 533.79 | 541.98 | 536.36 | 570.77 |

| | Seed no. | 7 | 8 | 9 | 10 | Average | Std. dev. |
|---|---|---|---|---|---|---|---|
| $M_x$ | 1 comp. | 591.22 | 587.83 | 569.45 | 532.88 | 558.41 | 47.06 |
| | 3 comp. | 488.63 | 603.70 | 477.99 | 586.38 | 543.78 | 39.55 |

## 4.4 Summary of the results

In this chapter, we have used the proposed turbulence model to parametrize the autoregressive wind generation method. The autoregressive method can be used in its original form, without link to the measured data (artificial case); it can also be used with a link to the measured wind speed time series (linked case).

A turbulent wind field has been generated using both methods, and applied in CAsT to compute aerodynamic loads and obtain the response of the structure under each wind field. We have compared the simulated results with the measurements of the moment at the tower base. It appears that the linked wind generation method yields improved correlation between the simulated and measured moment time series, and that the estimation of the maximum moment at the tower base is also much more accurate.

Moreover, we have compared the effect of including three components of measured wind rather than one. The results indicate that a larger amount of included information from measurements increase the stability of the estimations

over several realizations. In this study, only a numerical validation has been conducted since actual measurements with three components were not available for the 400 kW wind turbine; additional studies should be done to confirm this result and assess the improvement quantitatively.

Improvements in the maximum load estimation is crucial for issues like fatigue estimation. For example in the case we have studied, thanks to the reduced overestimation, we could conclude that the structure may have borne less than the design fatigue loads, and decide to extend the lifetime of the wind turbine.

Conversely, in some cases, the improved method might reduce the underestimation of loads, and make us realize that the actual loads are larger than the design loads. Then, the operator can control the load on the wind turbine by adjusting the blade pitch or forcing the turbine to stall. It can also lead to an updated estimation of fatigue loads, and induce a shorter lifespan for the structure.

# Chapter 5

# Conclusion

In the physical model-based condition monitoring method, one of the major conditions to have an accurate load estimation is to provide an accurate external force. For wind turbines, the main forces to consider are the aerodynamic loads, which are nonlinearly dependent on the turbulent wind flow. More generally, a time-domain simulation is necessary to understand the dynamic response of the wind turbine, but common turbulence descriptions are only provided in the frequency domain. The main objective of this thesis was to develop a new approach to describe turbulence, by proposing a new turbulence model available in both frequency and time-domain. The proposed model must satisfy the IEC requirements and be validated by measurements. Additionally, the new turbulence model shall be used to generate a wind field, which is then applied on a finite element simulation to estimate the wind turbine response.

First, Kaimal's and von Karman's turbulence models were reviewed. The IEC suggested the Kaimal model, which has the advantage of being empirical but is only available in the frequency domain. On the other hand, Von Karman's turbulence model is a theoretical model provided in both time and frequency domain. The shortcoming of von Karman's model was that it did not describe lateral and vertical turbulence accurately. The proposed model takes advantage of von Karman's relationships between time and frequency domain descriptions, and modifies it based on the empirical observations of Kaimal's model. Additionally, parameters of the model are adjusted to satisfy the IEC requirements. The proposed model has been validated using long-term measurements of a sonic anemometer.

To evaluate the quality of the proposed turbulence model, it was used to

parametrize an autoregressive wind generation method. The wind generation method is given in two forms: the "artificial" method, where only the mean wind speed and standard deviation of the measured wind speed are used, and the "linked" one, which also allows to include the whole time series of the measured wind speed. It is implemented in the WND3D software, in which Iwatani's autoregressive method is modified to take the time domain descriptions of turbulence as an input, directly. Wind fields are generated with and without link with measured data, and as a first approach by neglecting the Reynolds stress; they were shown to satisfy the target turbulence characteristics.

The generated wind fields were then applied on a finite element simulation and the estimated responses were compared to measurements. To quantify the accuracy of the estimation, we compared the correlation between the estimated and measured tower base moment time series as well as the accuracy of the estimated maximum tower base moment. The first part of the study compares the estimated responses using the artificial and the linked method. It shows that, as expected, the wind generated with the linked method leads to a much higher correlation between estimated and measured moment time series, and the maximum moment is also better estimated. A second study aimed at evaluating the benefit of linking with three components of measured data rather than just one. Although there were no measured response available for comparison, the results were shown to differ quite significantly between linking with one and three components, and it is expected that including more measurement data will improve the estimation.

These results show that the proposed turbulence model not only satisfies the international standards' requirements and empirical data, but it also yields better estimation results for application in physical model-based condition monitoring of wind turbines. It also indicates that linking the generated wind field with some measurement data is beneficial for the accuracy of the response estimation.

This research has, however, shown some limits. In particular, although the proposed turbulence model provides a description for the Reynolds stress correlation between the longitudinal and vertical components, it neglects the correlation between the longitudinal and lateral components which appears to be non-negligible in the measured data. Additionally, the autoregressive wind generation method, in its current implementation, cannot be solved accurately and reliably when cross-component correlations are considered. The current algo-

rithm is using the Yule-Walker equations to find the autoregressive model parameters; another way to estimate the parameters should be considered in future implementations.

In any case, a generalization and automation of the wind generation process, in particular real time updating of the autoregressive parameters, shall be conducted for practical application in a condition monitoring context.

Arguably, additional steps towards mathematical and statistical rigour might also be necessary. As often happens with first approaches, random variables were generally supposed to be Gaussian. A closer look at the probabilistic aspects of stochastic wind modelling might give interesting insights.

# Appendix A

# Spectral analysis of signals

This appendix gives an idea of the basic spectral analysis concepts used in the thesis. Detailed mathematical background can be found in textbooks such as *Spectral Analysis of Signals* by Stoica and Moses [21], from which the title of this appendix is taken. Another useful book is *Numerical Recipes* [19], which gives the reader a more practical vision on spectral analysis, although one must be careful of the simplifications and unspoken assumptions of the authors.

The reader is invited to read more about other methods not mentioned here, such as the maximum entropy method (MEM) to estimate the power spectral density. Although it has been used in the thesis rather than the periodogram estimate described here, the periodogram approach is easier to understand and implement as a first approach, and has the advantage of being less sensitive to parameter choices than the MEM.

## A.1 Definitions

### A.1.1 Notation

Some general variables to be used in this appendix are given below.

- ⋆ $t$ is generally a real variable, representing time in seconds, and $\Delta t$ is generally a time interval,
- ⋆ $f$ is a frequency in Hz, and $f_s = 1/\Delta t$ is the sampling frequency,
- ⋆ $\omega$ is an angular frequency in rad/s,
- ⋆ a normalized angular frequency is defined as $\overline{\omega} = \omega \Delta t$, in cycles per sampling interval,

⋆ $n, k, m$ are integers, used to index discrete sequences.

We will use small letters (such as $x$) to denote signals in the time domain, and the corresponding capital letter (like $X$) to denote their Fourier transform. Also, we will use brackets to denote functions of a discrete variable (such as $f[n]$) and parentheses for functions of a continuous variable (such as $f(t)$).

### A.1.2 Fourier transform

#### A.1.2.1 Integral definition

For an integrable function $x : \mathbb{R} \to \mathbb{C}$, we can define its Fourier transform by

$$X(\xi) = \int_{-\infty}^{\infty} x(t) \exp(-2\pi i f t) \mathrm{d}t \tag{A.1}$$

where $i = \sqrt{-1}$, $t$ represents time (seconds) and $f$ represents frequency (Hertz). The sign of the argument for the exponential term depends on conventions; we will use this expression as it is the one found in most of the references used for this study.

Under suitable conditions, which are related to the Fourier inversion theorem and that we will assume are satisfied, the original function $x$ can be recovered by the inverse Fourier transform,

$$x(t) = \int_{-\infty}^{\infty} X(f) \exp(2\pi i f t) \mathrm{d}f \tag{A.2}$$

We can also write these expressions using the angular frequency $\omega = 2\pi f$ (in rad/s), giving

$$X(\omega) = \int_{-\infty}^{\infty} x(t) \exp(-i\omega t) \mathrm{d}t$$
$$x(t) = \frac{1}{2\pi} \int_{-\infty}^{\infty} X(\omega) \exp(i\omega t) \mathrm{d}\omega$$

$x$ is typically a continuous-time signal. In the next sections, we will see how the Fourier transform can be applied to discrete samples of such a signal, and how it can be used when only a limited number of samples is available.

#### A.1.2.2 Discrete-time Fourier transform (DTFT)

Let $\{y[n], n \in \mathbb{Z}\}$ be a deterministic discrete-time data sequence, for example obtained from sampling a continuous-time signal, such as the function $x$ of the previous section. We have, for a sampling interval $\Delta t$,

$$y[n] = x(n\Delta t) \tag{A.3}$$

Under the assumption that $\{y[n]\}$ has finite energy, i.e. $\sum |y[n]|^2 < \infty$, we can define the DTFT of the sequence by

$$Y(\overline{\omega}) = \sum_{t=-\infty}^{\infty} y[t] \exp(-i\overline{\omega}t) \tag{A.4}$$

where $\overline{\omega}$ is the normalized angular frequency, or number of cycles per sampling interval, i.e. $\overline{\omega} = \omega\Delta t$. The corresponding inverse DTFT (iDTFT) is obtained by

$$y[n] = \frac{1}{2\pi} \int_{-\pi}^{\pi} Y(\overline{\omega}) \exp(i\overline{\omega}n) \mathrm{d}\overline{\omega} \tag{A.5}$$

We can also define the frequency $f = 2\pi\omega$ and the normalized frequency $\overline{f} = 2\pi\overline{\omega} = f/f_s$, where $f_s = 1/\Delta t$ is the sampling frequency.

#### A.1.2.3 Discrete Fourier transform (DFT)

The discrete Fourier transform is related to the DTFT, but instead of having an infinite sequence, we consider a sequence with a finite number of values. The finite sequence can be obtained by windowing the infinite sequence $\{y[n]\}$ that we used to define the DTFT. Let's denote this finite sequence $\{\tilde{y}[n], n = 0, \ldots, N-1\}$.

The DFT is defined as

$$\tilde{Y}[k] = \sum_{n=0}^{N-1} \tilde{y}[n] \exp(-2\pi i \frac{k}{N} n); \tag{A.6}$$

and the inverse DFT (iDFT) is

$$\tilde{y}[n] = \frac{1}{N} \sum_{k=0}^{N-1} \tilde{Y}[k] \exp(-2\pi i \frac{n}{N} k). \tag{A.7}$$

Table A.1: Properties of Fourier transform of a function depending on the function's characteristics

| Time-domain function | Fourier transform |
|---|---|
| $h(t)$ is real | $H(-f) = H(f)^*$ |
| $h(t)$ is imaginary | $H(-f) = -H(f)^*$ |
| $h(t)$ is even | $H(f)$ is even |
| $h(t)$ is odd | $H(f)$ is odd |
| $h(t)$ is real and even | $H(f)$ is real and even |
| $h(t)$ is real and odd | $H(f)$ is imaginary and odd |
| $h(t)$ is imaginary and even | $H(f)$ is imaginary and even |
| $h(t)$ is imaginary and odd | $H(f)$ is real and odd |

#### A.1.2.4 Properties of Fourier transforms

The Fourier transform has interesting properties that can be leveraged for spectral analysis.

**Special cases** When the signal has particular properties, such as symmetry, its Fourier transform also has remarkable properties. Table A.1 summarizes these properties.

**Convolution and correlation theorem** The convolution of two functions $g$ and $h$ is defined as

$$g * h(t) = \int_{-\infty}^{\infty} g(\tau)h(t-\tau)\mathrm{d}\tau. \tag{A.8}$$

The *convolution theorem* says that the Fourier transform of the convolution is the product of the Fourier transforms:

$$g * h(t) \underset{\text{Fourier transform}}{\Longleftrightarrow} G(f)H(f) \tag{A.9}$$

where $G$ and $H$ are the respective Fourier transforms of $g$ and $h$.

From there, we can derive the *correlation theorem*. The (continuous variable) correlation is defined by

$$\mathrm{Corr}(g,h)(t) = \int_{-\infty}^{\infty} g(t+\tau)h(\tau)\mathrm{d}\tau. \tag{A.10}$$

which gives us the correlation theorem:

$$\mathrm{Corr}(g,h)(t) \underset{\text{Fourier transform}}{\Longleftrightarrow} G(f)H(-f) \tag{A.11}$$

For the purpose of our study, we work with physical variables, therefore the signals or functions only take real values. The correlation theorem can then be rewritten:

$$\mathrm{Corr}(g,h)(t) \underset{\text{Fourier transform}}{\Longleftrightarrow} G(f)H(f)^* \tag{A.12}$$

from the properties in Table A.1.

The autocorrelation is a particular case, and for real signals it belongs to the Fourier transform pair

$$\mathrm{Corr}(g,g)(t) \underset{\text{Fourier transform}}{\Longleftrightarrow} |G(f)|^2 \tag{A.13}$$

This property is also called the *Wiener-Khinchin theorem*.

### A.1.3 Energy spectral density and Power spectral density

#### A.1.3.1 Energy spectral density of deterministic signals

The energy spectral density is defined from the DTFT as

$$S(\overline{\omega}) = |Y(\overline{\omega})|^2 \tag{A.14}$$

from which it appears that

$$\frac{1}{2\pi}\int_{-\pi}^{\pi} S(\overline{\omega})\mathrm{d}\overline{\omega} = \sum_{t=-\infty}^{\infty} |y[n]|^2 \tag{A.15}$$

(Parseval's theorem)

Defining the covariance series as

$$\rho(k) = \sum_{n=-\infty}^{\infty} y[n]y[n-k]$$

we can derive the following relationship with the energy spectral density.

$$\sum_{k=-\infty}^{\infty} \rho(k) = S(\overline{\omega})$$

#### A.1.3.2 Power spectral density of random signals

When the signal is no longer deterministic but is a random process, the sequence $\{y[n], n \in \mathbb{Z}\}$ is random sequence. Contrary to the deterministic sequence, the realizations of the random sequence *do not have finite energy*, and thus the previous definition cannot be used as is. However, the random signal has finite average power, which allows us to define an average power spectral density, or simply power spectral density (PSD).

In what follows, the discrete-time signal $\{y[n]\}$ is a *stationary* sequence of random variables with *zero mean*, i.e.

$$\forall n \in \mathbb{Z} \quad \mathbb{E}(y[n]) = 0 \tag{A.16}$$

$$\forall n, k \in \mathbb{Z} \quad r(k) = \mathbb{E}(y[n]y^*[n-k]) \tag{A.17}$$

Equation (A.17) defines the autocovariance sequence, or covariance function, of $y$. Some basic properties of the covariance function are:

$$r(k) = r^*(-k) \tag{A.18}$$

$$r(0) \geq |r(k)| \quad \text{for all } k \tag{A.19}$$

Equation (A.18) is easily derived from (A.17), while (A.19) comes from the positive semidefiniteness of the covariance matrix:

$$\begin{aligned} R_m &= \begin{pmatrix} r(0) & r^*(1) & \cdots & r^*(m-1) \\ r(1) & r(0) & \ddots & \vdots \\ \vdots & \ddots & \ddots & r^*(1) \\ r(m-1) & \cdots & r(1) & r(0) \end{pmatrix} \\ &= \mathbb{E}\left[ \begin{pmatrix} y^*(n-1) \\ \vdots \\ y^*(n-m) \end{pmatrix} \begin{pmatrix} y(n-1) & \cdots & y(n-m) \end{pmatrix} \right] \end{aligned} \tag{A.20}$$

for all $a \in \mathbb{C}^m$,

$$\begin{aligned} a^* R_m a &= a^* \mathbb{E}\left[z^*(n) z(n)\right] a \\ &= \mathbb{E}\left[|z(n)a|^2\right] \geq 0 \end{aligned} \tag{A.21}$$

The properties of positive semidefinite matrices lead to (A.19). The power spec-

tral density can then be defined two ways.

**First definition** The PSD can be defined as the DTFT of the covariance function

$$\phi(\overline{\omega}) = \sum_{k=-\infty}^{\infty} r(k)\exp(-i\overline{\omega}k) \tag{A.22}$$

and the inverse transformation to recover $r(k)$ is given by

$$r(k) = \frac{1}{2\pi}\int_{n=-\pi}^{\pi} \phi(\overline{\omega})\exp(i\overline{\omega}t)\mathrm{d}\overline{\omega} \tag{A.23}$$

**Second definition**

$$\phi(\overline{\omega}) = \lim_{N\to\infty} \mathbb{E}\left[\frac{1}{N}\left|\sum_{n=1}^{N} y[n]\exp(-i\overline{\omega}n)\right|^2\right] \tag{A.24}$$

The second definition is equivalent to the first under the condition that the covariance function $r(k)$ decays sufficiently rapidly.

For all these definitions, the power spectral density is a periodic function, with a period of $2\pi$. The description of the PSD can therefore be reduced to the interval $\overline{\omega} \in [-\pi, \pi]$. In terms of the "real" frequency, since we have $\overline{\omega} = 2\pi f/f_s$, the corresponding interval is $f \in [-f_s/2, f_s/2]$. The frequency $f_c = f_s/2$ is also called *Nyquist* or *critical frequency*; it defines the largest frequency range that can be used to reconstruct the original signal exactly without aliasing effects.

## A.2 Estimation of the Power Spectral Density

In all the previous definitions of the power spectral density, we have considered a discrete-time signal, made of an infinite number of samples of a continuous-time random signal. However, for practical applications, we can only obtain a finite number of data from observations of the random signal. Thus, the only available information that we have is an *estimate* of the PSD of the signal.

In this section we will study non-parametric methods to estimate the PSD of a random process when only a limited number of observations is available. The data will be denoted as a finite-length sequence of N observations, $\{y[n], n \in \{1, \ldots, N\}\}$.

### A.2.1 Periodogram and correlogram estimate

**Periodogram estimate** The periodogram method is based on the second definition of the PSD (A.24). It is defined as

$$\hat{\phi}_p(\overline{\omega}) = \frac{1}{N}\left|\sum_{n=1}^{N} y[n]\exp(-i\overline{\omega}n)\right|^2 \tag{A.25}$$

where we can see that the limit and expectation operators of the PSD definition have been ignored, since they cannot be applied.

As a side note, we can understand this formula as the "averaged" squared magnitude of the DFT, with $\overline{omega} = 2\pi\frac{k}{N}n$ to satisfy equation (A.6).

**Correlogram estimate** The correlogram is based on the other definition (A.22).

$$\hat{\phi}_c(\overline{\omega}) = \sum_{k=-(N-1)}^{N-1} \hat{r}(k)\exp(-i\overline{\omega}n) \tag{A.26}$$

in which the covariance function $r(k)$ has been replaced by its estimate $\hat{r}(k)$.

Two estimates are available for the covariance function:

⋆ Unbiased covariance estimate:

$$\hat{r}(k) = \frac{1}{N-k}\sum_{m=k+1}^{N} y[m]y^*[m-k] \quad 0 \le k \le N-1 \tag{A.27}$$

⋆ Biased covariance estimate:

$$\hat{r}(k) = \frac{1}{N}\sum_{m=k+1}^{N} y[m]y^*[m-k] \quad 0 \le k \le N-1 \tag{A.28}$$

Following the textbook [21], we will used the biased estimate as it guarantees the positive semidefiniteness of the covariance sequence, and thus the positivity of the PSD estimate. Additionally, using the biased estimate of the covariance function allows the periodogram and the correlogram estimates of the PSD to coincide for all $\overline{\omega}$.

In the next parts, we will mostly discuss the periodogram estimate as it is the most used method. Its advantage is that it can be easily computed by FFT of the data sequence, rather than needing the additional step of estimating the covariance function.

### A.2.2 Properties of the periodogram estimate

To evaluate the quality of the estimate, the statistical properties of the estimator must be assessed.

#### A.2.2.1 Bias

The periodogram estimate is asymptotically unbiased. It has however some leakage and smearing effects that might be troublesome for small samples.

#### A.2.2.2 Variance

The asymptotic variance/covariance of the periodogram estimate is given, for a general complex linear signal, by

$$\lim_{N\to\infty} \mathbb{E}\left([\hat{\phi}_p(\omega_1)-\phi(\omega_1)][\hat{\phi}_p(\omega_2)-\phi(\omega_2)]\right) = \begin{cases} \phi^2(\omega_1) & \text{if } \omega_1=\omega_2 \\ 0 & \text{if } \omega_1\neq\omega_2 \end{cases} \tag{A.29}$$

The result is similar for real-valued signals.

It means that the expectation and standard deviation of the periodogram estimate are equal to the corresponding true PSD value. Additionally, (A.29) implies that the periodogram values are asymptotically uncorrelated, thus making the estimator display an erratic behaviour similar to white noise.

Modified periodogram methods are introduced in the next section to improve the estimation by decreasing the variance.

### A.2.3 Modified periodogram methods

The large variance of the periodogram/correlogram estimate can be qualitatively explained by the fact that, according to the definition(A.26), the estimator of the covariance function $\hat{r}(k)$ is not very accurate especially for large absolute values of $k$, and the small errors in the covariance estimation are summed in $\phi_c(\overline{\omega})$. Intuitively, reducing the number of terms in the summation by removing the extreme ends of the covariance estimate could reduce this estimation error. The Blackman-Tukey (BT) method takes advantage of this idea, while other methods, such as the Welch method, are seeking to improve the BT estimator.

#### A.2.3.1 Blackman-Tukey estimator

The Blackman-Tukey estimator is defined as

$$\hat{\phi}_{BT}(\overline{\omega}) = \sum_{k=-(M-1)}^{M-1} w(k)\hat{r}(k)\exp(-i\overline{\omega}k) \tag{A.30}$$

with $M < N$, and where $w(k)$ is a window function, even (symmetric around 0) and such that $w(0) = 1$, $w(k) = 0$ for $|k| \geq M$ and decaying smoothly to zero.

Let $W(\overline{\omega})$ be the DTFT of $w(k)$.

$$W(\overline{\omega}) = \sum_{k=-\infty}^{\infty} w(k)\exp(-i\overline{\omega}k) = \sum_{k=-(M-1)}^{M-1} w(k)\exp(-i\overline{\omega}k) \tag{A.31}$$

Using the convolution theorem, we can write

$$\begin{aligned}
\hat{\phi}_{BT}(\omega) &= \sum_{k=-\infty}^{\infty} w(k)\hat{r}(k)\exp(-i\overline{\omega}k) \\
&= DTFT(\hat{r}(k)) * DTFT(w(k)) \\
&= \hat{\phi}_p(\omega) * W(\omega) \\
&= \frac{1}{2\pi}\int_{-\pi}^{\pi} \hat{\phi}_p(\psi)W(\omega-\psi)\mathrm{d}\psi
\end{aligned} \tag{A.32}$$

where $*$ denotes the convolution operator. The Blackman-Tukey estimator can therefore be interpreted as a "locally weighted average" of the periodogram, resulting in a "smoother" result.

It is shown in [21] that using this method, the resolution is proportional to $1/M$ while the variance is in the order of $M/N$, meaning that there is a trade-off between resolution and improvement of the variance.

#### A.2.3.2 Bartlett method and Welch method

The Bartlett method aims at reducing the fluctuations of the periodogram by splitting the available data, $N$ observations, into $K = N/M$ subsamples of M observations each. A periodogram estimate is obtained from each subsample, and all of them are then averaged. It has, however, a higher variance than the BT estimate, and lacks in windowing flexibility as it uses a fixed rectangular window (see details in [21]).

A variation on this method is proposed by Welch [28]. First, the subsamples

of data are allowed to overlap (increasing the number of data segments). Additionally, each segment is windowed before calculating the periodogram, in a similar way to the BT method. Let's define the data segments as

$$y_j(n) = y((j-1)L+n) \quad n = 1, ..., M \text{ and } j = 1, ..., K \tag{A.33}$$

where $M$ is the size of each segment, $K = N/M$ is the number of segments and $S$ depends on the overlap: $S = M$ if the segments do not overlap, and the recommended value is $S = M/2$ for 50% overlap.

For each segment, the windowed periodogram is computed as

$$\hat{\phi}_j(\omega) = \frac{1}{MW_s}\left|\sum_{n=1}^{M} w(n)y_j(n)\exp(-i\omega n)\right|^2 \tag{A.34}$$

where $W_s$ is the "power" of the window $w(n)$

$$W_s = \frac{1}{M}\sum_{n=1}^{M}|w(n)|^2 \tag{A.35}$$

The Welch estimate is then calculated as the average of the windowed periodograms.

$$\hat{\phi}_W(\omega) = \frac{1}{K}\sum_{j=1}^{K}\hat{\phi}_j(\omega) \tag{A.36}$$

In our study, we will use the Welch method to estimate the PSD.

**Remark:** The Bartlett and Welch methods can both be considered as a BT-type estimator. In [21], it is mentioned that although Welch's modified periodogram is the most commonly used method, and that it empirically gives better results that the Bartlett method, it is still theoretically less favourable than the Blackman-Tukey estimate.

### A.2.4 Cross-spectral densities

For cross-spectral densities, we can use the first definition of the PSD using the correlation, (A.22), using the cross-correlation instead of the autocorrelation.

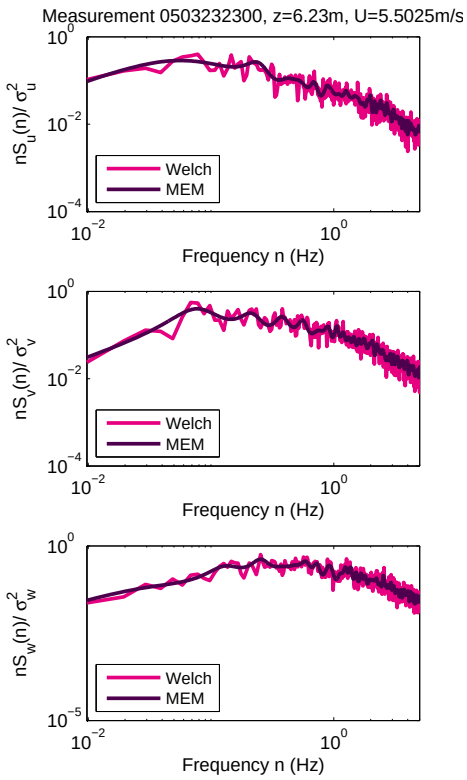


Figure A.1: Comparison of Welch's periodogram and MEM estimates.

The second definition, (A.24), becomes:

$$\phi(\overline{\omega}) = \lim_{N\to\infty} \mathbb{E}\left[\frac{1}{N}\left(\sum_{n=1}^{N} y_1[n]\exp(-i\overline{\omega}n)\right)\left(\sum_{n=1}^{N} y_2[n]\exp(-i\overline{\omega}n)\right)\right]. \quad \text{(A.37)}$$

The periodogram and correlogram estimates can be similarly adapted.

## A.3 Comparison of Welch's method and the MEM

The Maximum Entropy Method is another way to estimate the PSD. Although the choice of the MEM order can be tricky sometimes [19], we used Welch's periodogram estimate to calibrate this parameter. The comparison of the two methods, Fig. A.1, shows that the MEM is a smoother PSD estimate.

# Appendix B

# Reynolds stress

The proposed turbulence model includes a relationship between the longitudinal and vertical component, that we have called "$u\,w$ Reynolds stress". Although this relationship has been observed on real wind (as seen in this thesis in section 2.5), we have decided to neglect it due to issues with the autoregressive model, mentioned in 3.3.

In fact, the addition of Reynolds stress in the correlation matrix increases the complexity of the AR model, by adding a relationship between the $u$ and $w$ components, which are already conditioned by their own correlation models.

This appendix summarizes the observations that have been made when trying to generate a wind with Reynolds stress and suggests some corrections.

## B.1 Generation of a wind field with Reynolds stress

It appeared quite early that using the same AR order than for the generation without Reynolds stress lead to errors in the numerical resolution of the Yule-Walker equations. This order has been reduced, but still problems appears when we tried to generate a full field covering the entire area of the wind turbine. The following results have been obtained using the proposed model, without link to measurements, with the parameters described in section 4.2. The AR order has been reduced to 30, and the turbulence has been generated at only three different points, aligned on a vertical axis. These points are node 2, 7 and 10 of the wind turbine model; their respective height above ground is 4.5 m, 27 m and 35 m.

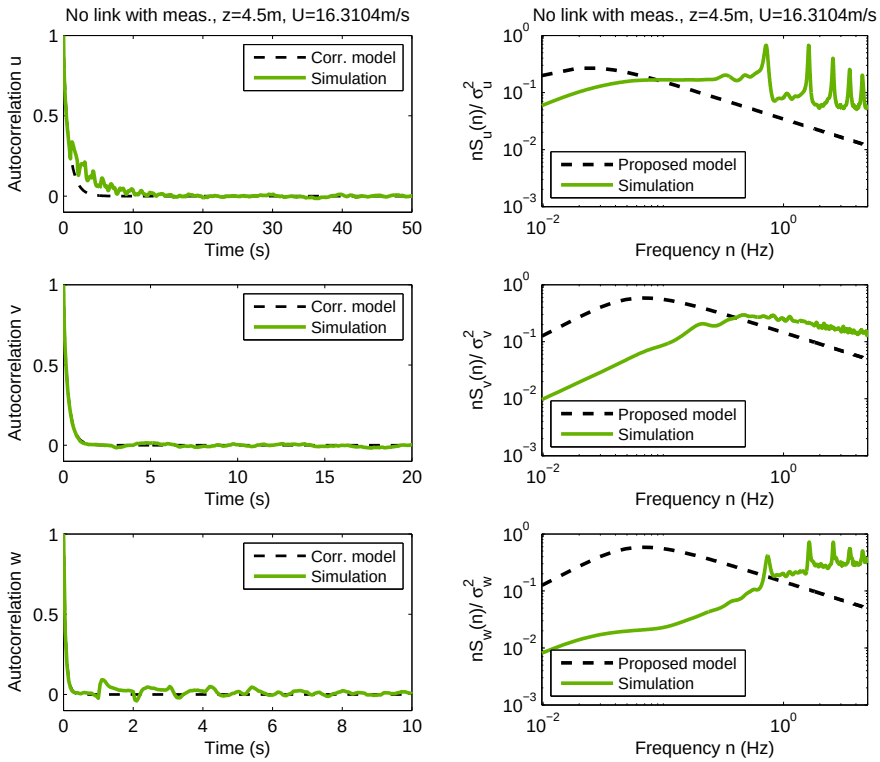


Figure B.1: Autocorrelation and PSD of the three components of the generated wind with Reynolds stress, at 4.5 m above ground.

### B.1.1 Autocorrelation and power spectral density

Fig. B.1 shows the autocorrelation and PSD of the generated wind at node 2, close to the ground. At this point, the effect is the most visible. We can clearly observe that the autocorrelations of the longitudinal and the vertical component display oscillations, with the corresponding peaks in the PSD. This phenomena is due to the AR parameters hitting, or getting to close to, producing a root of the AR model's characteristic polynomial (see 3.3.1) that is too close to unity in magnitude.

At other points such as node 7, the effect is less visible but still present, Fig. B.2.

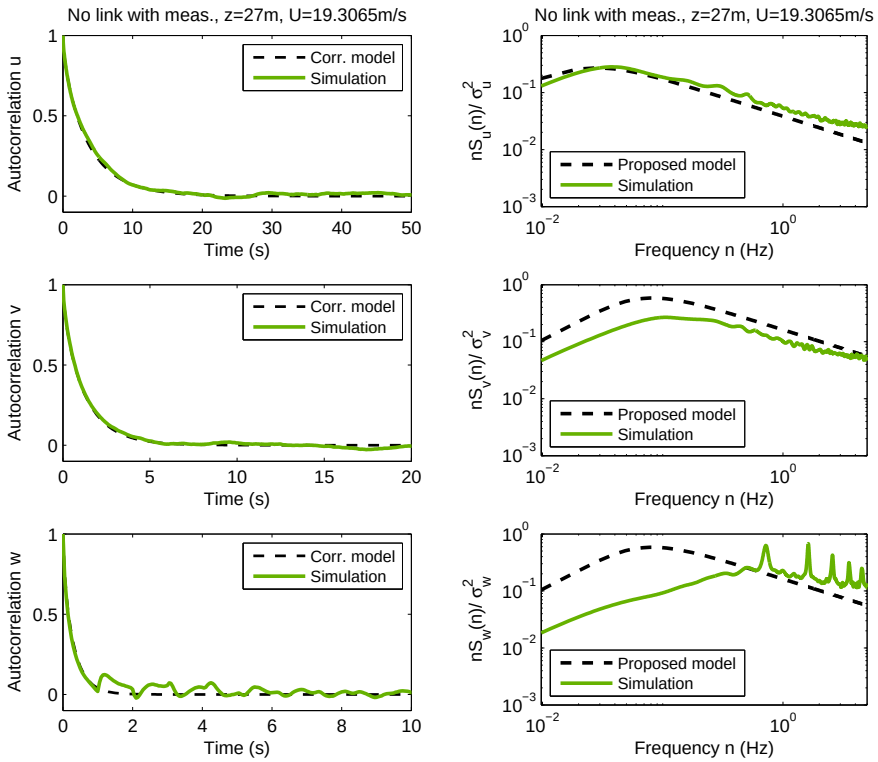


Figure B.2: Autocorrelation and PSD of the three components of the generated wind at 27 m above ground.

### B.1.2 Coherence and co-spectrum

The coherence is also impacted. In Fig. B.3(a), it is interesting to see that the vertical component's coherence seems to take on characteristics of the longitudinal component. We can guess that this is due to the Reynolds stress creating a link between the longitudinal and vertical components.

The Reynolds stress model is however well reproduced, Fig. B.3(b).

## B.2 Spectrum correction

During the study of Reynolds stress, we have investigated possibilities to correct the spectrum numerically after the generation. Actually, forgetting about the oscillations produced by a badly fitted AR model, it appears that when we add Reynolds stress relationships, the PSD and coherence are impacted while

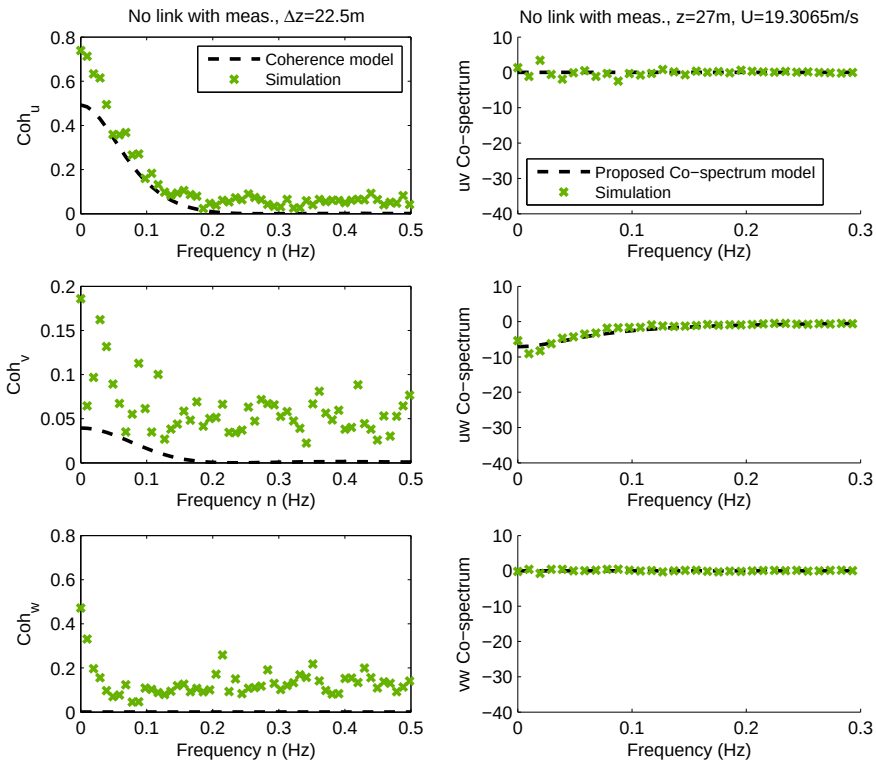


(a) Coherence, three components, between node 2 and 7

(b) Co-spectrum at 27 m

Figure B.3: Coherence and co-spectrum for the wind generated with Reynolds stress.

the Reynolds stress is well reproduced by the simulated wind. The following is a tentative method to correct the autospectrum without impacting the other features such as coherence and co-spectrum.

In the end, the method did not succeed and the issue with Reynolds stress lies more deeply in the AR method, so it clearly cannot be corrected this way. In hindsight, methods such as digital filtering would give better results that this method anyway. However, the investigation give some idea of how spectral analysis can practically be applied, which is why it has been included here as a part of the appendix.

### B.2.1 Basics

Our idea is to modify the autospectrum so that it takes on the target values, but without modifying the phase, which does not influence the value of the autospectrum but might have an effect on other properties. This report reviews the definition of the power spectral density, looks at the various power spectral density estimation techniques, and suggests a method to do the correction.

Let's denote $u_i, v_i, w_i$ the wind speed time series for the three components at point $i$. We consider two points, thus $i = 1, 2$. We define:

- ⋆ $S_{u_1}$ the autospectrum of the u component at point 1,
- ⋆ $S_{u_1 u_2}$ the cross-spectrum of the u component between points 1 and 2,
- ⋆ $Co_{u_1 w_1}$ the co-spectrum of the u and w components at point 1,

and all other spectra follow this notation.

### B.2.2 Spectrum correction

To correct the autospectrum, we will adjust the magnitude of the Fourier transform, without modifying the phase. Let's denote with an exponent $t$ the modified ("target") values of the autospectrum, such as

$$S^t_{u_1} = (R^t_{u_1})^2 \tag{B.1}$$

First, the actual value of the phase is calculated.

$$\varphi_{u_1} = \arctan\left(\frac{Im(\mathscr{F}(u_1))}{Re(\mathscr{F}(u_1))}\right) \tag{B.2}$$

Then, we replace the magnitude by the target magnitude:

$$R_{u_1} \rightarrow R^t_{u_1} \tag{B.3}$$

Finally, the adjusted Fourier transform of $u_1$ can be calculated:

$$\begin{aligned} Re(\mathscr{F}(u_1)^t) &= R^t_{u_1} \cos(\varphi_{u_1}) \\ Im(\mathscr{F}(u_1)^t) &= R^t_{u_1} \sin(\varphi_{u_1}) \end{aligned} \tag{B.4}$$

Eventually, we can calculate the modified time series as an inverse Fourier

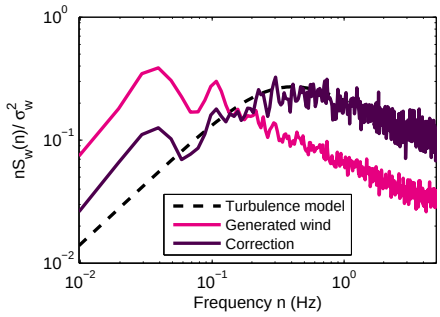


Figure B.4: PSD correction applied on a typical case, where the generated wind's PSD is very different from the target model.

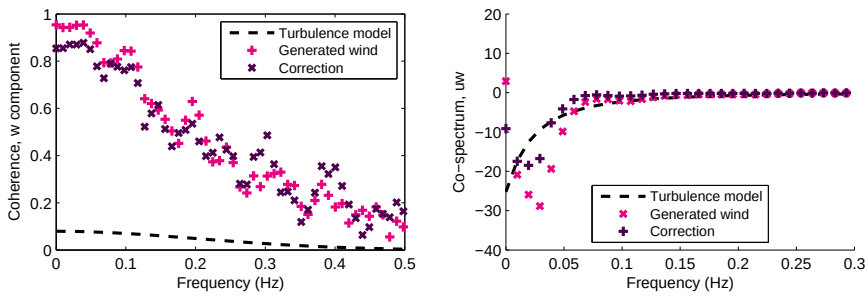


(a) Coherence

(b) Co-spectrum, $uw$

Figure B.5: Coherence and co-spectrum before and after PSD correction. They are not impacted by the PSD correction method.

transform:

$$u_1^t = \mathscr{F}^{-1}(\mathscr{F}(u_1)^t) \tag{B.5}$$

Applying this technique modifies the autospectrum without modifying the coherence or the co-spectrum, as shown in Fig. B.4 and Fig. B.5. Note that for this study we used Welch's periodogram estimate and not the MEM.

# Appendix C

# Response estimation with von Karman's model

In this appendix, an additional result is introduced. The suitability of von Karman's original model is compared to the proposed model.

The main objective of this thesis was to propose an improved description of turbulence, which we have introduced in Chapter 2. Therefore, we would like to compare the variation in the response estimation due to a different choice of turbulence models.

Hence, we will also simulate a wind field with the original von Karman model, that we have shown to be flawed in section 2.3.3. We have shown that linking with measurement data will improve the result, so we will only compute a linked wind field simulation. The objective is to show that the proposed turbulence model leads to better results than the original von Karman model.

Table C.1: Description of the generated turbulent wind fields studied in each section.

| | Wind generation method | Link with measured data | Turbulence model | Standards |
|---|---|---|---|---|
| Wind 1 | Linked | 1 component | von Karman | AIJ |
| Wind 2 | Linked | 1 component | Proposed | IEC |

## C.1 Wind field generation with the original von Karman model

Turbulent wind fields are generated using the original von Karman model and the proposed model. The wind properties are summarized in Table C.1. Wind 2 is the same as in Section 4.2. Wind 1 is generated using the parameters described thereafter.

### C.1.1 Simulation parameters

For the simulation, the parameters have been chosen as follows.

**Wind speed and turbulence intensity profile** WND3D includes the power law profile for the wind speed and turbulence intensity described in section 2.4.4.1 and 2.4.4.2 with

- ⋆ $U_0 = 19.87$ m/s and $z_0 = 36$ m (from measurements),
- ⋆ $\alpha = 0.1$,
- ⋆ $I_0 = 0.108$ and $z_0 = 36$ m (from measurements),
- ⋆ $\beta = 0.15$ following the AIJ recommendations.
- ⋆ For both profiles, $z_b = 5$ m is set up as the lower boundary.

Turbulence is supposed to be isotropic (2.38).

**Turbulence length scale** The turbulence length scale is calculated using the expression (2.40) and the ratios (2.39). To keep the same logic as the wind and turbulence intensity profiles, a lower boundary is set up at 5 m, under which the length scale is constant and equal to the length scale at 5 m.

**Correlations** The correlations are evaluated using the original von Karman turbulence model of section 2.3.3. We will not use the measured data to estimate the correlation due to the issues mentioned in 3.2.3. Like the first wind, we also neglect the Reynolds stress.

### C.1.2 Quality of the generated wind field

We can compare the generated wind fields' power spectral densities. Fig. C.1 shows the differences between simulated wind number 1 (proposed model) and

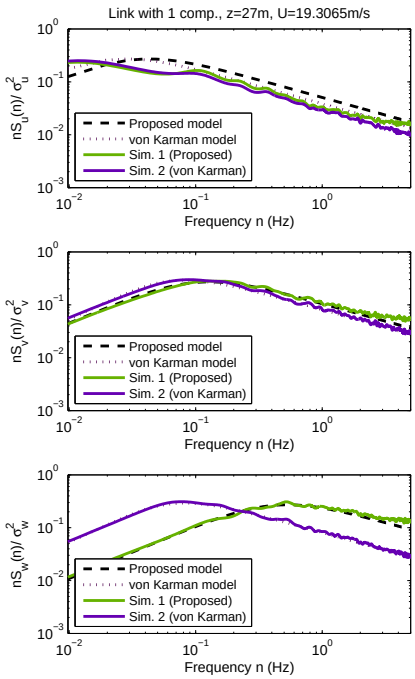


Figure C.1: PSD comparison of winds generated with proposed turbulence model versus von Karman's turbulence model, linked case.

wind number 2 (von Karman model). Actually, the shape of the autospectrum is the same for both proposed and von Karman model, but because of the different length scales the results differ. The effect is even more important for the lateral and vertical components as the length scales and target spectral shapes are even more different.

We can expect that these differences will have effects on the estimation of the structural response.

## C.2 Response estimation

### C.2.1 Moment time series

When looking at the time series of the simulated moments, Fig. C.2, we can barely see any difference between the two cases. Since the winds have been generated with a link to measurement data, the simulated responses look rather similar to the measured response.

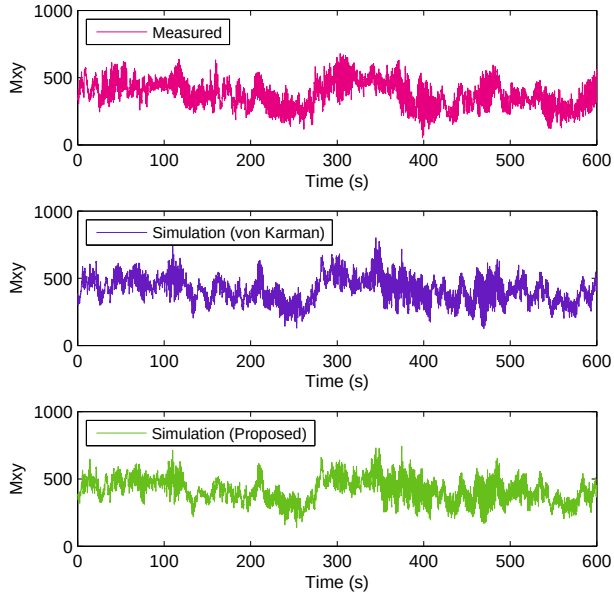


Figure C.2: Time series of the moment at tower base for one realization. Comparison between measurement, artificial and linked case.

A quantitative study shall be conducted to evaluate the quality of each estimation; the correlation coefficient is a good measure of the phase similarity between each response and the measurements.

### C.2.2 Correlation between simulation and measurement

Indeed, differences appear when we take a closer look at the results. Fig. C.3 and Table C.2 describe the correlation coefficients between the simulated and measured time series of the tower base moment. It appears that although the linked wind generation method allows the von Karman based turbulence to produce a nicely correlated response, our proposed model leads to a better response estimation, with a correlation coefficient almost 10% higher on average.

Table C.2: Correlation coefficients between simulated and measured moment, with responses estimated using von Karman and proposed turbulence models.

| Seed no. | 1 | 2 | 3 | 4 | 5 | 6 | 7 | 8 | 9 | 10 |
|---|---|---|---|---|---|---|---|---|---|---|
| Karman | 0.474 | 0.454 | 0.452 | 0.484 | 0.517 | 0.518 | 0.495 | 0.527 | 0.421 | 0.507 |
| Prop. | 0.510 | 0.511 | 0.505 | 0.537 | 0.528 | 0.552 | 0.556 | 0.580 | 0.493 | 0.549 |

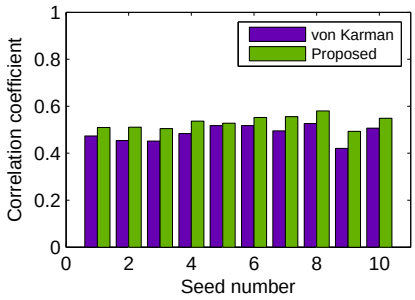


Figure C.3: Correlation coefficients, with responses estimated using von Karman and proposed turbulence models.

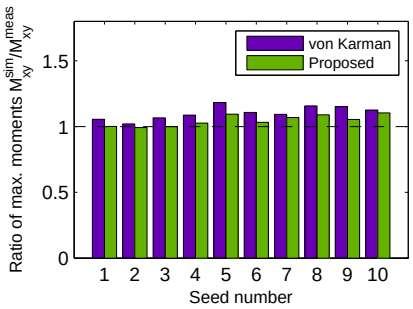


Figure C.4: Maximum moment ratio, with responses estimated using von Karman and proposed turbulence models.

Table C.3: Maximum moment ratios, with responses estimated using von Karman and proposed turbulence models.

| Seed no. | 1 | 2 | 3 | 4 | 5 | 6 | 7 | 8 | 9 | 10 |
|---|---|---|---|---|---|---|---|---|---|---|
| Karman | 1.055 | 1.020 | 1.066 | 1.087 | 1.183 | 1.107 | 1.092 | 1.158 | 1.150 | 1.126 |
| Prop. | 1.000 | 0.992 | 0.999 | 1.026 | 1.094 | 1.033 | 1.069 | 1.089 | 1.054 | 1.104 |

| Seed no. | Average | Std. dev. |
|---|---|---|
| Karman | 1.104 | 0.051 |
| Proposed | 1.046 | 0.042 |

### C.2.3 Estimation of the maximum tower base moment

Following the observations on the correlation coefficients, Fig. C.4 and Table C.3 are another measure of how the proposed turbulence model improves the estimation of the structural response.

When the response is estimated using a von Karman-based turbulent wind field, the average overestimation of the maximum moment stands at 10.4% of the measured value, still better than with the artificial generation method but not as good as with the proposed turbulence model. The standard deviation of error is also larger, at 5.1% of the measured maximum moment value against 4.2% for the proposed model.

These results show, rather clearly, that the proposed turbulence model is superior to the legacy von Karman turbulence model for simulating a realistic and accurate turbulent wind flow.

# Appendix D

# Modified turbulence standard deviation ratios

In the thesis, the proposed model has been described assuming that the ratios of turbulence standard deviations were, like the Kaimal model in the IEC 61400-1, defined as

$$\begin{cases} \sigma_v = 0.8\sigma_u \\ \sigma_w = 0.5\sigma_u. \end{cases}$$

This choice is actually conservative, especially for the lateral component $v$. Wind tunnel tests [ref], as well as the ratios recommended in the IEC for other models, seem to indicate that a more optimal choice would be

$$\begin{cases} \sigma_v = 0.7\sigma_u \\ \sigma_w = 0.5\sigma_u. \end{cases} \tag{D.1}$$

Consequently, the turbulence length scale ratios derived from the second IEC requirement are also modified. The equations derived from the IEC requirements are:

$$\frac{L_v}{L_u} = \left(\frac{3}{4}\right)^{3/2} \left(\frac{\sigma_v}{\sigma_u}\right)^3$$
$$\frac{L_w}{L_u} = \left(\frac{3}{4}\right)^{3/2} \left(\frac{\sigma_w}{\sigma_u}\right)^3,$$

which, using the new ratios of equation (D.1), lead to

$$\begin{cases} L_u = 3.49\Lambda_1 \\ L_v = 0.22 L_u \\ L_w = 0.08 L_u . \end{cases} \tag{D.2}$$

In this appendix, the results of Chapter 4 are reproduced using these new standard deviation and length scale ratios.

## D.1 No link and link with one component

In this section I will study the case of Miyakojima wind turbine, using the measured data to generate a wind field without measured data, and a wind field linked to one component of measured wind speed, at hub height.

### D.1.1 Generated wind fields

#### D.1.1.1 Wind generation parameters

**Wind speed and turbulence intensity profile** WND3D includes the power law profile for the wind speed and turbulence intensity described in section 2.4.4.1 and 2.4.4.2 with

- ⋆ $U_0 = 19.87$ m/s and $z_0 = 36$ m (from measurements),
- ⋆ $\alpha = 0.1$,
- ⋆ $I_0 = 0.108$ and $z_0 = 36$ m (from measurements),
- ⋆ $\beta = 0.1$ to have a constant standard deviation as required by the IEC.
- ⋆ For both profiles, $z_b = 5$ m is set up as the lower boundary.

The length scales and standard deviation ratios are obtained from (D.2) and (D.1).

**Correlations** The correlations are evaluated using the proposed turbulence model of section 2.4. We will not use the measured data to estimate the correlation.

The Reynolds stress is neglected, i.e. there is no correlation between different components of the wind.

Table D.1: Correlation coefficients between simulated and measured tower base moment time series, comparison of artificial and linked case, modified turbulence standard deviation ratios.

| Seed no. | 1 | 2 | 3 | 4 | 5 | 6 | 7 | 8 | 9 | 10 |
|---|---|---|---|---|---|---|---|---|---|---|
| Artificial | 0.042 | 0.155 | 0.029 | 0.020 | 0.055 | 0.090 | 0.105 | 0.072 | 0.088 | 0.018 |
| Linked | 0.509 | 0.513 | 0.513 | 0.543 | 0.532 | 0.558 | 0.562 | 0.582 | 0.501 | 0.550 |

#### D.1.1.2 Quality of the generated wind field

**Time series** The time series of the generated wind for both cases are compared in Fig. D.1.

**Power spectral density** The power spectral density of the generated wind is calculated using the MEM estimation. The averaged PSD are shown in Fig. D.2.

**Coherence** Coherence of the generated wind field is shown in Fig. **??**.

**Reynolds stress** The wind has been generated with no Reynolds stress. This assumption is respected by the generated wind as shown on Fig. 4.6.

### D.1.2 Reponse estimation

In this section, the results obtained with the artificial and linked wind fields described in the previous section are compared.

#### D.1.2.1 Moment time series

The time series of the tower base moment are shown in Fig. D.4. We can see that the low-frequency trends are closer to measurements in the case where measured wind speed is included in the generated wind field.

#### D.1.2.2 Correlation between simulation and measurement

Fig. 4.8 and Table **??** show the correlation coefficients between the simulated and the measured time series of tower base moment. The coefficients are increased when the external force is calculated from the wind generated with link to measured wind speed.

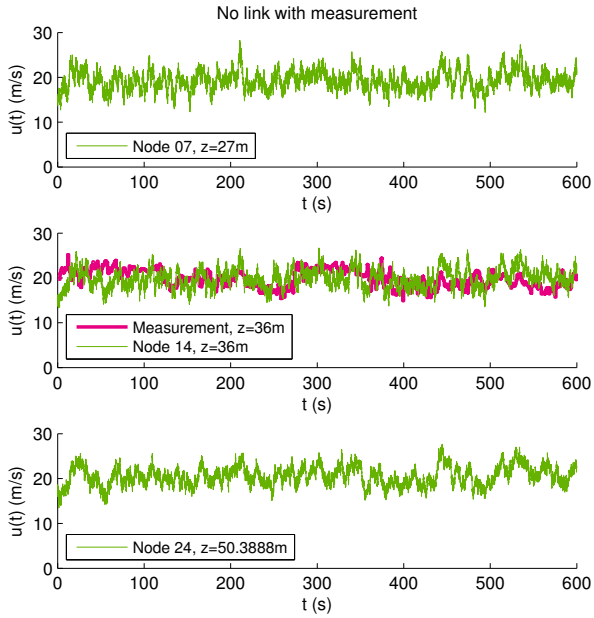


(a) Artificial case

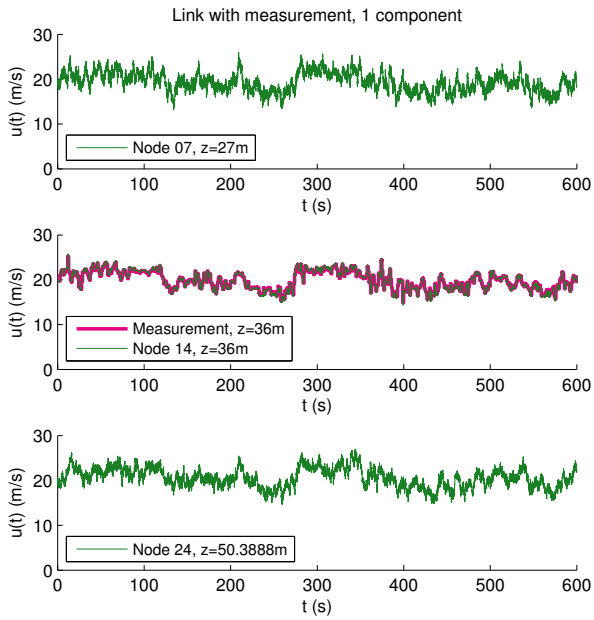


(b) Linked case

Figure D.1: Time series of the wind speed generated using WND3D, for one realization, artificial and linked case, modified turbulence standard deviation ratios.

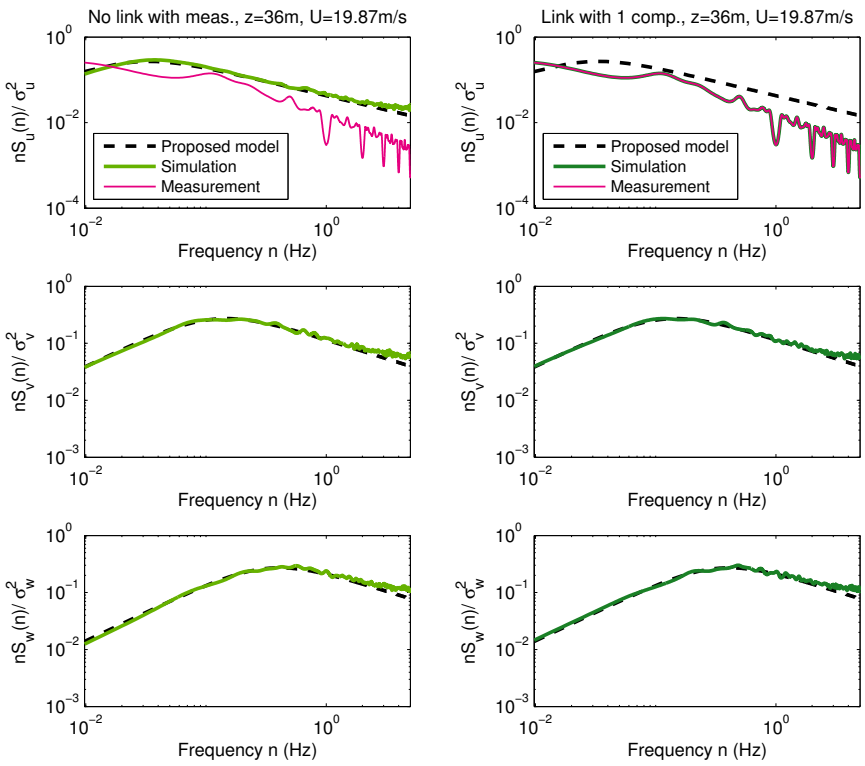


(a) Artificial case

(b) Linked case

Figure D.2: Power spectral density of the generated wind speed at measurement height (36 m), average over 10 realizations, artificial and linked case, modified turbulence standard deviation ratios.

#### D.1.2.3 Estimation of the maximum tower base moment

In Fig. D.6, we have plotted the ratios between the maximum moment estimated by simulation and the maximum measured moment. Results are also shown in Table D.2.

## D.2 Numerical validation: linking with three components of measured wind

In this section, similar to 4.3, I will consider the case of including 1 and 3 components of measured wind speed as a constraint to the generated wind fields.

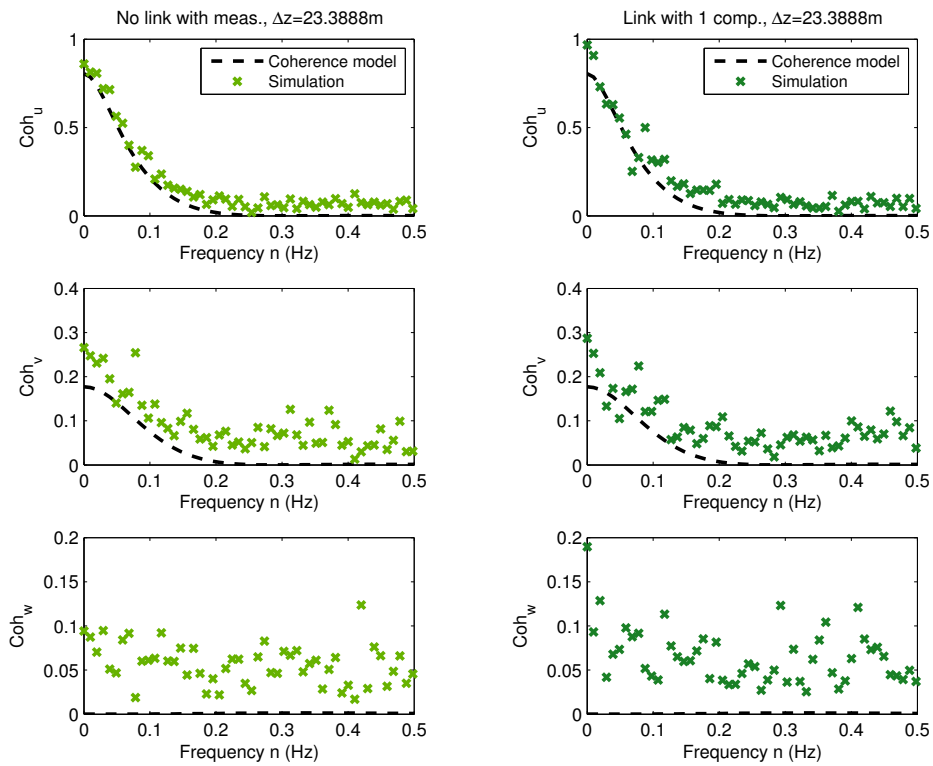


(a) Artificial case, between blade tip (node 24) and two-thirds of tower height (node 7)

(b) Linked case, between blade tip (node 24) and two-thirds of tower height (node 7)

Figure D.3: Coherence for longitudinal component, artificial and linked case, using the proposed turbulence model; modified turbulence standard deviation ratios.

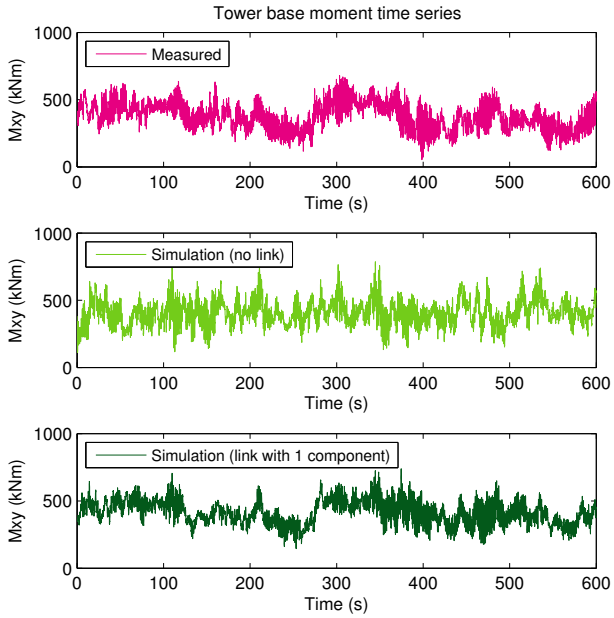


Figure D.4: Time series of the moment at tower base for one realization. Comparison between measurement, artificial and linked case, modified turbulence standard deviation ratios.

### D.2.1 Generated wind fields

#### D.2.1.1 Wind generation parameters

**Wind speed and turbulence intensity profile** WND3D includes the power law profile for the wind speed and turbulence intensity described in section 2.4.4.1 and 2.4.4.2 with

- ⋆ $U_0 = 17.31$ m/s and $z_0 = 36$ m,
- ⋆ $\alpha = 0.15$ (terrain category II),
- ⋆ $I_0 = 0.198$ and $z_0 = 36$ m (from measurements),
- ⋆ $\beta = 0.15$ to have a constant standard deviation as required by the IEC.
- ⋆ For both profiles, $z_b = 5$ m is set up as the lower boundary.

The length scales and standard deviation ratios are obtained from (D.2) and (D.1).

**Correlations** The correlations are evaluated using the proposed turbulence model of section 2.4. We will not use the measured data to estimate the cor-

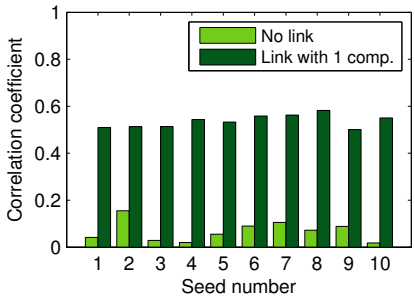


Figure D.5: Correlation coefficients between measurement and simulations done with artificial and linked wind fields, modified turbulence standard deviation ratios.

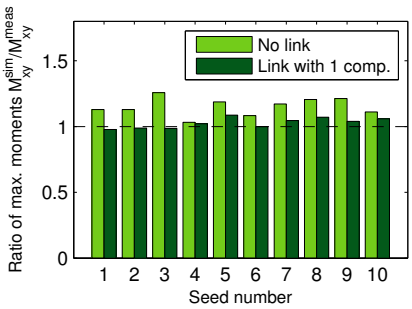


Figure D.6: Maximum moment ratio between measurement and simulations done with artificial and linked wind fields, modified turbulence standard deviation ratios.

Table D.2: Maximum moment ratios, comparison of artificial and linked case, modified turbulence standard deviation ratios.

| Seed no. | 1 | 2 | 3 | 4 | 5 | 6 | 7 | 8 | 9 | 10 |
|---|---|---|---|---|---|---|---|---|---|---|
| Artificial | 1.129 | 1.129 | 1.258 | 1.032 | 1.188 | 1.083 | 1.171 | 1.206 | 1.213 | 1.111 |
| Linked | 1.012 | 0.972 | 0.994 | 1.028 | 1.090 | 1.006 | 1.065 | 1.069 | 1.045 | 1.087 |

| Seed no. | Average | Std. dev. |
|---|---|---|
| Artificial | 1.152 | 0.068 |
| Linked | 1.037 | 0.041 |

relation.

The Reynolds stress is neglected, i.e. there is no correlation between different components of the wind.

#### D.2.1.2 Quality of the generated wind field

**Time series** The time series of the generated wind for both cases are compared in Fig. D.7 and Fig. D.8.

**Power spectral density** The power spectral density of the generated wind is calculated using the MEM estimation. The averaged PSD are shown in Fig. D.9.

**Reynolds stress** Since the sequence of correlation matrices in the AR model have been parametrized to neglect Reynolds stress, the AR process itself will not include any cross-component correlations. However, when linking with three

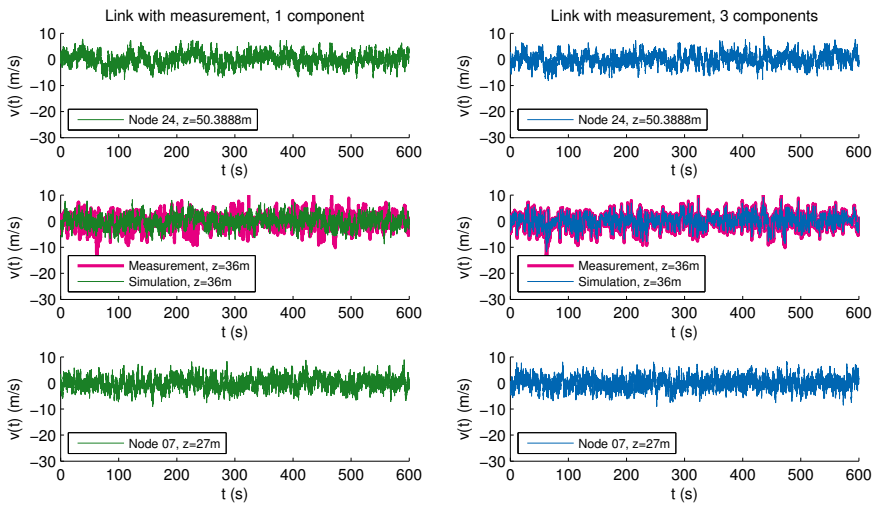


(a) Link with 1 component

(b) Link with 3 components

Figure D.7: Time series of the generated lateral wind at several heights, link with 1 and 3 components.

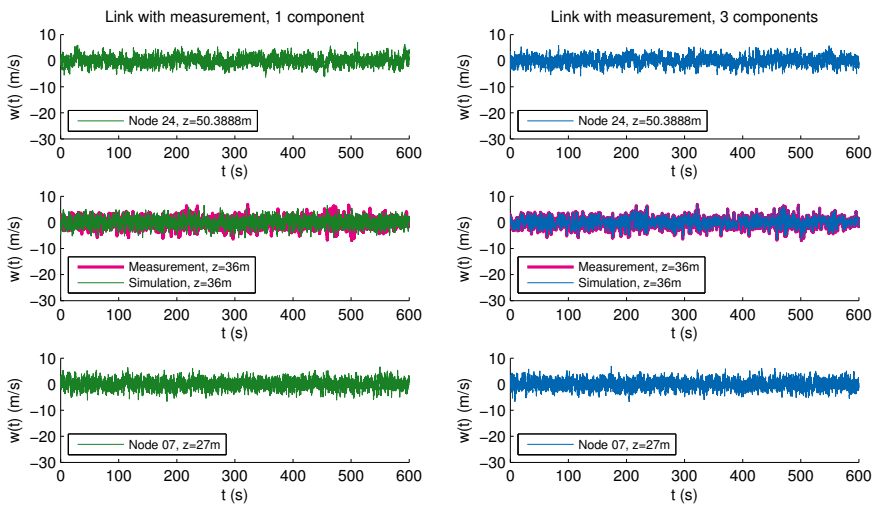


(a) Link with 1 component

(b) Link with 3 components

Figure D.8: Time series of the generated vertical wind at several heights, link with 1 and 3 components.

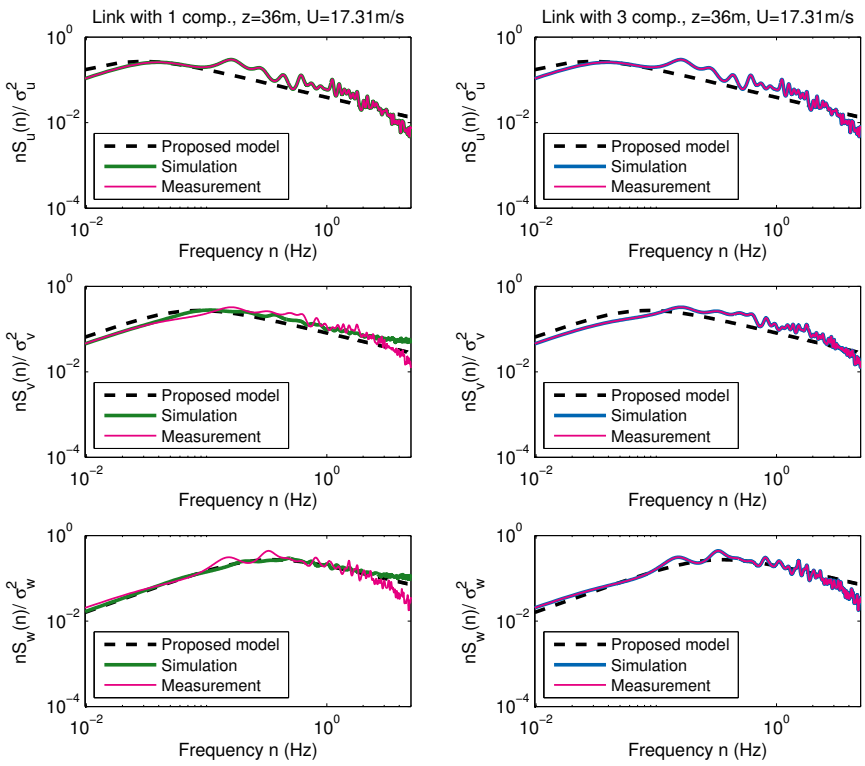


(a) Link with 1 component

(b) Link with 3 components

Figure D.9: Power spectral densities of winds generated with link to 1 and 3 components of measured data, proposed model, at hub height (measurement point).

components of measured wind speed, the Reynolds stress correlations do exist between these three components at the measurement point. Fig. D.10 shows the co-spectra in both cases at measurement point.

### D.2.2 Reponse estimation

#### D.2.2.1 Moment time series

The time series of the tower base moment are shown in Fig. D.11. We can see that the low-frequency trends are closer to measurements in the case where measured wind speed is included in the generated wind field.

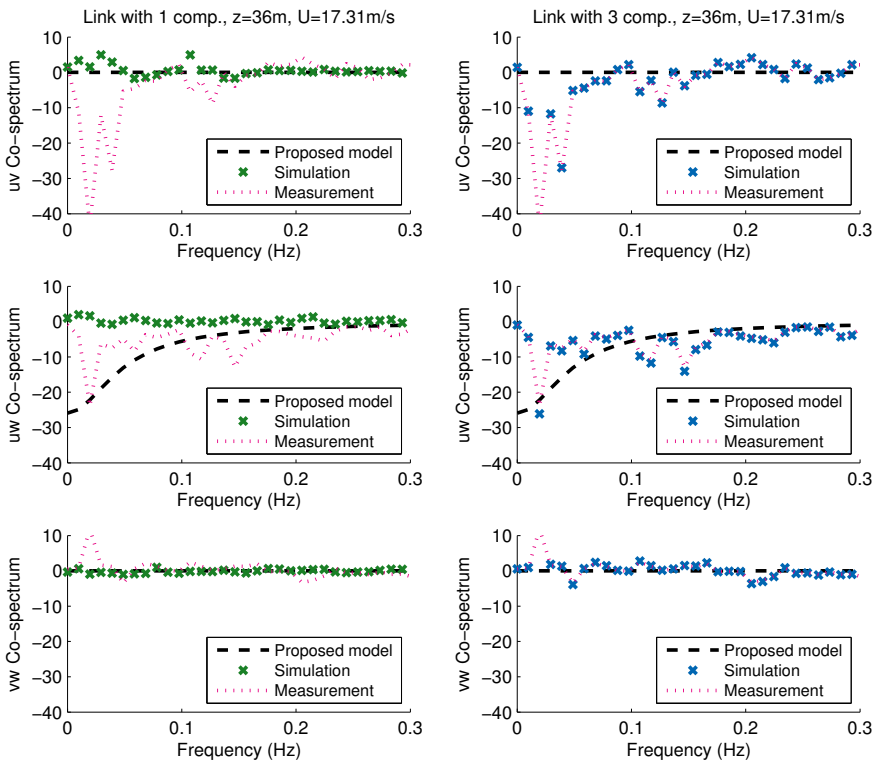


(a) Link with 1 component

(b) Link with 3 components

Figure D.10: Co-spectrum (Reynolds stress), link with 1 and 3 components, hub height (measurement point).

#### D.2.2.2 Estimation of the maximum moment

To quantify the differences, the maximum estimated moment for each simulation is compared, Fig. **??**. Numerical values are also given in Table D.3 and Table D.4.

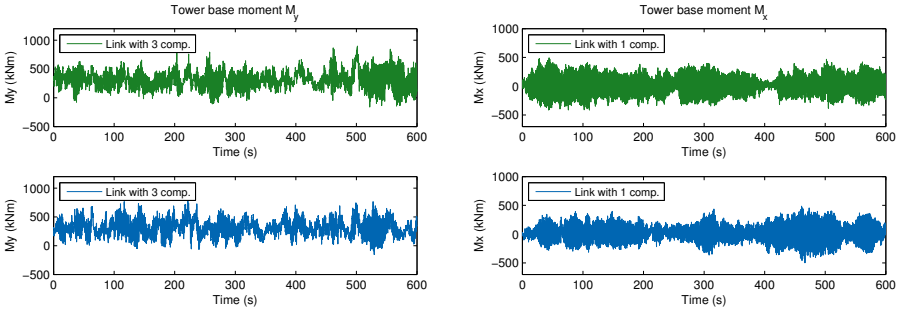


(a) Fore-aft (b) Side-by-side

Figure D.11: Times series of the tower base moment, simulation using wind fields with link to 1 and 3 components of measured data. The moments are shown in kNm.

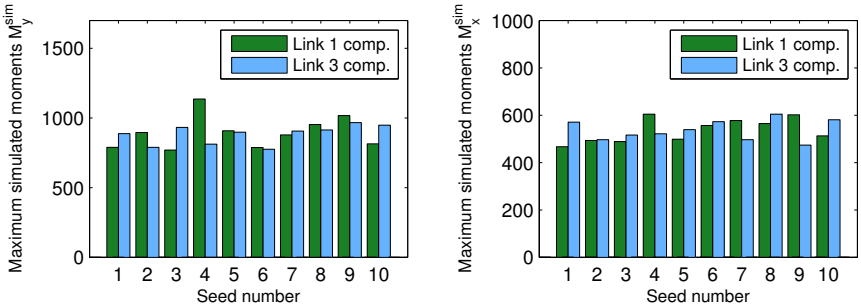


(a) Fore-aft (b) Side-by-side

Figure D.12: Maximum tower base moment, simulation with link to 1 and 3 components of measured wind speed. The moments are shown in kNm.

Table D.3: Values of the maximum simulated fore-aft moment when linked to 1 and 3 components of measured wind speed, 10 realizations. The moments are shown in kNm.

| | Seed no. | 1 | 2 | 3 | 4 | 5 | 6 |
|---|---|---|---|---|---|---|---|
| $M_y$ | 1 comp. | 789.60 | 895.40 | 770.10 | 1136.50 | 908.00 | 788.20 |
| | 3 comp. | 887.60 | 789.30 | 932.80 | 812.00 | 898.60 | 775.50 |

| | Seed no. | 7 | 8 | 9 | 10 | Average | Std. dev. |
|---|---|---|---|---|---|---|---|
| $M_y$ | 1 comp. | 878.10 | 953.40 | 1017.10 | 814.10 | 895.05 | 116.31 |
| | 3 comp. | 906.00 | 914.30 | 966.40 | 948.30 | 883.08 | 67.37 |

Table D.4: Values of the maximum simulated side-by-side moment when linked to 1 and 3 components of measured wind speed, 10 realizations. The moments are shown in kNm.

| | Seed no. | 1 | 2 | 3 | 4 | 5 | 6 |
|---|---|---|---|---|---|---|---|
| $M_x$ | 1 comp. | 466.90 | 493.45 | 488.38 | 604.64 | 498.38 | 556.29 |
| | 3 comp. | 570.58 | 496.49 | 516.20 | 521.39 | 539.17 | 572.64 |

| | Seed no. | 7 | 8 | 9 | 10 | Average | Std. dev. |
|---|---|---|---|---|---|---|---|
| $M_x$ | 1 comp. | 577.62 | 564.98 | 601.53 | 512.52 | 536.47 | 50.34 |
| | 3 comp. | 496.91 | 604.10 | 473.83 | 580.72 | 537.20 | 43.12 |

# Bibliography


[1] Architectural Institute of Japan. AIJ Recommendations for Loads on Buildings (English), 2004.

[2] T. Burton, D. Sharpe, N. Jenkins, and E. Bossanyi. *Wind Energy Handbook*. John Wiley & Sons, 2001.

[3] A. Davenport. The Spectrum of Horizontal Gustiness Near the Ground. *Quarterly Journal of the Royal Meteorological Society*, 87(372):194–211, 1960.

[4] M. de Hoon, T. van der Hagen, H. Schoonewelle, and H. van Dam. Why Yule-Walker Should Not Be Used for Autoregressive modelling. *Annals of Nuclear Energy*, 23(15):1219–1228, 1996.

[5] DNV/Risø. Guidelines for the Design of Wind Turbines, 2001.

[6] M. Fujimura and J. Maeda. Cross-correlation of Fluctuating Components of Wind Speed Based on Strong Wind Measurement. In *Proceedings of the 7th Asia-Pacific Conference on Wind Engineering*, Taipei, Taiwan, 2009.

[7] GL Garrad Hassan. Bladed Theory Manual, version 4.1, 2010.

[8] J. Hinze. *Turbulence*. McGraw-Hill, 2nd edition, 1975.

[9] International Electrotechnical Commission. *Wind turbines - Part 1: Design requirements*. Number 918025243. International Electrotechnical Commission, 3rd edition, 2005.

[10] T. Ishihara, P. V. Phuc, Y. Fujino, K. Takahara, and T. Mekaru. A Field Test and Full Dynamic Simulation on a Stall Regulated Wind Turbine. In *Proceedings of the 6th Asia-Pacific Conference on Wind Engineering*, pages 599–612, 2005.

[11] Y. Iwatani. Simulation of Multidimensional Wind Fluctuations Having Any Arbitrary Power Spectra and Cross Spectra. *Journal of Wind Engineering*, 11:5–17, 1982.

[12] Y. Iwatani. Simulation of Multidimensional Wind Fluctuations Linked to Measured Data. *Journal of Wind Engineering*, 69:1–13, 1996.

[13] J. C. Kaimal, J. C. Wyngaard, Y. Izumi, and O. R. Coté. Spectral Characteristics of Surface-layer Turbulence. *Quarterly Journal of the Royal Meteorological Society*, 98(417):563–589, July 1972.

[14] M. Lange and U. Focken. *Physical Approach to Short-Term Wind Power Prediction*. Springer, 2010.

[15] J. Maeda and M. Makino. Power Spectra of Longitudinal and Lateral Wind Speed Near the Ground in Strong Winds. *Journal of Wind Engineering and Industrial Aerodynamics*, 28:31–40, 1988.

[16] J. Maeda and M. Makino. Characteristics of Gusty Winds Simulated by an ARMA Model. *Journal of Wind Engineering and Industrial Aerodynamics*, 44:427–436, 1992.

[17] P. Morthorst. Wind Energy - The Facts, Volume 1. Technical report, European Wind Energy Association, 2009.

[18] P. V. Phuc. Numerical and Theoretical Study on the Wind Response of Wind Turbine in the Strong Wind Condition. Master's thesis, The University of Tokyo, 2005.

[19] W. H. Press, S. A. Teukolsky, W. T. Vetterling, and B. P. Flannery. *Numerical Recipes in Fortran 77: The Art of Scientific Computing, Volume 1*. Cambridge University Press, 2nd edition, 1992.

[20] M. Shinozuka. Simulation of Multivariate and Multidimensional Random Processes. *Journal of the Acoustical Society of America*, 49(1):357–368, 1971.

[21] P. Stoica and R. Moses. *Spectral Analysis of Signals*. Prentice Hall, 2004.

[22] M. Takeuchi and J. Maeda. Multidimensional Simulation of Fluctuating Wind Field Including Lateral Components Under Strong Winds. In *The Fifth International Symposium on Computational Wind Engineering*, Chapel Hill, North Carolina, USA, 2010.

[23] I. Troen and E. L. Petersen. *European Wind Atlas*. Commission of the European Communities, Directorate-General for Science, Research, and Development, 1989.

[24] P. S. Veers. Three-dimensional Wind Simulation. 1988.

[25] T. von Karman. Progress in the Statistical Theory of Turbulence. *Proceedings of the National Academy of Sciences of the United States of America*, 34(11):530–539, 1948.

[26] T. von Karman and L. Howarth. On the Statistical Theory of Isotropic Turbulence. *Proceedings of the Royal Society of London*, 164(917):192–215, Jan. 1938.

[27] G. Walker. On Periodicity in Series of Related Terms. *Proceedings of the Royal Society of London*, 131(818):518–532, 1931.

[28] P. Welch. The Use of Fast Fourier Transform for the Estimation of Power Spectra: a Method Based on Time Averaging over Short, Modified Periodograms. *IEEE Transactions on Audio and Electroacoustics*, AU-15(2):70–73, 1967.

[29] J. Yoon. *Prediction of Dynamic Response of Wind Turbines Using SCADA Data and Updated Aeroelastic Model*. PhD thesis, The University of Tokyo, 2011.

[30] G. U. Yule. On a Method of Investigating Periodicities in Disturbed Series, with Special Reference to Wolfer's Sunspot Numbers. *Philosophical Transactions of the Royal Society of London Series A Containing Papers of a Mathematical or Physical Character*, 226(636-646):267–298, 1927.